Winter 2018

Development of a Novel and Dynamic Shear Rheometer Based Extensional Deformation Test to Replace Force Ductility Test

Waleed M. Omer
Louisiana Tech University

DEVELOPMENT OF A NOVEL AND DYNAMIC SHEAR RHEOMETER BASED EXTENSIONAL DEFORMATION TEST TO REPLACE FORCE DUCTILITY TEST

by

Waleed Mohammed Omer, B.S.

A Thesis Presented in Partial Fulfillment
of the Requirements of the Degree
Master of Science

COLLEGE OF ENGINEERING AND SCIENCE
LOUISIANA TECH UNIVERSITY

March 2018

ABSTRACT

Modification of asphalt binders is essential to improve the physical and rheological properties of asphalt and to reduce the aging effect. The use of polymers to modify asphalt is the most common approach in asphalt modification. Force ductility test has been a challenging topic as an indicator of asphalt performance, especially for the modified asphalt binders. The significance of the force ductility test as a measure of fatigue and thermal cracking has been debated because of its low reproducibility, empirical nature and the unclear relationship with the fundamental asphalt properties, especially with modified asphalt binders [1]. Extensional deformations tests where converging flows occur have been used by many for polymer characterizations (2). In this study, the extensional deformation behavior of binders Performance Graded 58-28, PG 64-22, and PG 76-22 and its parameters including geometry and temperature were investigated through an extensional rheological approach using a DSR-based Sentmanat Extensional Rheometer (SER). Furthermore, a test method and a sample preparation procedure especially for asphalt binders were developed as a replacement to the conventional force ductility test. The sample preparation method has been simplified and detailed in a way that it can be performed in all asphalt labs. A detailed analysis indicates that the average second peak and first peak elongation forces increase due to the increase of the sample's area, with R^2 values of 0.85 and 0.84, respectively. However, the same areas with different dimensions derived different values of elongation force that is due to

the dominant role of the width. The elongation force of all samples with the same area but different dimensions increases due to the width's increment even though the thickness decreases.

Based on this study, the recommended test specifications are as follows: the selected geometry is 9 mm x 0.72 mm (width x thickness). The second peak elongation force F_2 value was chosen as a recommended force ductility parameter. The minimum F_2 value recommended is 14 N, which was lower than the lowest limit of 99% confidence interval (14.45N – 15.99 N). Also, the minimum ratio of the second peak elongation force over the first peak elongation force F_2/F_1 of 1.25 is recommended for PG 76-22. This is also lower than the lowest value of 99% confidence interval (1.29-1.51). The recommended temperature is 4ºC, the recommended strain rate is $0.1s^{-1}$, and the recommended final strain is 3.4 rad. Therefore, with a more reproducible, significantly less material and time consuming, and with a more mechanistic approach, the developed novel method can help improve the durability of modified asphalt pavements.

DEDICATION

To

My mother Hind Freigoun

TABLE OF CONTENTS

LIST OF TABLES

LIST OF FIGURES

ACKNOWLEDGMENTS

First and foremost, I wish to thank God Almighty for the life He gave me. I owe all that I am to Him. Special thanks to my father Mohammed Omer, my mother Hind Freigoun, and my brother Wael Mohammed for their unwavering support along the way.

I also wish to express my deepest appreciation and gratitude to my masters committee chairman, Dr. Nazimuddin Wasiuddin, for his invaluable help, constant support and considerable patience throughout my masters' studies. Without his dedication, effort and active involvement, this work would not have been possible.

I would also like to thank Dr. Xingran Wang and Dr. Norm Pumphrey for serving as my committee members and for their valuable comments and suggestions.

I want to thank my research colleague, Shams Arafat, for his help since day one; he played a major role with the laboratory work, and my life in Ruston.

At last, I want to thank Dr. Amel O. Bakhiet "my second mother", and Dr. Rashid A. Saeed at Sudan University of Science & Technology for their constant support during the admission process.

CHAPTER 1

INTRODUCTION

1.1 Introduction

The Force ductility test, as described in the writing, is used to estimate the potential of asphalt binder for fatigue and thermal cracking, and/or raveling. In this test, an asphalt binder sample is elongated typically at 4°C and 5 cm/min deformation rate until a fragile fracture occurs or it reaches the elongation of at least 30 cm, AASHTO T300. However, due to the increasing stress on the highways, the use of the polymer-modified asphalt binder has grown tremendously. Many studies failed to correlate the force ductility test with the polymer-modified asphalt binder performance. In the last decade, relating the polymer modified asphalt binder's proprieties to its molecular structure through shear rheometers has become increasingly advocated. Many studies tried to develop a linear and non-linear visco-elastic rheological parameter to correlate it with the modified-asphalt performance. Extensional rheometers can be much more accurate in describing the polymer characterization than the above mentioned rheological measurements. To this end, the following thesis has been initiated to replace AASHTO T300 with an extensional deformation test using Sentmanat Extensional Rheometer (SER).

1.2 Background

The U.S. has the longest total road network size in the world by more than 4 million miles of public roads (FHWA 2015). With the economy improving, the traffic and the heavy loads utilizing the road are enormously increasing. However, among all the challenges that the roads paving is facing, asphalt binder plays a major role on improving the roads performance. Throughout the last two decades, many methods have been developed to implement a breakthrough in paving challenges. One of the new successful approaches is the use of the modifiers to improve the asphalt binder characteristics. With the widest use of the polymer modifications in the asphalt binder, many testing methods and specifications must be modified in order to be validated with the modified asphalt binders' microstructure behavior. Of these methods, force ductility test is still a challenge difficulty for researchers and DOTs. New test methods and specifications with different approaches have been adopted by different DOTs to replace or modify force ductility test, but still there is no clarified replacement for the force ductility test till now.

1.3 Objectives

The primary objective of this study is to develop a new extensional deformation test method using a Sentmanat Extensional Rheometer inside the DSR to fulfill the acknowledged gap in the current PG System by replacing the force ductility test. The specific objectives are as follows:

1. Develop a sample preparation method.
2. Perform a parametric study for the effect of sample geometry (thickness and width), and select the final geometry.
3. Investigate the effect of temperature and select the test temperature.

4. Analyze the reproducibility of the results.
5. Recommend test parameters and specifications.

1.4 Thesis Organization

This thesis is organized into five sections: Introduction, Literature Review, Methodology, Results and Discussion, and Conclusions. Chapter 1 is an introduction to this study. It gives a brief summary of the force ductility test, use of polymer modifications, describes the needs, and states the research objectives. Chapter 2 is the literature review, which introduces a background of AASHTO 300, an overview on the force ductility test and the polymer modified asphalt's characterization methods, a survey of all the states that still use AASHTOO 300 as a PG plus requirement, and a detailed description of Sentmanat Extensional Rheometer. Chapter 3 is the Research Methodology, which gives details about the test parameters, selection of materials used, experimental plan, sample preparation, and the test procedure. Chapter 4 is the results and discussions, which introduces an analysis of the data obtained, and the recommended parameters and specifications of the developed test method. The report closes with the final conclusions. Literature used as supporting material are cited in references.

.

CHAPTER 2

LITERATURE REVIEW

2.1 Introduction

2.1.1 Background

One of the popular techniques to enhance asphalt pavement performance is the modifications use in the asphalt binder by utilizing materials such as polymer, lime, carbon black, fibers, and rubbers [3]. The use of polymer-modified asphalt binders has grown tremendously in North America due to the increasing stress on the highways from higher traffic volumes and heavier loads. The Strategic Highway Research Program (SHRP) on asphalt was carried out almost exclusively with unmodified asphalt cements, so the applicability of the Superpave Performance Graded (PG) AASHTO M320 specifications and test methods to modified binders was not validated. Consequently, Departments of Transportation (DOT) in most of the states have added supplemental specifications known as "PG-Plus" tests, to identify the presence of polymers. Louisiana is among the states that are currently using a PG-Plus specification. Separation of polymer, force ductility, and elastic recovery are the required tests for the Louisiana Department of Transportation and Development's PG-Plus specifications. The use of polymer modifiers in asphalt binders was found to be a promising technique to improve the performance of asphalt mixtures. However, an insight impact of polymer modifiers on asphalt binders relevant to the performance is yet to be researched [3].

2.1.2 Overview on force ductility test

The force ductility test is used to estimate the asphalt binder potential for fatigue and thermal cracking, and/or raveling [4]. It was first introduced by Anderson and Wiley in 1976 [5] to indicate expected low temperature performance of asphalt binders by comparing their relative strength at low temperatures while being pulled at a fixed deformation rate [6]. Later, in 1985, Shuler [7-8] modified the test procedure to improve the precision and practicality, particularly for use with polymer modified asphalt binders. Many agencies have adopted the rheology characterization methods. However, there are some agencies still using AASHTO T300 for characterizing polymer modified asphalt binders in which an asphalt binder sample is elongated typically at 4°C and 5 cm/min deformation rate until fragile fracture or reaching the elongation of at least 30 cm. AASHTO T300 specifies the force ratio (ratio of the force at the second peak to the force at the initial peak) to be reported. The first peak is related to the base asphalt and the second peak characterizes the polymer [7-8].

However, performing force ductility test is a time and material consuming process. It is subject to reproducibility difficulties and can exhibit significant variability at low to intermediate temperatures (4º-25ºC) [4, 9, 10]. Besides variability in results, force ductility test requires the use of a ductility bath, which has several disadvantages including inconsistency of the testing sample geometry. Also, the force ductility test reflects the structure response of the sample not the material properties response. Most importantly, these tests are empirical [11] and often fail to accurately and comprehensively characterize the performance characteristics associated with polymer modified asphalt [10-11]. Many studies failed to correlate force ductility results with the asphalt binder performance. One of these studies is a study conducted by Tabatabaee [12]. No correlation was found between the force ductility results and the number of cycles to fatigue failure N_f which was calculated based on linear Amplitude Sweep LAS results at the intermediate grade temperature. It was also reported that force ductility test was not able to consistently detect the presence of the elastomeric modification. A survey was conducted of several state DOTs (such as Louisiana and Illinois) that specify force ductility test in their requirements; we observed the diversity of specifications in the force ductility test. Table 2-1 shows the PG plus requirements for performance graded asphalt binder (modified) for four different states.

Table 2-1. PG Plus Requirement for Performance Graded Asphalt Binder (Modified) for Four Different States

State	Criteria	Temp	Test Method	Requirements by Performance Grade							
Illinois	(f2/f1)	4ºC	T300	Binder (SB/SBS)	64-29	70-22	70-28	76-22	76-28		
				Requirements	0.30 min	0.30 min	0.30 min	0.35 min	0.35 min		
Louisiana	(f2/f1)	4ºC	T300	Binder	76-22M						
				Requirements	0.30 min						
	f2 in kg			Binder	70-22M						
				Requirements	0.23 min						
Michigan	(f2/f1)	4ºC	T 300	Binder	58-34 P	64-28 P	64-34 P	70-22 P	70-28 P	76-22 P	76-28 P
				Requirements	0.30 min	0.30 min	0.35 min	0.30 min	0.30 min	0.35 min	0.35 min
Oregon	(f2/f1)	4ºC	ODOT TM 427	Binder	AC-15-5TR						
				Requirements	0.30 min						

Figures 2-1 and 2-2 were reported on the LTRC Project No. 11-2B [13]. It shows a visual of how the ductility test failed to consistently detect the second peak elongation force f_2.

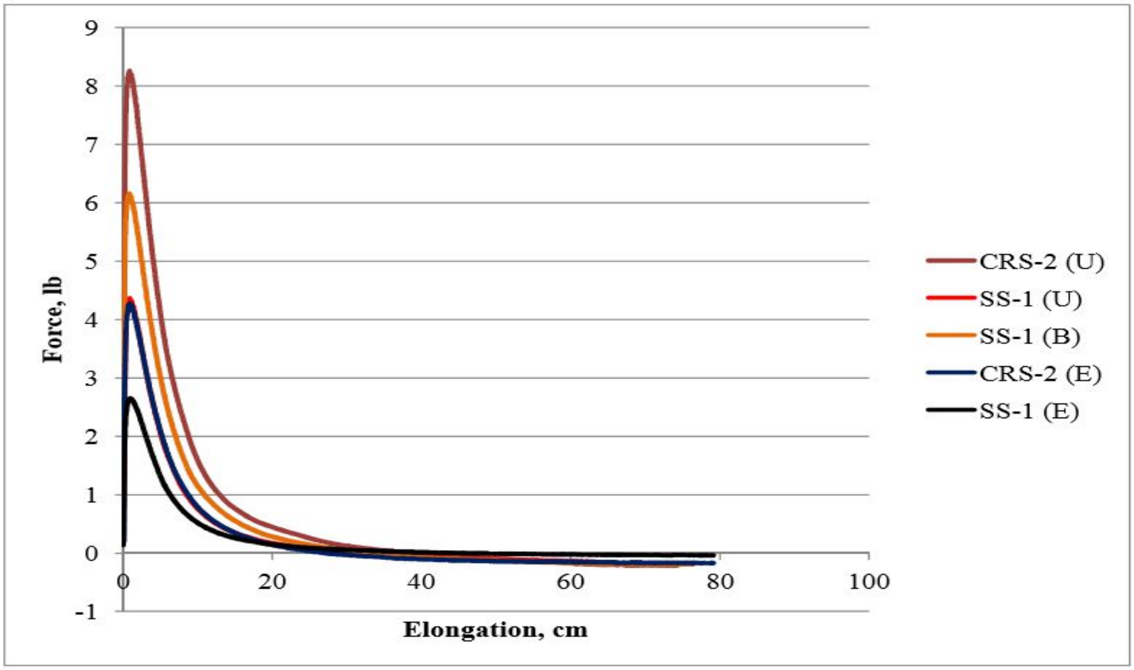

Figure 2-1. Force ductility results of non-polymer modified asphalt emulsion [13]

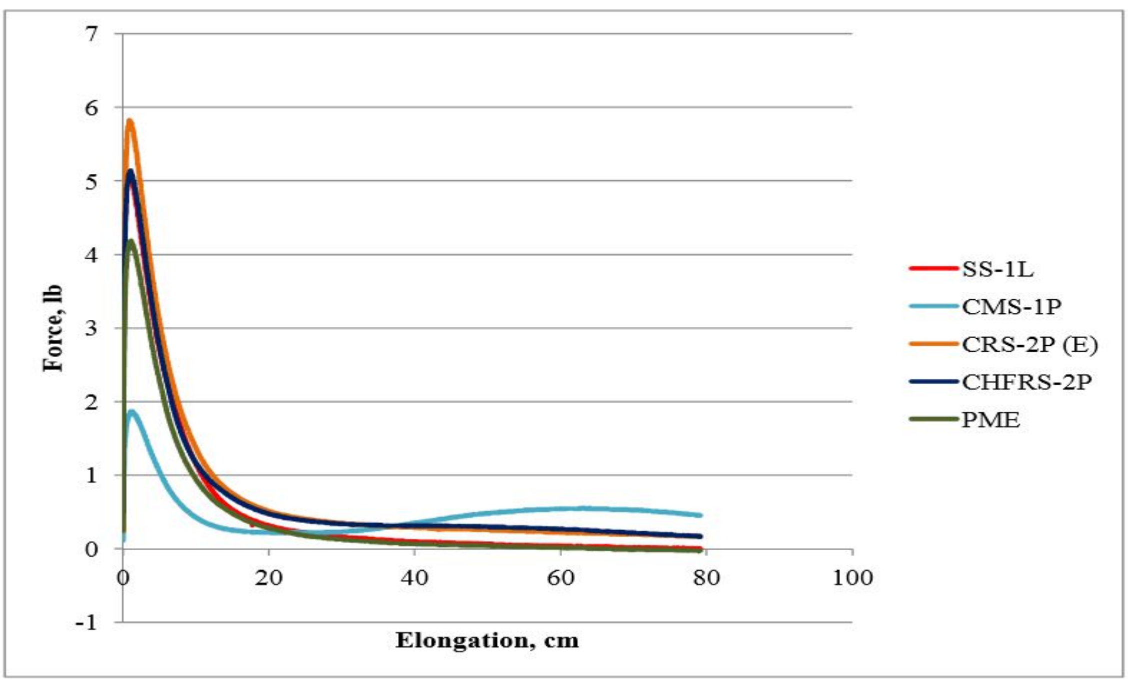

Figure 2-2. Force ductility results of polymer modified asphalt emulsion [13]

2.1.3 Overview on the polymer modified asphalt's characterization methods

Relating the polymer modified asphalt binder's proprieties to its molecular structure has become increasingly advocated. Simple shear is the most common method that has been used to generate most of the material's deformation. Characterizing the polymer's extensional flow behavior has historically been quite difficult because the deformations experienced by polymers during processing are both rapid and large [2]. Therefore, shear rheometers failed to differentiate between certain polymer's micro-structure features. One of the attempts to replace the simple shear methods was by the United States Federal Highway Administration when they proposed to replace AASHTO M 320-05 high temperature specifications and parameters, by the multi-stress creep recovery [15]. In NCHRP Project 9-10 [14], it was reported that linear binder tests ($G^*/\sin\delta$) which are performed in the LVE (linear visco-elastic) region such as high temperature tests of the current PG System do not correlate with high temperature mixture failure such as rutting unless the binder is a viscous fluid in those temperatures.

Therefore, to address mix failure accurately, non-linear binder properties should be evaluated. Multiple Stress Creep Recovery MSCR testing (AASHTO TP70) and the specifications (ASHTO MP19) were developed to describe binder properties in the non-linear range. The MSCR consists of a multiple stress-creep recovery. In its current form, it consists of 10 cycles of each stress level of 0.41 and 3.2 kPa; each cycle consists of 1 s of creep loading followed by 9 s recovery period [15]. There are two crucial parameters of the MSCR test: 1-The temperature of the test and 2-The applied shear stress [15]. It is now believed that MSCR based AASHTO MP19 provides asphalt binder specifications blind to modifications. Furthermore, some studies (NCHRP Project 9-10) do show that for some modifications, MSCR based high temperature grading is not significantly different than AASHTO M320. A new parameter Jnr has been developed, which is currently considered as a replacement for the parameter $G^*/\sin\delta$ at high temperatures. Jnr is the average of the non-recovered strain in every 10 cycles group over the applied stress appropriate for the group. However, when relating Jnr to the pavement rutting through the wheel tracking test results, the correlation between Jnr and the rutting depth exist just in the high stress levels of the MSCR test. As reported by D'Angelo [2009a, 2009b], the linear viscoelastic description of the asphalt is not applicable when MSCR large shear stresses applied to the material.

Extensional flows have a high sensitivity towards the polymer's molecular microstructure, such as the polymer's long-chain branching [2]. Extensional rheometers can be much more accurate describing the polymer characteristics than the other type of rheological measurements mentioned above. In 2004, Sentmanat [2] developed the dual wind-up extensional rheometer "Sentmanat Extensional Rheometer" SER for short that achieved a truly uniform extensional deformation. Additionally, SER invests the fiber wind-up technique in applying the true strain rate to the specimen during the uniaxial extensional experiment. Furthermore, this fixture can convert a conventional rotational rheometer host system into a universal testing station capable of performing extensional melt rheology experiments, all within the controlled environment of the host system's environmental chamber. To this end, this study has been initiated to replace AASHTO T300 with an extensional deformation test using SER.

2.2 Advantages of Using SER for Characterization of Polymer in Asphaltic Materials Replacing Force Ductility Tests

- The SER fixture can be accommodated in currently used commercially available DSR models and will therefore replace the force ductilimeter with DSR.
- Less than 1 gm of materials is needed for the test.
- SER results reflect the material properties response.
- More four samples can be tested in 1 hour. The SER will provide Hencky strain rate, Elongation Viscosity, and it is more mechanistic.
- Most importantly, SER identifies polymer network (branching) through strain hardening measurements.

2.3 Description of the SER

As shown in Figure 2-1 and described in detail by Sentmanat [2], SER consists of a paired master, and slave wind-up drums mounted on bearing housed within a chassis, and mechanically coupled via termeshing gears. The rotational motion of the rheometer spindle drives the rotation of the drive shaft which results in the rotation of the master drum, and an equal opposite rotation of the slave drum, which causes the wound up of the two ends of the sample “secured by the clamps to the drums” onto the drums, rustling the sample stretched over an unsupported length, $L_{\circ}$.

For a constant drive shaft rotational rate, Ω, equal dimension wind-up drums R, and fixed unsupported length of the sample$L_{\circ}$, the applied Hencky strain rate to the sample can be expressed as [2]:

$$\varepsilon_H = \frac{2\Omega R}{L_{\circ}}. \qquad \textbf{Eq.2.1}$$

The resistance of the sample to stretch in both drums, torque T, is measured by the torque transducer attached to the fixture which can be expressed as [2]:

$$T(t) = 2RF(t). \quad \textbf{Eq.2.2}$$

For a constant strain rate experiment, the instantaneous cross-sectional area A(t) can be expressed as [2]:

$$\mathrm{A(t)} = A_0 \exp\left[-\boldsymbol{\varepsilon_H} t\right]. \quad \textbf{Eq.2.3}$$

For a constant strain rate, the tensile stress function $\eta_E{}^{+}(t)$, can be expressed as [2]:

$$\eta_E{}^{+}(t) = \frac{F(t)}{\varepsilon_H A(t)}. \quad \textbf{Eq.2.4}$$

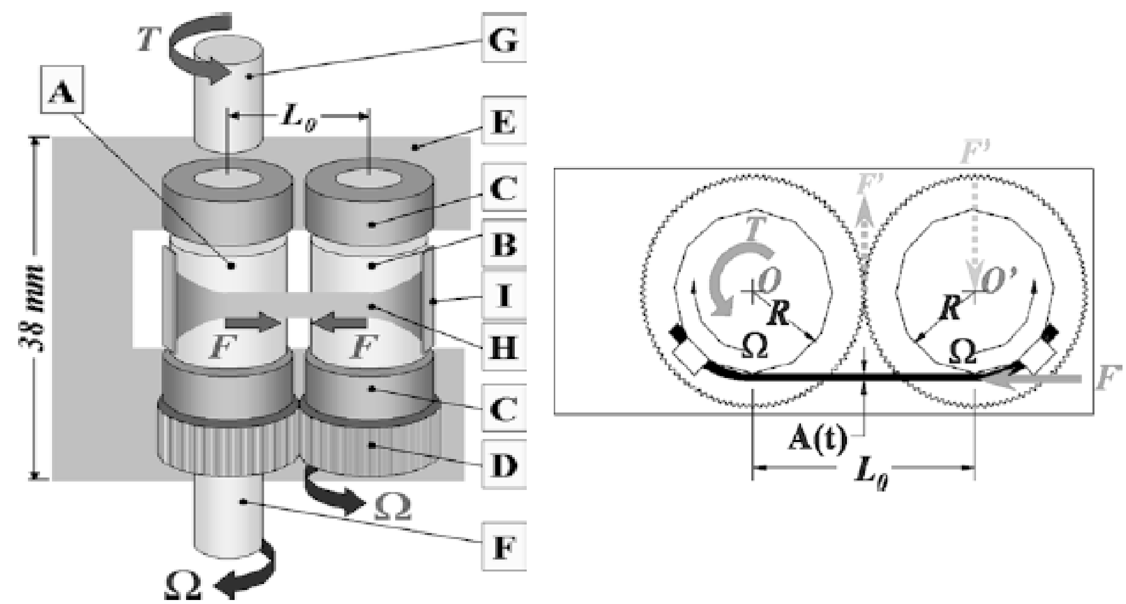

(a) (b)

Figure 2-3. a: Side view of the Sentmanat Extensional Rheometer (SER) during Operation. Inside Squares: A. Master Drum, B. Slave Drum, C. Bearings, D. Intermeshing Gears, E. Chassis, F. Drive Shaft, G. Torque Shaft, H. Sample, I. Securing Clamps. **b:** Elevation the SER during an experiment. Symbols: L_0 Unsupported Length, Ω Drive Shaft Rotation Rate, T Torque, F Tangential Force

2.4 Validation of SER Results with Previous Extensional Rheology Results

2.4.1 Extension experiment with commercial Poly-Isobutylene (PIB) (BASF Oppanol (B15) (2)

Extensional experiments were performed at 23°C. The poly-isobutylene macular characteristics are as follows: macular number (M_n) of 44,000 and macular weight (M_w) of 88,000. The same material has been tested through uniaxial extension experiments by other independent laboratories [16, 17]. Figure 2-4 shows the tensile stress curves results from the SER superposed with the stress growth results reported from the other laboratories. The agreement between the SER data and the data reported in the other studies can be observed through a variety of extensional rheometer technologies.

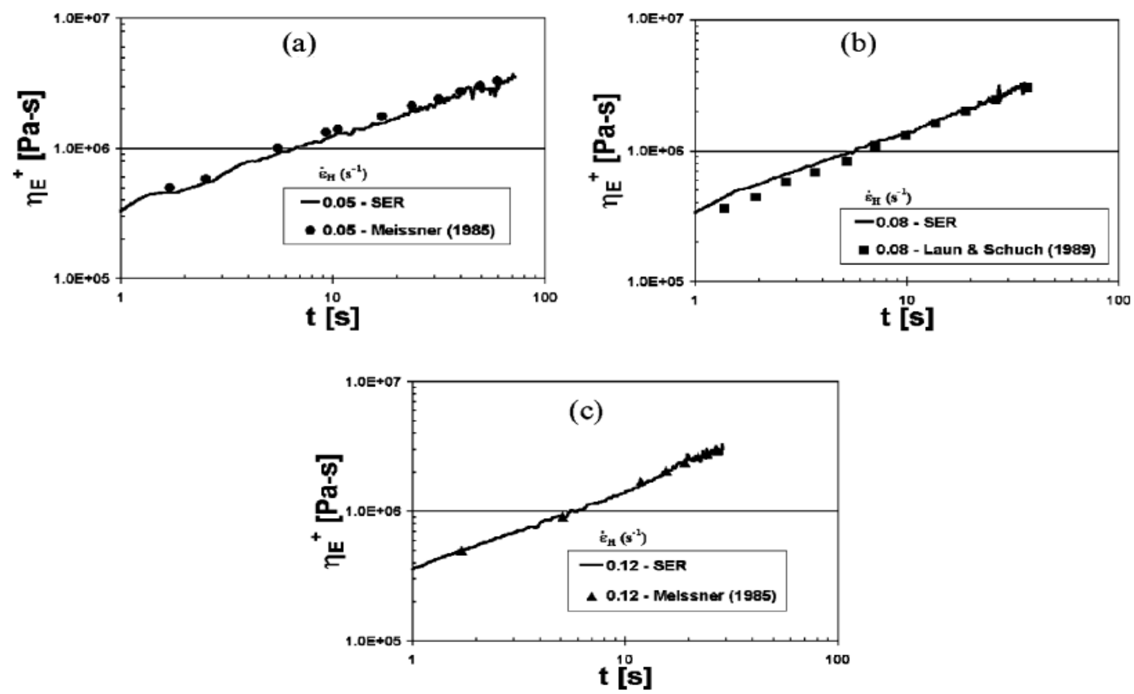

Figure 2-4. Comparison of tensile stress growth curves data from SER and another extensional rheometer technology [3]

2.4.2 Extensional experiment with natural rubber [2]

Due to the extreme resilient of uncured natural rubber, it can be hard to characterize its rheological properties especially at room temperature. Therefore, the linear viscoelastic (LVE) properties of natural rubber can be a challengeable task to obtain by the simple shear method due to the slipping associate with the experiments of simple shear. Even though the relaxation modulus G(t) of the LVE shear stress of natural rubber can be difficult to determine at room temperature without the use of the rheometer fixture sample bonding, it can be easily determined through the step extensional experiment with the SER. Figure 2-5 shows the LVE stress relaxation modulus for natural rubber NR-RSS2 using the SER.

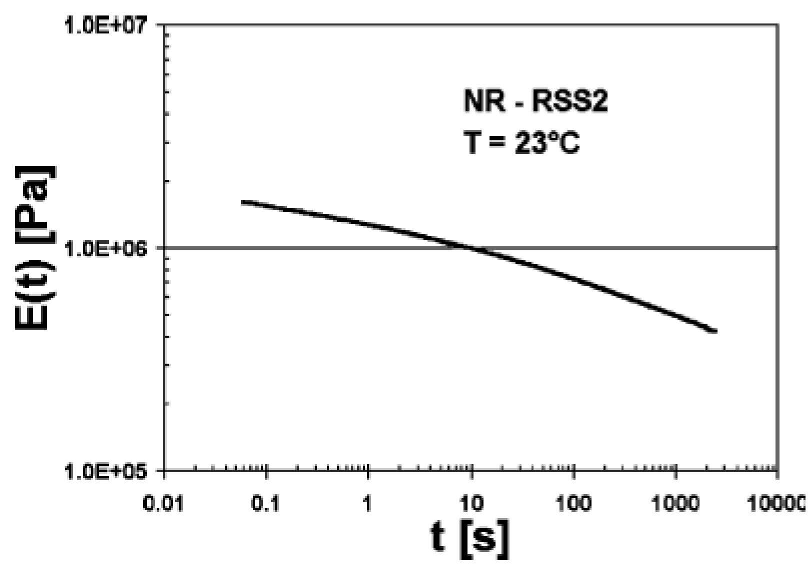

Figure 2-5. Extensional stress relaxation modulus for NR-RSS2 at 23°C [2]

Figure 2-6 indicates tensile stress growth curves plot for uncured NR-RSS2 at room temperature and constant Hencky strain rates ranging from $0.001 s^{-1}$ to $10\ s^{-1}$. Also included in the graph is a LVE stress relaxation modulus data plot from Figure 2-5 integrated with respect to time, which theoretically defines the LVE envelope of tensile stress growth behavior. Note the perfect agreement between the low-strain portion of all five tensile stress growth curves.

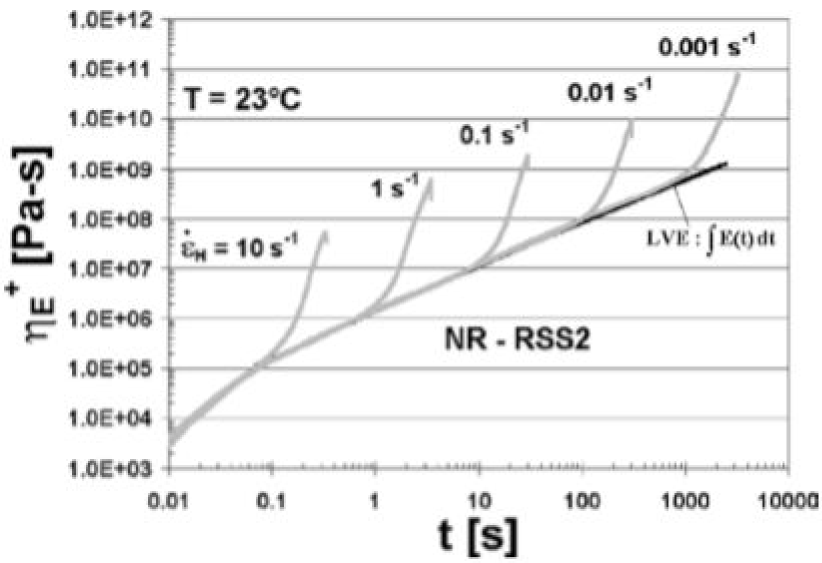

Figure 2-6. Tensile stress growth curves for NR-RSS2 for constant Hencky strain rates ranging from 0.001s + to 10 s^{-1}

2.4.3 Shear rheology of Lupolen 1840H [18]

Figure 2-7 shows the extensional rheology of the transient extensional viscosity function $\eta_E{}^+(\varepsilon_{H,}t)$ for affinity LLDPE. The results were generated by a SER-HV-P01 mounted on Anton Paar MCR501 torsional rheometer. The solid line illustrates the linear viscoelastic envelop $\eta_E{}^+ = 3\eta^+$generated from shear experiment with a cone and plate fixture. The similarity of results between the two methods can be observed.

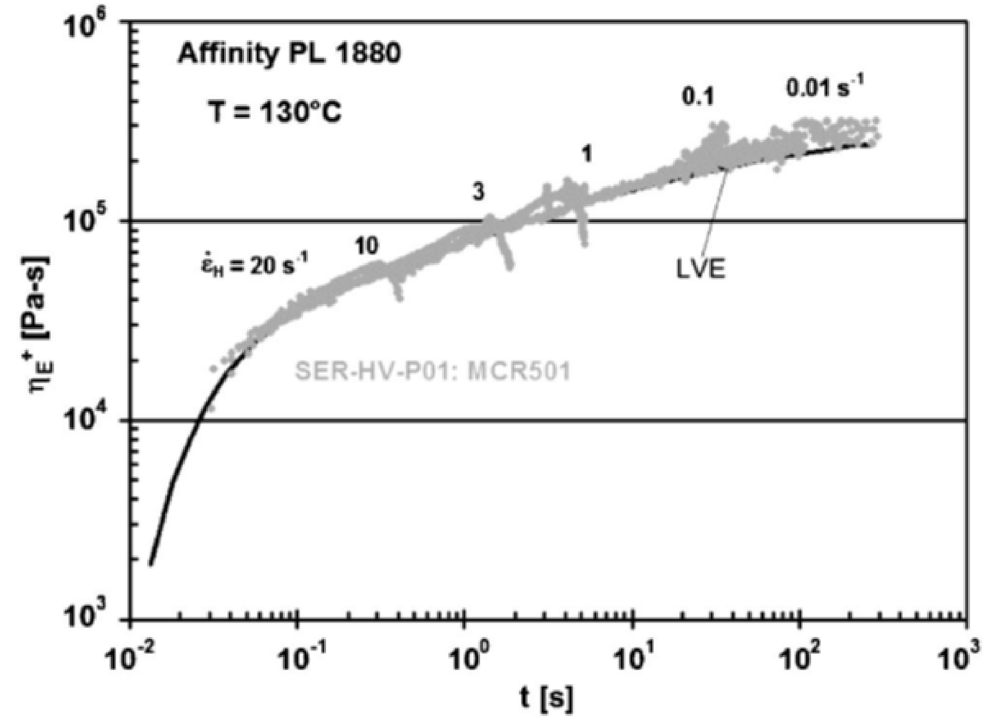

Figure 2-7. Tensile stress growth curves at 130°C for Affinity PL 1880 LLDPE obtained from the SER. Also shown LVE given by $\eta_g^+ = 3\eta^+$ generated by the cone and the plate measurements in start-up steady shear flow

CHAPTER 3

METHODOLOGY

3.1 Introduction

In this study, the applicability of Sentmanat Extensional Rheometer (SER) to accurately detect the second peak elongation force was investigated. The effect of geometry, temperature, and polymer on the elongation force were investigated. Sample preparation and the test procedure were developed for asphalt binders to be tested in the SER.

3.2 Extensional Test Parameters

1. Sample geometry (width, thickness, and area)
2. Test temperature
3. Extensional rate
4. Asphalt binder grade (PG)
5. Existence of polymer

3.3 Selection of Asphalt Binder Grades

Three asphalt binder grades were chosen to be investigated in this study: PG 76-22, PG 64-22 and PG 58-28. PG 76-22 is a polymer modified binder, PG 64-22 and PG 58-28 are neat binders. The main objective of selecting the above-mentioned binder grades is to explore the hypothesis that the SER will detect the second peak elongation force in PG 76-22 but not in PG 64-22 accurately and PG 58-28 due to the polymer's modification.

The secondary objective is to investigate the accuracy of the SER in detecting the elongation force through verifying the principle rule that PG 76-22 should show greater first peak elongation force than PG 64-22, and PG 58-22 should display the least elongation force among the three binders.

3.4 Selection of Geometry

In this study, nine different geometries were chosen to investigate the effect of geometry in the second peak elongation force. Eight geometries were specified during the experimental plan stage. Then, the ninth geometry was added during the experimenting stage to improve the understanding of geometry's effect on the elongation force. The nine geometries are as follows:

1. (W= 5 mm x T= 0.6 mm) A= 3.0 mm^2
2. (W= 7.5 mm x T= 0.4 mm) A = 3.0 mm^2
3. (W= 6 mm x T= 0.6 mm) A= 3.6 mm^2
4. (W= 9 mm x T= 0.4 mm) A= 3.6 mm^2
5. (W= 5 mm x T= 0.83 mm) A= 4.2 mm^2
6. (W= 6 mm x T= 0.83 mm) A= 5.0 mm^2

7. (W= 8 mm x T= 0.72 mm) A= 5.8 mm^2
8. (W= 9 mm x T= 0.72 mm) A= 6.5 mm^2
9. (W= 10 mm x T= 0.83 mm) A= 3.6 mm^2

3.5 Selection of Temperature

In order to recommend the appropriate testing temperature for the newly developed test procedure, 4°C, 10°C and 16°C were chosen to be explored as testing temperatures. No testing temperature above 16°C was chosen because at higher temperature, lower viscosity of asphalt sample causes higher final strain. That exceeds the maximum recommended Hencky strain specified by the SER manufacturer, which is equal to four per drum.

3.6 Experimental Plan

As mentioned earlier, PG 76-22, PG 64-22, and PG 58-28 were used in this study to verify SER results' reproducibility. One hundred twenty-two extensional deformation tests were performed as shown in Table 3-1. Ninety-five tests out of the total 122 were performed in PG 76-22 polymer modified binder to investigate the capability of the SER to accurately detect the second peak elongation force. Eighty-three tests out of the 95 were performed at 4°C with nine different geometries to analyze the effect of the width and the thickness on the elongation force. The nine geometries were chosen according to the following categories:

1. Same initial areas with different width and thickness
2. Different initial areas with different width and different thickness
3. Different initial areas with different width but same thickness
4. Different initial areas with different thickness but same width

Ten replicates of each of the eight geometries were tested, then the ninth geometry was added with three replicates for more detailed investigation on the effect of width and thickness. Six samples of PG 76-22 were tested at 10°C using two geometries (three tests each). Six more samples were tested at 16°C using two geometries (three tests each) to investigate the temperature effect on the extensional deformation and its parameters.

Fifteen PG 64-22 samples were tested at 4°C with five different geometries and every geometry was tested three times to analyze the differences in elongation force behavior between modified and neat binders. Twelve PG 58-28 samples were prepared and tested at 4°C using four different geometries with three replicates for each geometry.

Table 3-1. Summary of Materials and Experimental Plan

<table>
<tr><th colspan="3">Sample Geometry</th><th rowspan="2">No. of Samples</th><th rowspan="2">Temperature</th><th rowspan="2">Binder</th></tr>
<tr><th>W mm (+/- 0.25)</th><th>T mm (+/- 0.06)</th><th>A mm^2 (+/- 0.39)</th></tr>
<tr><td>5</td><td>0.6</td><td>3.0</td><td>10</td><td rowspan="6">4°C</td><td rowspan="13">PG 76-22</td></tr>
<tr><td>7.5</td><td>0.4</td><td>3.0</td><td>10</td></tr>
<tr><td>6</td><td>0.6</td><td>3.6</td><td>10</td></tr>
<tr><td>9</td><td>0.4</td><td>3.6</td><td>10</td></tr>
<tr><td>5</td><td>0.83</td><td>4.2</td><td>10</td></tr>
<tr><td>6</td><td>0.83</td><td>5.0</td><td>10</td></tr>
<tr><td rowspan="3">8</td><td rowspan="3">0.72</td><td rowspan="3">5.8</td><td>10</td><td>4°C</td></tr>
<tr><td>3</td><td>10°C</td></tr>
<tr><td>3</td><td>16°C</td></tr>
<tr><td rowspan="3">9</td><td rowspan="3">0.72</td><td rowspan="3">6.5</td><td>10</td><td>4°C</td></tr>
<tr><td rowspan="12">3</td><td>10°C</td></tr>
<tr><td>16°C</td></tr>
<tr><td>10</td><td>0.83</td><td>6.5</td><td rowspan="10">4°C</td></tr>
<tr><td rowspan="2">7.5</td><td rowspan="2">0.4</td><td rowspan="2">3.0</td><td>64-22</td></tr>
<tr><td>58-28</td></tr>
<tr><td rowspan="2">9</td><td rowspan="2">0.72</td><td rowspan="2">6.5</td><td>64-22</td></tr>
<tr><td>58-28</td></tr>
<tr><td rowspan="2">6</td><td rowspan="2">0.83</td><td rowspan="2">5</td><td>64-22</td></tr>
<tr><td>58-28</td></tr>
<tr><td>8</td><td>0.72</td><td>5.8</td><td>64-22</td></tr>
<tr><td>9</td><td>0.4</td><td>3.6</td><td>64-22</td></tr>
<tr><td>6</td><td>0.6</td><td>3.6</td><td>58-28</td></tr>
</table>

3.7 Sample Preparation

PG 76-22, PG 64-22 and PG 58-28 Samples were prepared using the following steps:

3.7.1 Preparing the binder

a. The binder in the main can was heated in the oven at 150°C for 45 minutes.

b. Around 100 g of binder was placed in each of 5 different small metal cans to reduce the aging that occurs due to the repeated heating process as shown in Figure 3-1.

c. The binder in one of the small cans was heated in the oven at 150°C for around 20 minutes until it liquified.

Figure 3-1. The binder placed into the small can

3.7.2 Controlling the sample thickness

a. The binder was poured in a 1 in diameter silicon mold to control the amount of binder needed as shown in Figure 3-2. Silicon was selected to be the molding material because asphalt does not adhere to silicon. The size of the mold was selected to be 1-in in diameter to simplify the thickness control process by reducing the amount of binder under the loads.

b. The liquid binder that was poured in the silicon mold was left in room temperature for 15 to 20 minutes until it cooled down, so it could be removed from the silicon mold as shown in Figure 3-3.

c. In order to control the sample thickness, the sample was placed onto a silicon mat between two stainless steel plates with the exact desired thickness as shown in Figure 3-4. After few trials, 1.7 in was found to be the suitable spacing dimension between the stainless-steel plates to allow the binder to spread to a uniform thickness.

d. To block the adhesion between the asphalt sample and the glass plate from the next step, a minimum 2 in x 2 in silicon mat was placed over the sample overlapping with the stainless-steel plate as shown in Figure 3-5. The overlapping is to ensure that the silicon mat will not slip from the stainless-steel plates and affect the sample's thickness control process. The other dimension of the silicon mat is to ensure that the sample was covered after spreading.

e. In order to ensure a uniform distribution of the loads over the sample, a 2 in x 2 in thick glass plate was placed over the silicon mat, overlapping with the stainless-steel plates as shown in Figure 3-6.
f. Twenty lbs of loads were placed over the thick glass plate. For the polymer modified binders' the loads were kept over the sample for 18 to 24 hours as shown in Figure 3-7. Several trials of 8, 12 and 14 hours were made but the sample's thickness increased by around 1 mm after removing the loads due to the increasing of the softening point as a result of polymer modification, which to increase its elastic properties [19-23]. As for the non-modified binders, the loads were kept over the sample for 10 to 12 hours.
g. The loads were removed along with the glass plate and the silicon mat as shown in Figure 3-8.

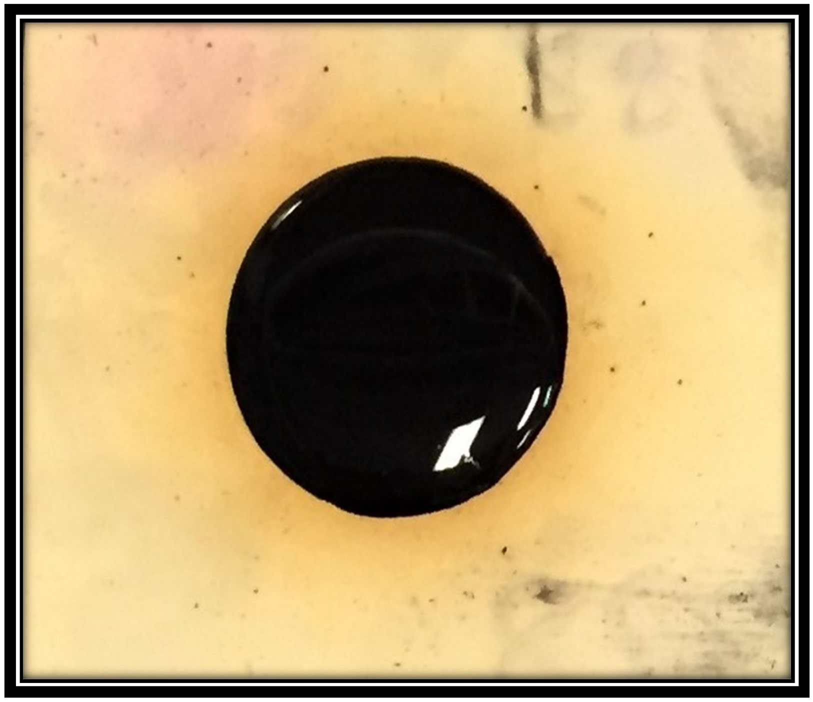

Figure 3-2. The binder poured into the silicon mold

Figure 3-3. The binder was removed from the silicon mold

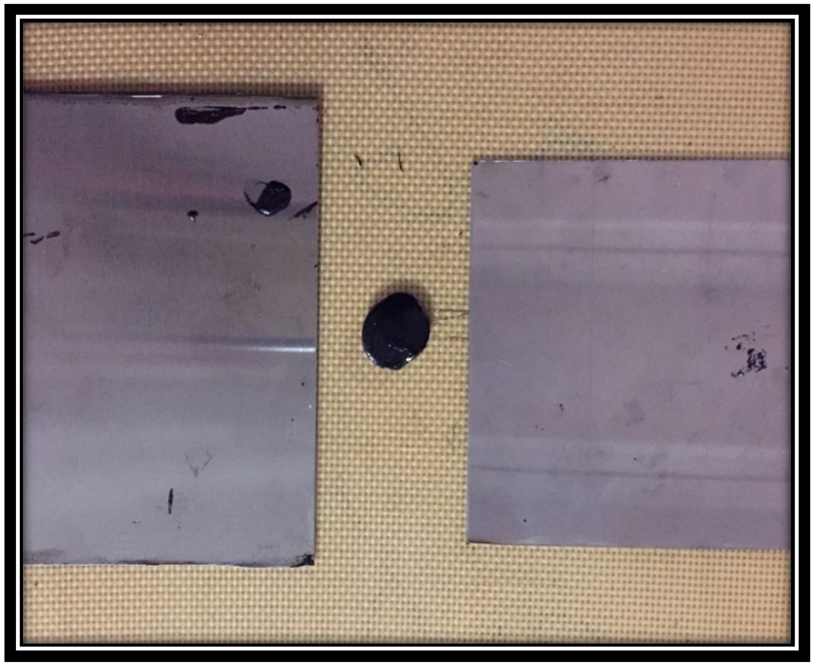

Figure 3-4. Binder placed between two stainless steel plates

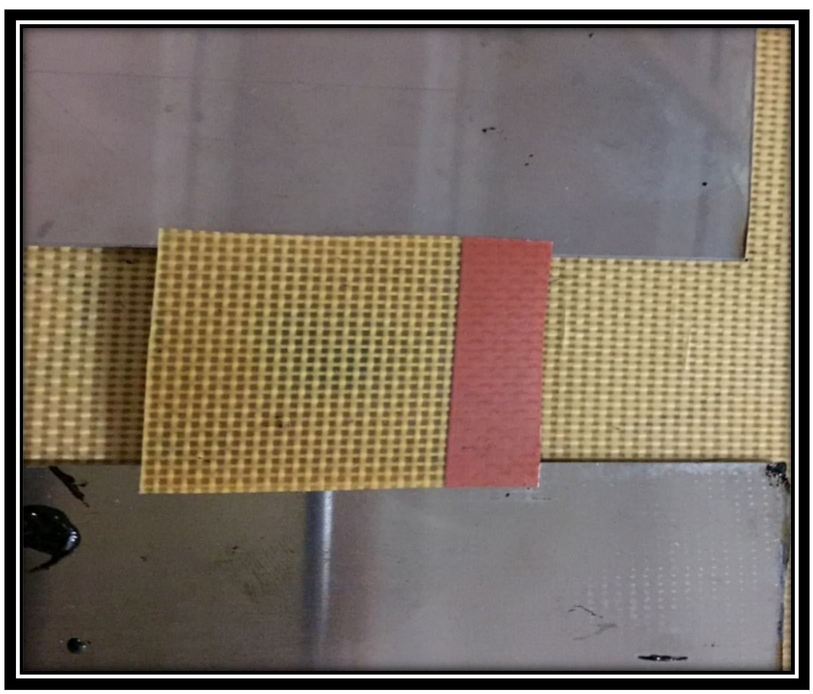

Figure 3-5. Silicon mat placed above the binder

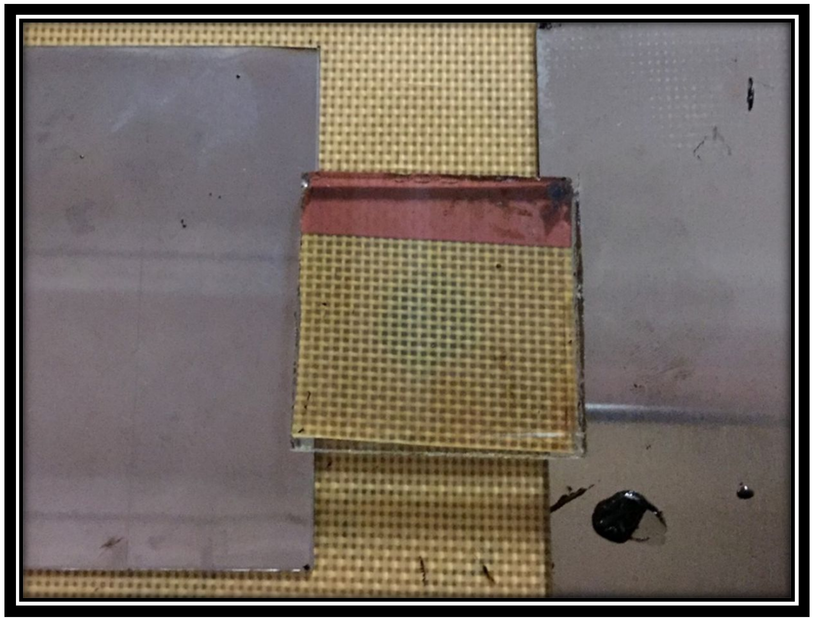

Figure 3-6. The thick glass placed over the silicon mat

Figure 3-7. The loads placed over the thick glass

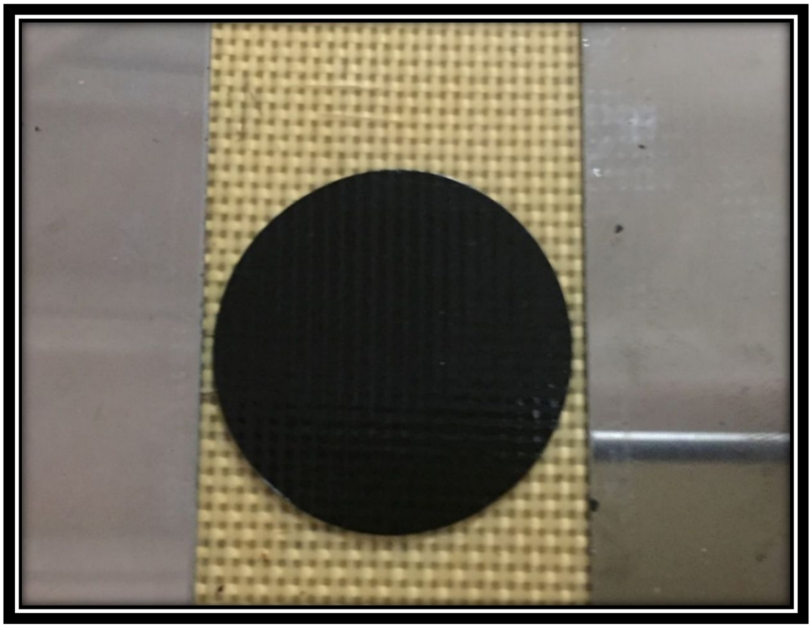

Figure 3-8. The binder's shape after removing the loads

3.7.3 Cutting the sample to the desired dimensions

a. The sample was placed in a refrigerator at 5°C for 1 to 2 minutes.

b. The sample was removed carefully from the big silicon mat to a smaller 4 in x 4 in silicon mat.

c. The sample was placed in a refrigerator at 5°C for 2 to 3 minutes. If the sample is left at 5°C for longer than 2 to 3 minutes the sample will crack during the cutting process as shown in Figure 3-9. If the sample is left at 5°C for less than 2 to 3 minutes, the sample will stick to the metal edge during the cutting process as shown in Figure 3-10.

d. Immediately after removing the sample from the refrigerator, the sample was cut with a sharp metal edge to the desired dimensions as shown in Figure 3-11 and Figure 3-12. The sample was measured by a slide caliper to ensure the desired dimensions as shown in Figure 3-13.

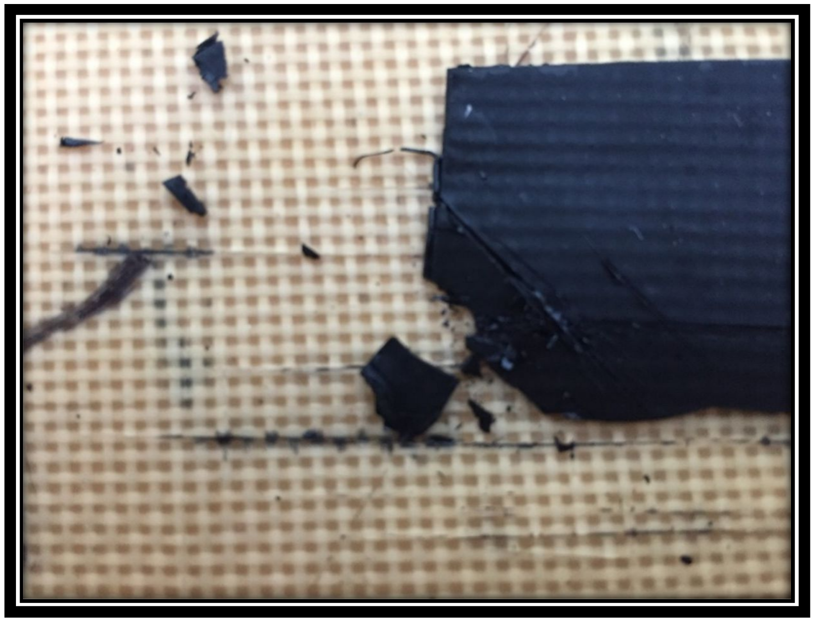

Figure 3-9. Cracked during the cutting process due to a long cooling period

Figure 3-10. Sticking to the metal edge due to a short cooling period

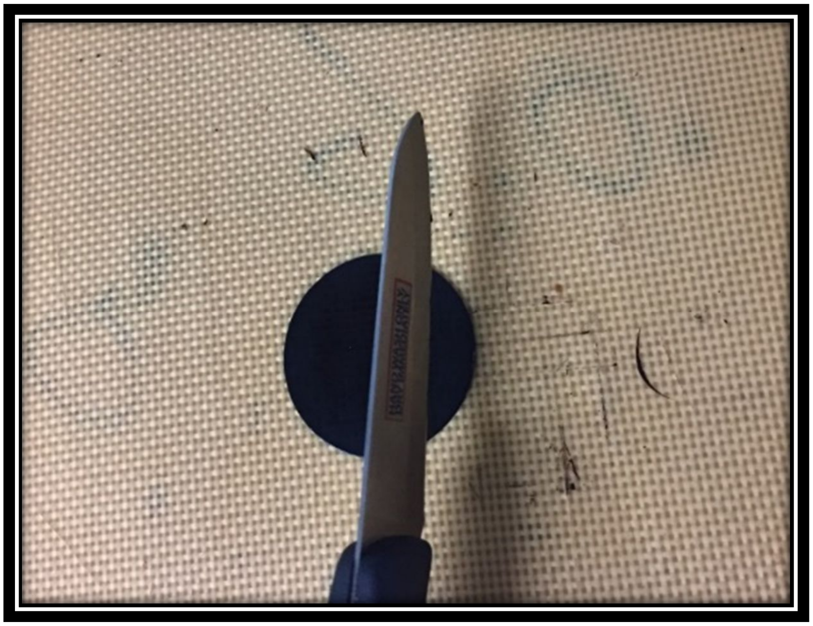

Figure 3-11. Cutting the binder to the desired length

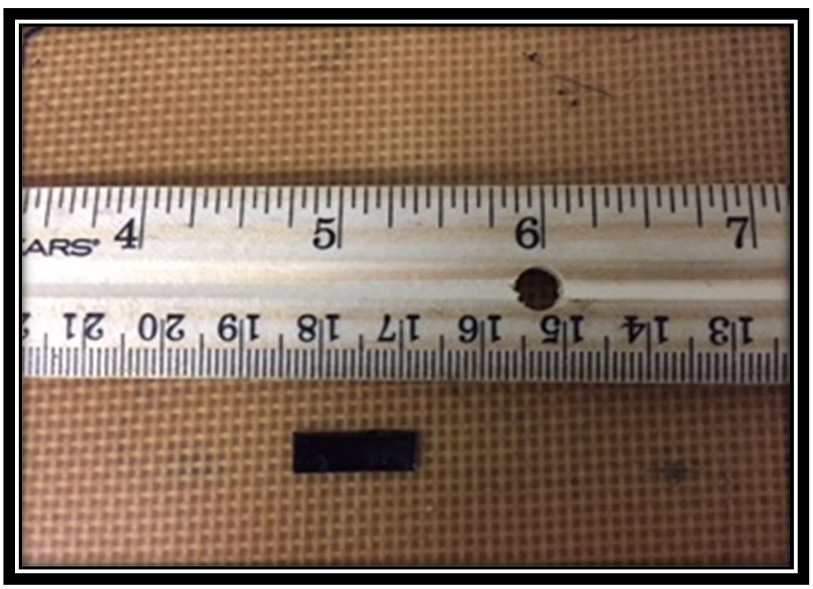

Figure 3-12. Sample with desired dimensions

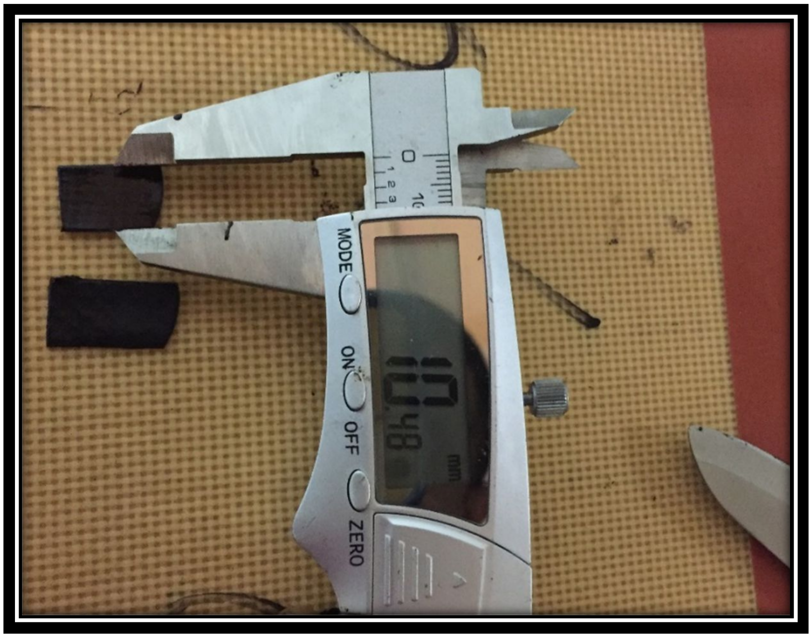

Figure 3-13. Sample with desired dimensions

3.8 Test Procedure

Measurements were performed on a Universal Testing Platform model SER3-G, manufactured by Xpansion Instruments LLC. Connected to DSR model AR2000 Ex with an environmental chamber.

1. Before fixing the SER to the DSR, the smart swap and the SER bracket should be placed into the DSR as shown in Figures 3-14 and 3-15.
2. As shown in Figure 3-16, SER consists of paired master and slave wind-up drums connected to a drive shaft. Rotation of the drive shaft results in the rotation of the master drum and an equal and opposite rotation of the slave drum, which results in the stretching of the sample.

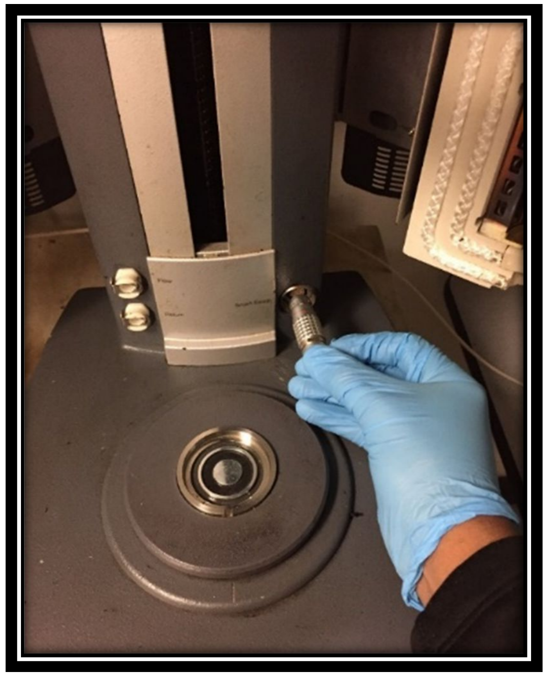

Figure 3-14. Inserting the smart swap

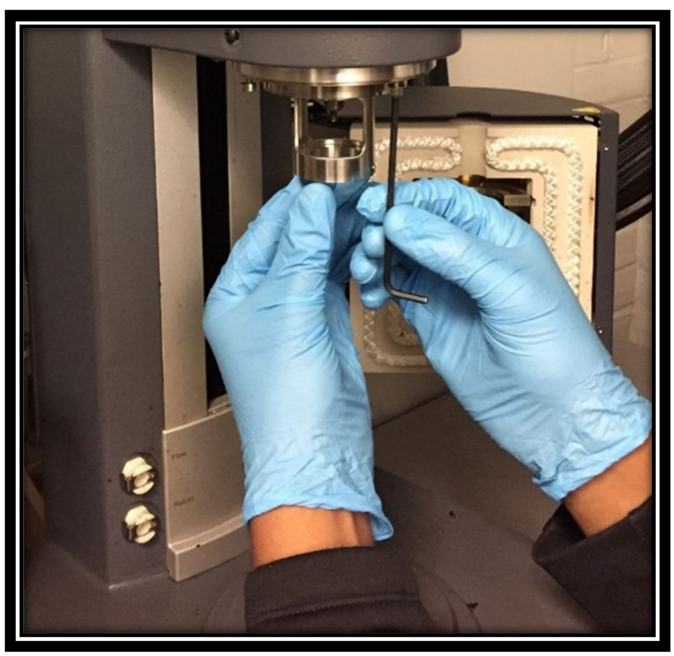

Figure 3-15. Fixing the SER bracket

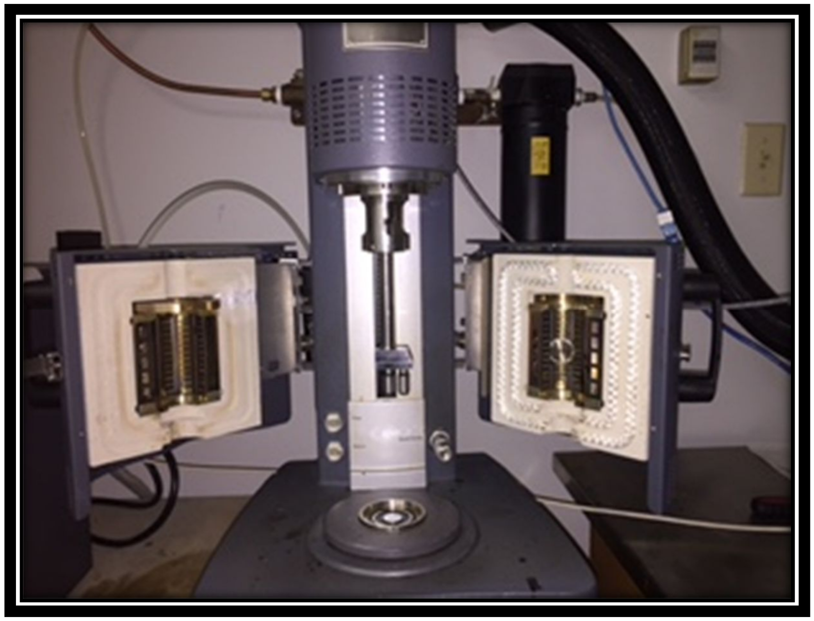

Figure 3-16. The SER fixture prior to the sample loading

3. The sample was loaded and secured at each end by clamps as shown in Figures 3-17 and 3-18, and then the chamber was closed.

Figure 3-17. SER fixture after loading the sample

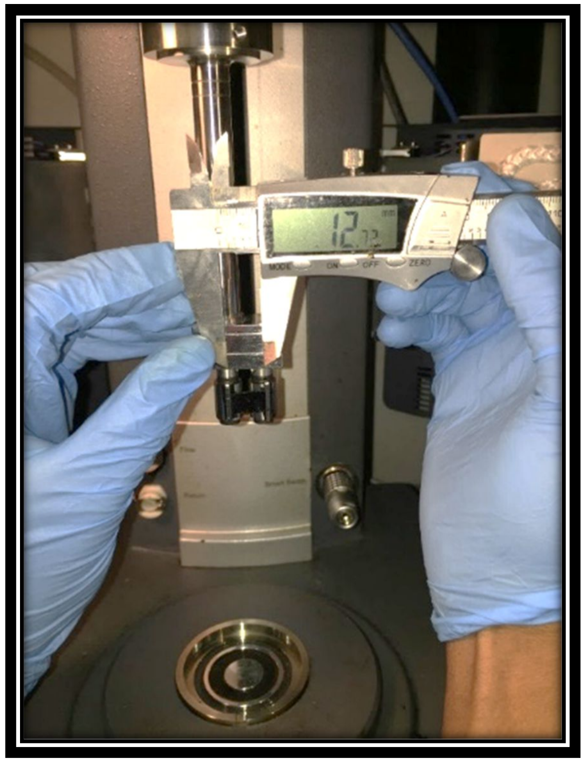

Figure 3-18. Length of the sample 12.75 mm

4. At the beginning, samples slipped several times during the tests because of the high stresses resulting from the solid tensile testing as shown in Figure 3-19.
5. Therefore, an ultra-thin double-sided adhesion tape with a thickness of 0.1 mm was placed into the drum prior to the sample loading to prevent the sample from slipping as shown in Figures 3-20 and 3-21.

Figure 3-19. Clamps kicked out due to the hard stresses

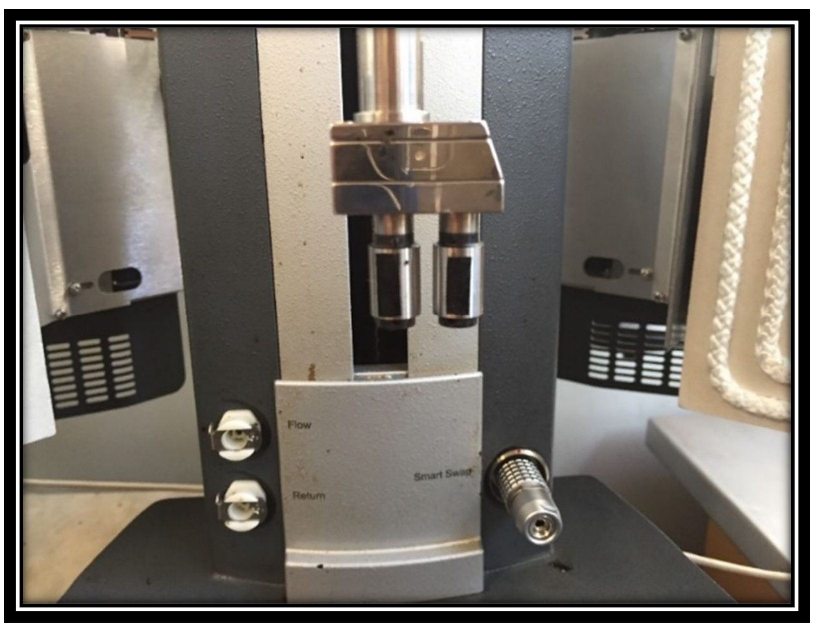

Figure 3-20. Double-sided adhesion tape fixed to the drums

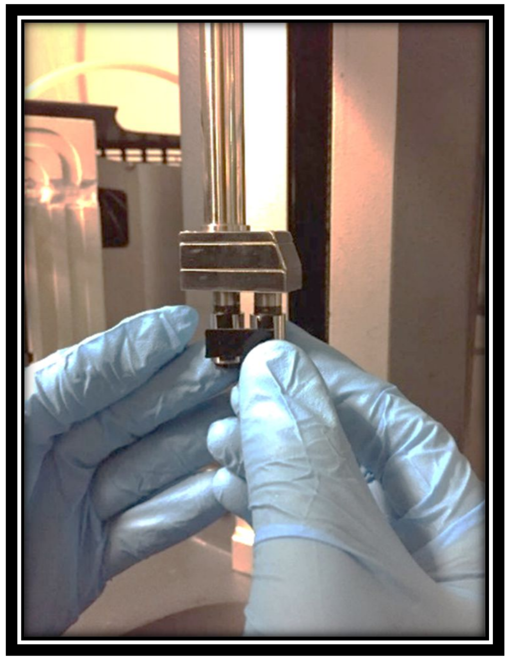

Figure 3-21. Loading the sample post to the double-side adhesion tape

6. As for the test parameters, as shown in Figure 3-22 the environmental control was set to 4ºC, the soak time was 600 s, and the wait for temperature option was activated to ensure temperature equilibrium, Figure 3-23 shows the DSR control panel. The solid density was set to 1.0 g/cm^3, and the melt density was set to 0.95 g/cm^3. Final strain was 3.4 rad, with a strain rate of 0.1 s^{-1}. For more accurate measurements, the fast sampling option was activated.

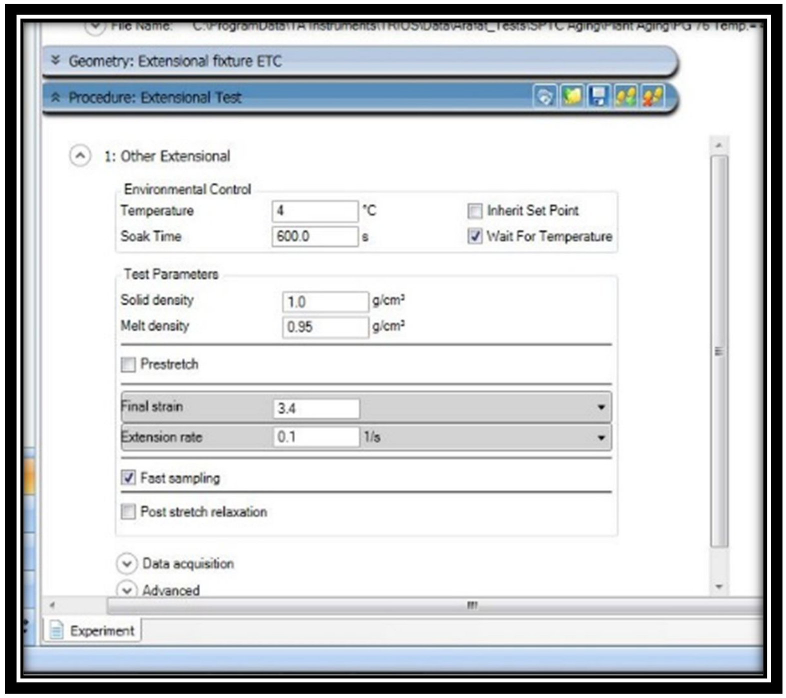

Figure 3-22. Software screenshot shows the test Parameter

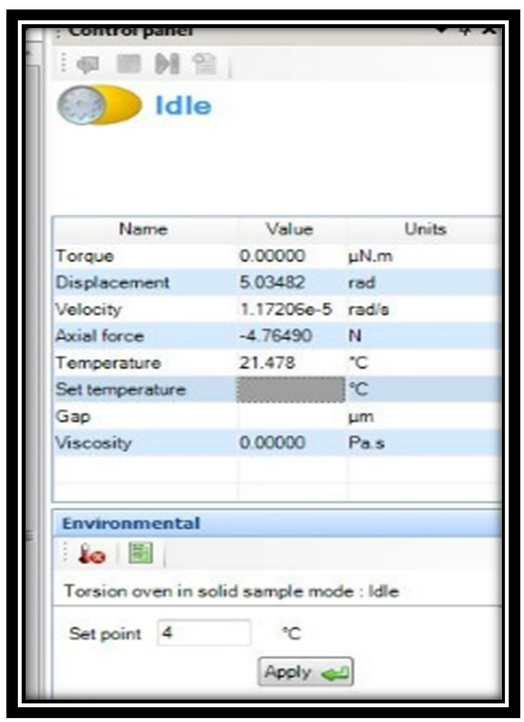

Figure 3-23. Software screenshot shows the DSR control panel

7. Figure 3-24 shows the sample during the extensional deformation. Figure 3-25 shows the sample at the end of the test. Upon completion of the test, the sample was removed immediately, and the drums were carefully cleaned with a soft wipe, and paint thinner was used as needed.

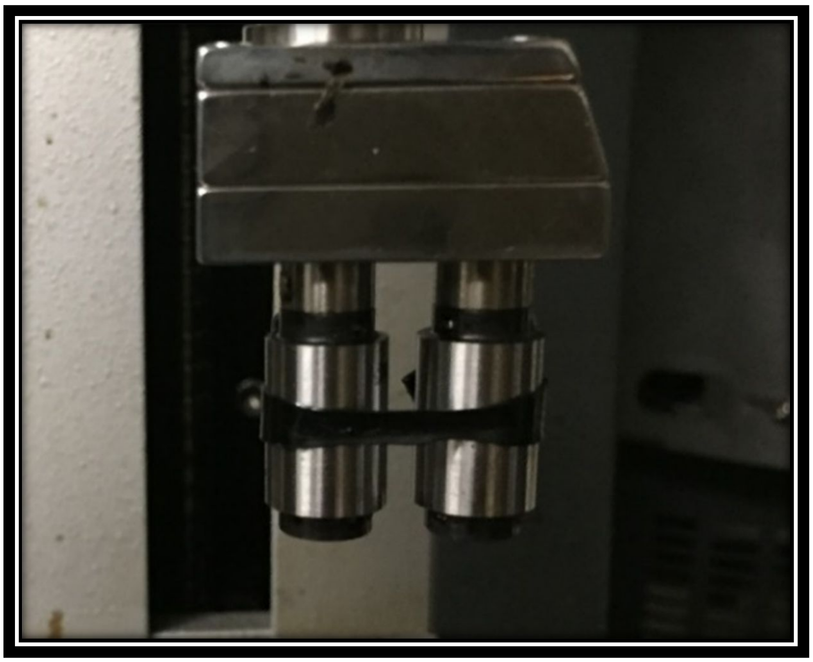

Figure 3-24. Sample during the extensional deformation test

Figure 3-25. Sample after the end of the test

CHAPTER 4

RESULTS AND DISCUSSIONS

4.1 Simulating Second and First Peak Elongation Force

4.1.1 Introduction

Polymer modified binder is a non-homogeneous material [24]. The first part of the "elongation force vs. time" graph reflects the asphalt yielding due to the tensile force, so it is primarily due to the base asphalt's behavior. The second part of the curve describes polymer behavior, so it depends on the polymer modification type and level of the [25].

One of the major objectives of this study was to simulate second peak elongation force of asphalt modified binders using Sentmanat Extensional Rheometer (SER).

In pursuit of this objective, PG 76-22, PG 64-22, and PG 58-28 samples were prepared to be tested in the SER according to the procedure described earlier. The results showed that SER can accurately detect the polymer effect in modified asphalt binder through simulating the second peak elongation force.

4.1.2 Simulating second peak elongation force

Three types of asphalt binders with three different geometries were illustrated in Figures 4.1 to 4.9. Binders were PG76-22, PG 64-22 and PG 58-22. Every binder was tested with three different geometries: W = 9 mm x T = 0.72 mm, W = 7.5 mm x T = 0.4 mm, and W = 6 mm x T = 0.83 mm.

It can be observed from Figures 4.1 through Figure 4.9 that, PG 76-22 showed second peak elongation force for all the above mentioned three geometries. Comparatively, no second peak elongation force has been detected for PG 64-22 and PG 58-22. This demonstrates the above-mentioned statement: the second part of the Elongation Force vs Step Time curve describes the polymer's behavior.

The general elongation force trend of PG 76-22 can be described as follow: Elongation force sharply increased immediately after starting the test until it reached the first peak elongation force F_1. Then it started to decrease gradually for less than 2N until it reached the point of inflection F_m. As mentioned in Section 4.1.1, polymer modified binders are non-homogeneous material. Therefore, at the point of inflection, elongation force started to rise again due to` the polymer yielding behavior until it reached the second peak elongation force. Immediately after that, the binder sample reached the final strain or the failure point 0 N, after which it can be described as sharp failure criteria. The time between the second peak elongation force and the final strain point is less than five seconds for all three geometries.

4.1.3 Simulating first peak elongation force

As mentioned in Section 4.1.3, the first part of the Elongation Force vs Step Time curve reflects the asphalt yielding due to the tensile force. Hence, to evaluate the asphalt binder performance, the first peak elongation force is an important parameter to analyze.

It can be observed from Figures 4.1 to 4.9 that PG 64-22 showed less first peak elongation force than PG 76-22, and PG 58-28 showed less first peak elongation force than PG 64-22. This was expected because PG 76-22 has the highest stiffness among the three binders, and PG 58-28 has the lowest stiffness.

As for the failing criteria of PG 64-22 and PG 58-28, they are more ductile than PG 76-22. In the cases of PG 64-22 and PG 58-22, the time between the highest peak elongation force, which the first peak elongation force, and the final strain point is around 25 seconds. This variance of failing criteria is because of the polymer impact on the elongation force curve characteristics. The polymer inverts the elongation force at the point of inflection as shown in Figures 4.1, 4.4, and 4.7.

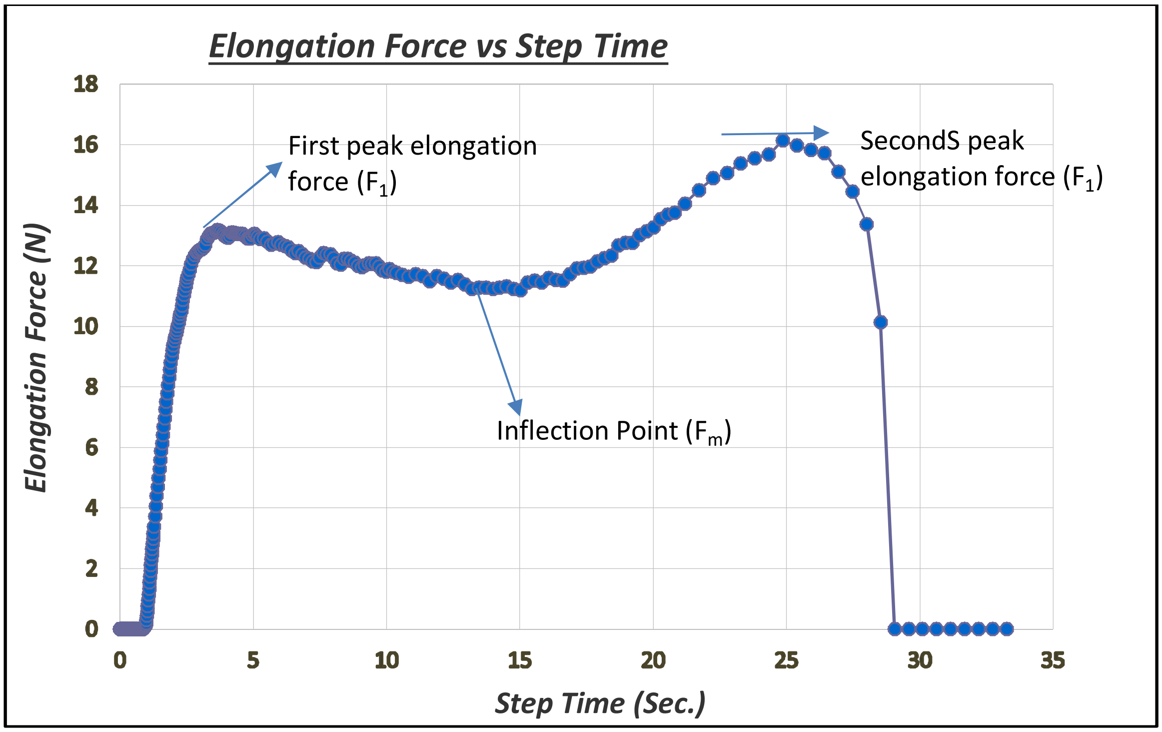

Figure 4-1. Elongation Force vs. Step Time for PG 76-22 geometry of 9.0 mm x 0.72 mm

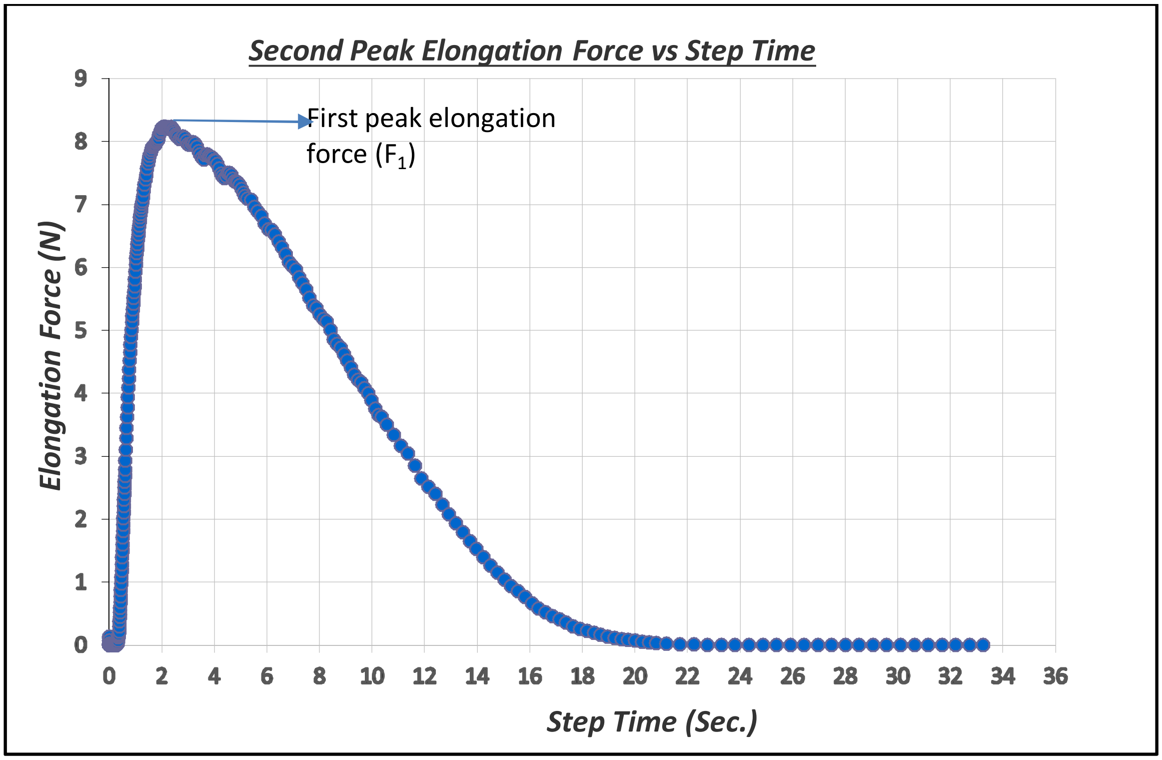

Figure 4-2. Elongation Force vs. Step Time for PG 64-22 geometry of 9.0 mm x 0.72 mm

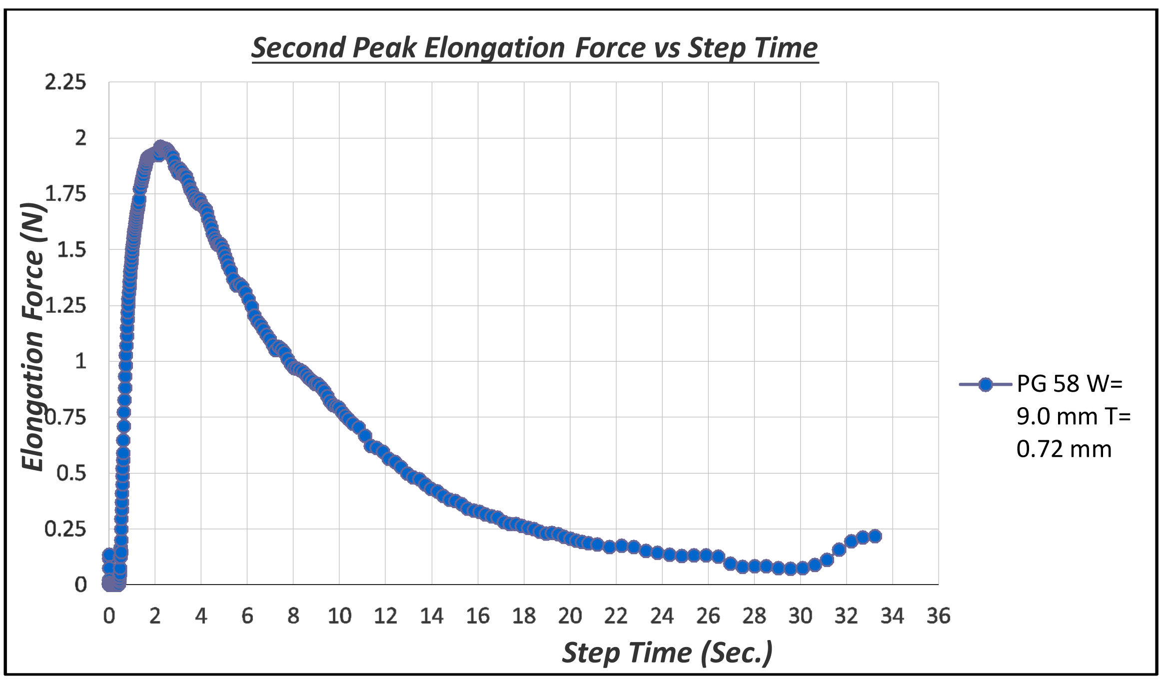

Figure 4-3. Elongation Force vs. Step Time for PG 58-28 geometry of 9.0 mm x 0.72 mm

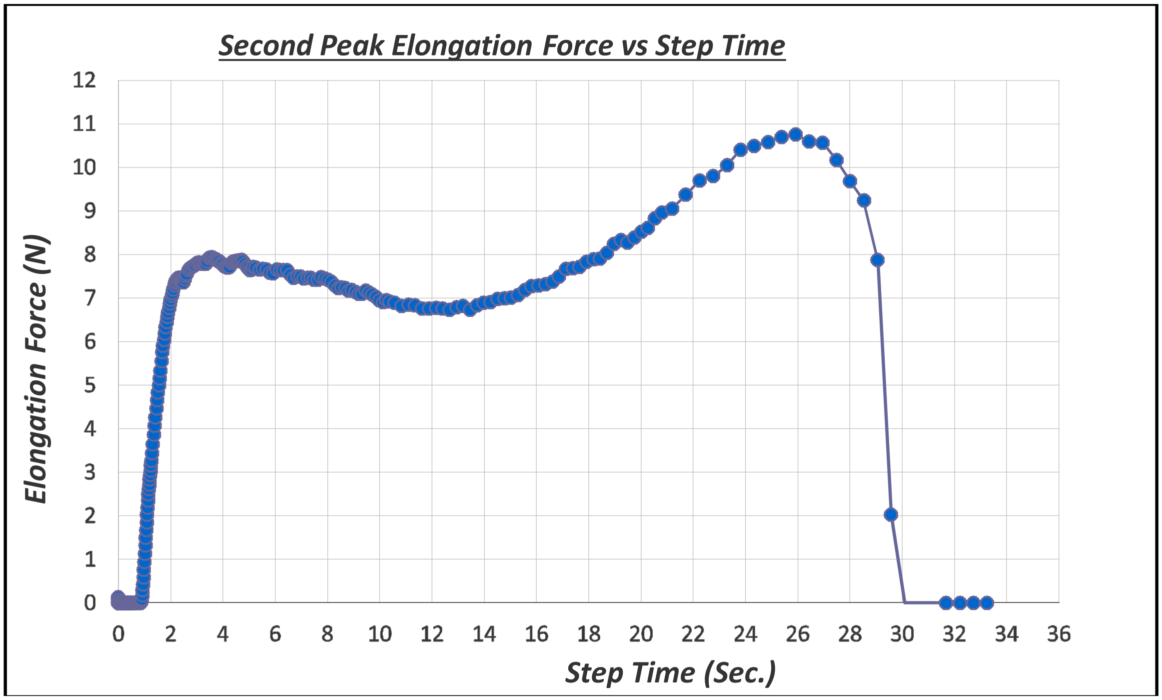

Figure 4-4. Elongation Force vs. Step Time for PG 76-22 geometry of 6.0 mm x 0.83 mm

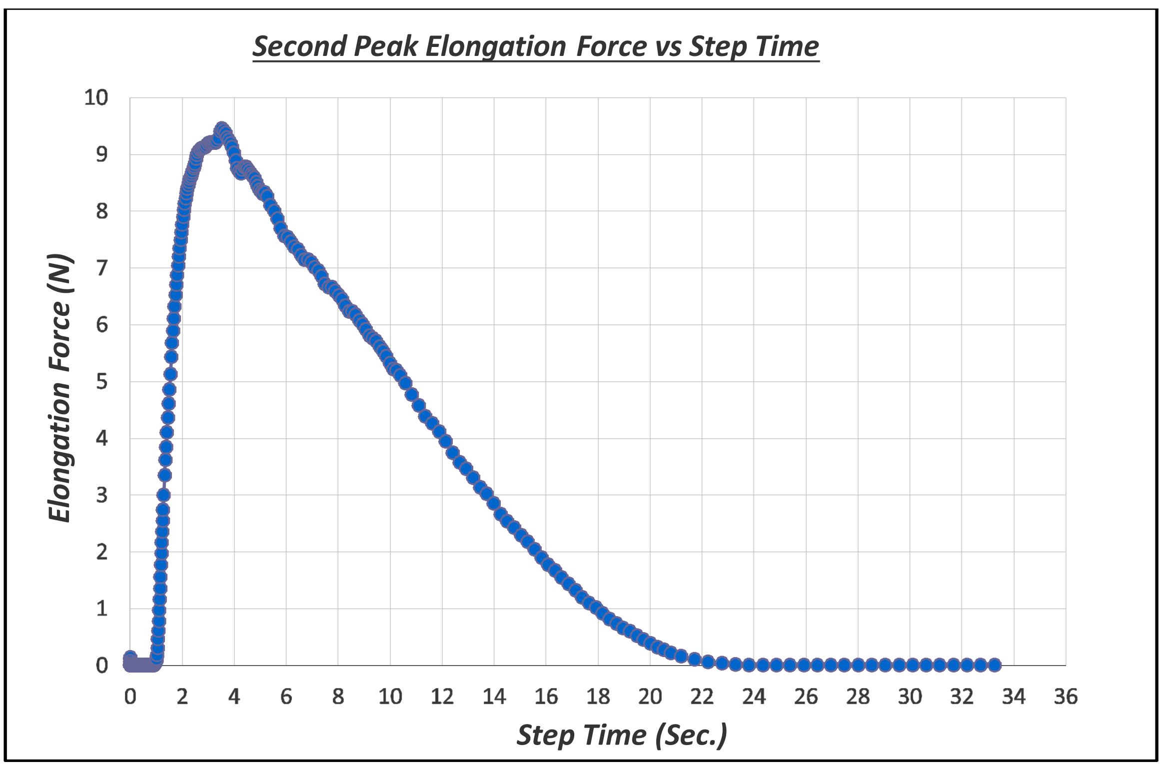

Figure 4-5. Elongation Force vs. Step Time for PG 64-22 geometry of 6.0 mm x 0.83 mm

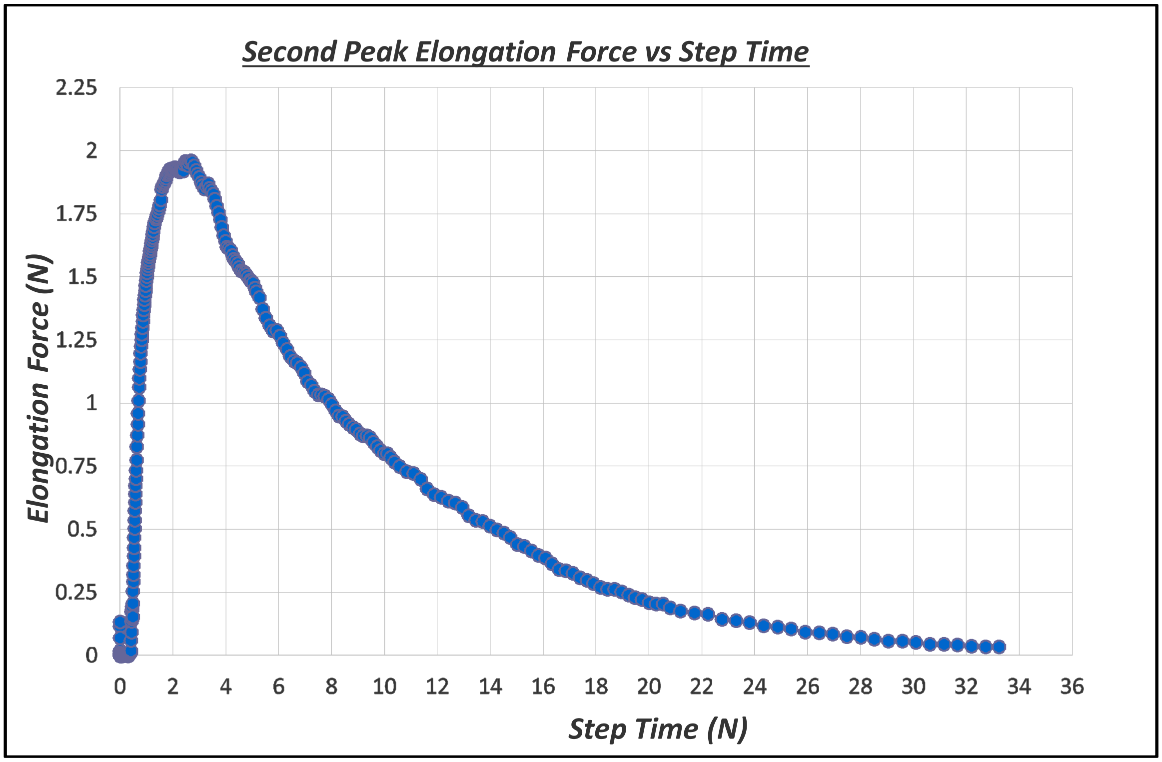

Figure 4-6. Elongation Force vs. Step Time for PG 58-28 geometry of 6.0 mm x 0.83 mm

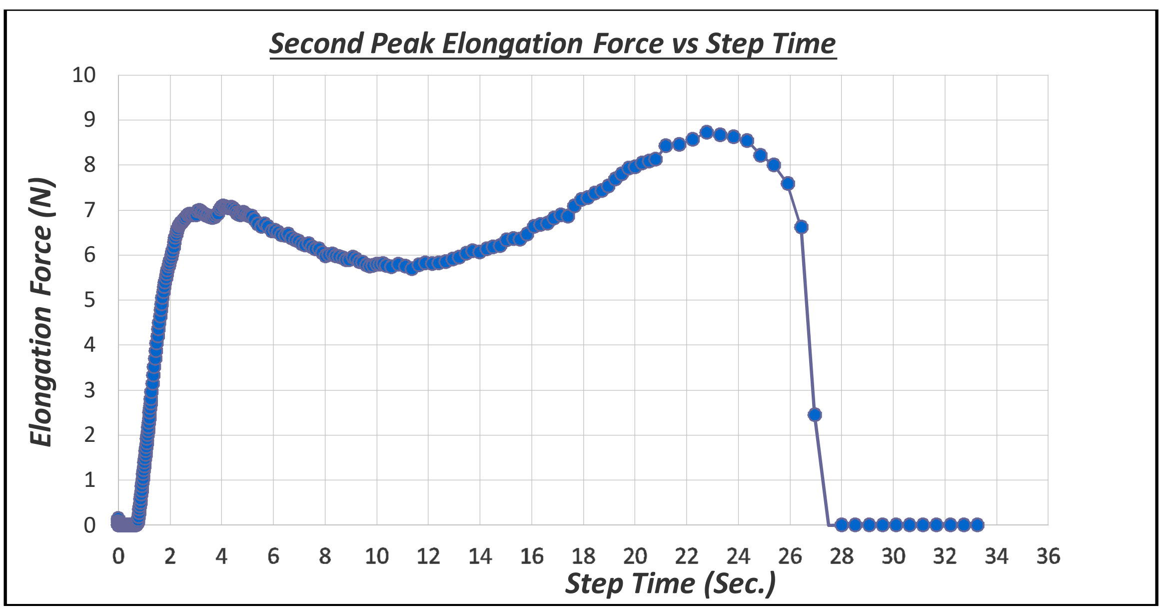

Figure 4-7. Elongation Force vs. Step Time for PG 76-22 geometry of 7.5 mm x 0.4 mm

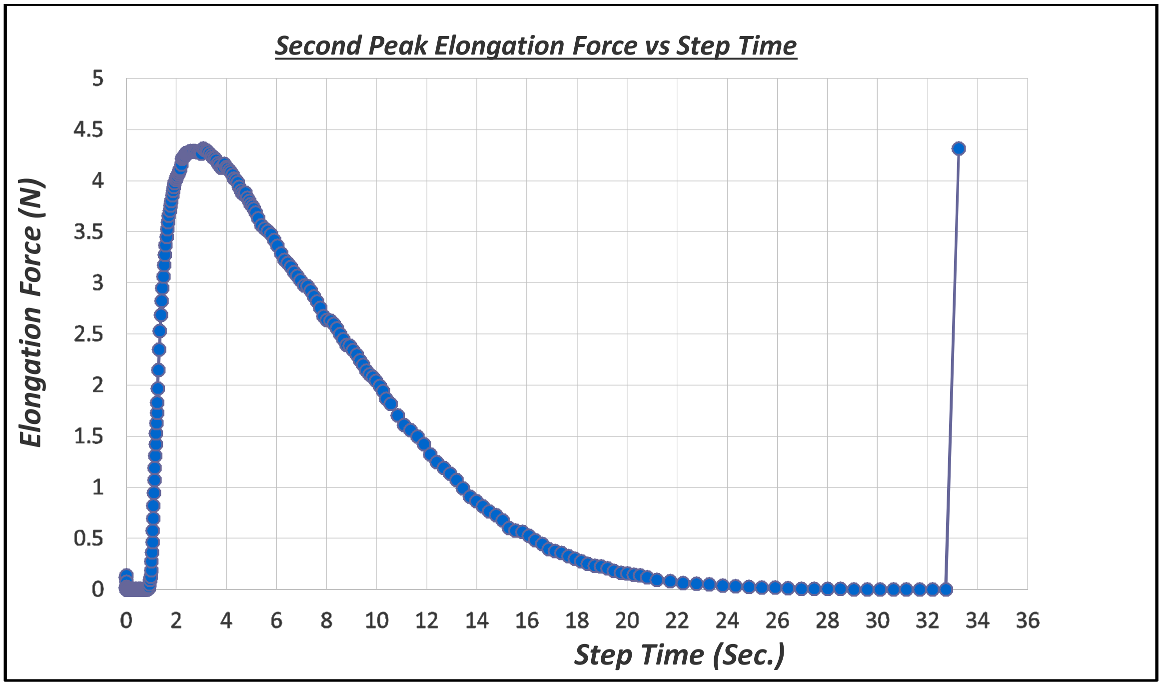

Figure 4-8. Elongation Force vs. Step Time for PG 64-22 geometry of 7.5 mm x 0.40 mm

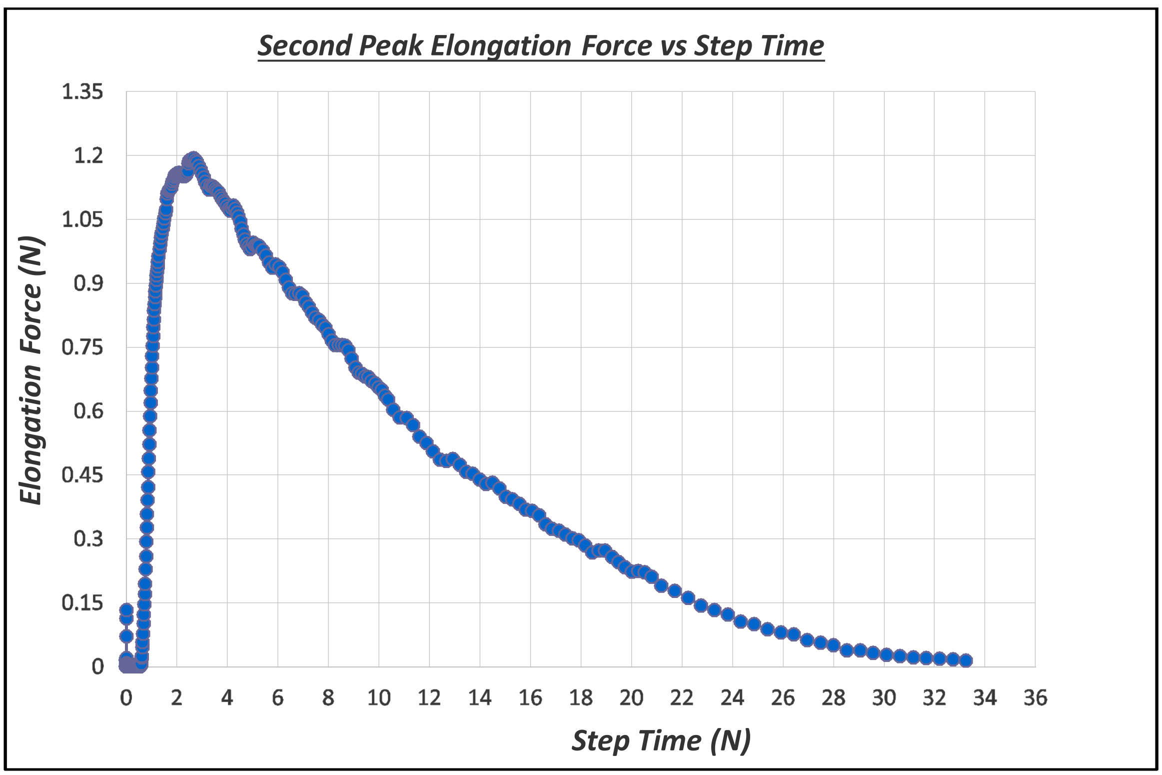

Figure 4-9. Elongation Force vs. Step Time for PG 58-28 geometry of 7.5 mm x 0.40 mm

4.2 Selection of a Geometry

4.2.1 Correlation between sample initial X-sectional area and elongation force

The potential effect of sample width and thickness on the elongation force was analyzed through four approaches: different initial cross-sectional areas, same initial cross-sectional areas with different geometries, different initial cross-sectional areas with the same width, and different initial cross-sectional areas with the same thickness.

4.2.1.1 *Correlation between sample initial X-sectional area and second peak elongation force.* Figure 4-10 demonstrates the correlation between the second peak elongation force F_2 and initial area for 122 samples. In general, as the initial area increases the second peak elongation force increases. It can be observed that each of the three initial areas that have been tested with two different geometries have shown different F_2 values. For clearer results projection, an average of ten samples for every geometry was plotted in Figure 4-11 (except geometry W= 10 mm x T= 0.83 mm was tested three times as mentioned in Section 3.6). The R^2 value was found to be 0.85, which indicates the linear correlation between the second peak elongation force and the initial area. As for the same initial areas with different geometries, 3.0 mm^2, 3.6 mm^2, and 6.5 mm^2, it can be clearly observed that as the initial area increases, the gap between the average second peak elongation force relatively increases. This indicates that the width and the thickness have different effects on the elongation force.

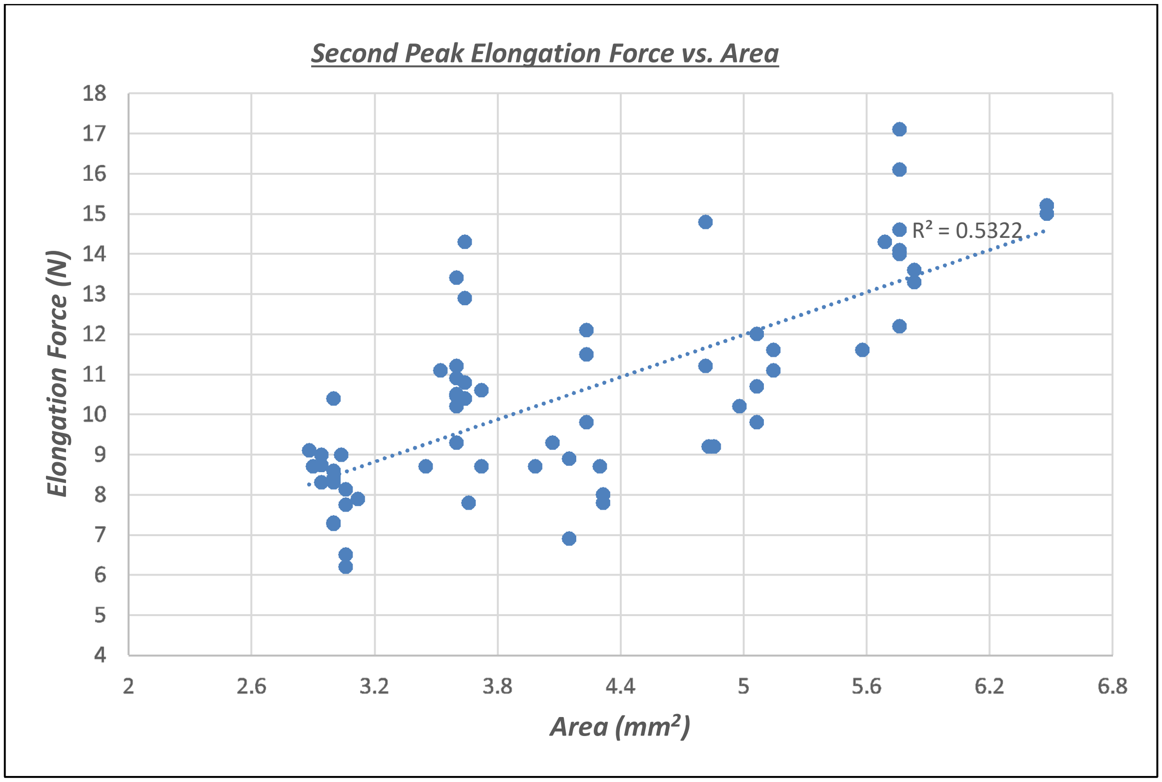

Figure 4-10. Second Peak Elongation Force vs. Initial Area

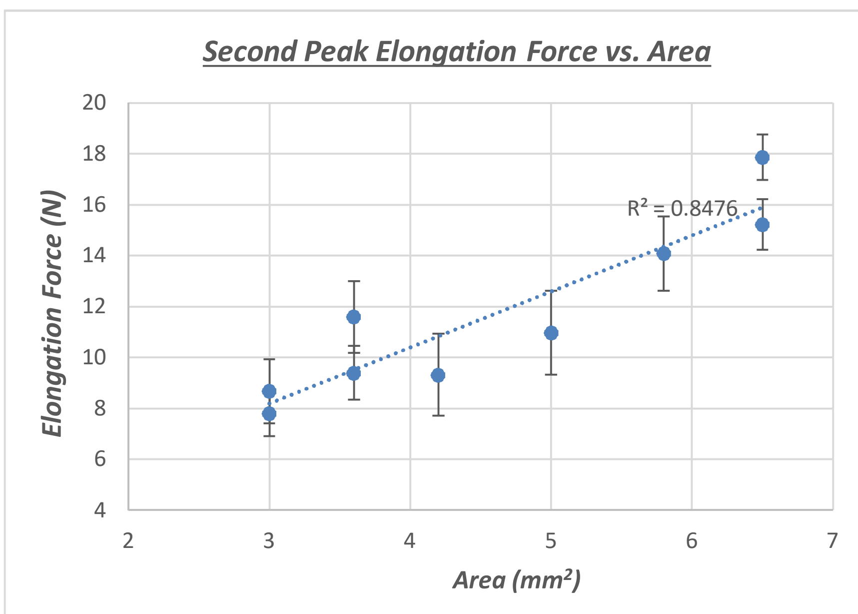

Figure 4-11. Average Second Peak Elongation Force vs. Initial Area

4.2.1.2 *Correlation between sample initial X-sectional area and first peak elongation force*. Figure 4-12 shows the correlation between the first peak elongation force F_1 and the initial area. It can be observed that F_1 has almost the same increasing trend of F_2 been showed in Figure 4-10 but exhibits slightly lesser increase with respect to the initial area than F_2. Figure 4-13 illustrates the average F_1 elongation force vs initial area. The R^2 value was found to be 0.84.

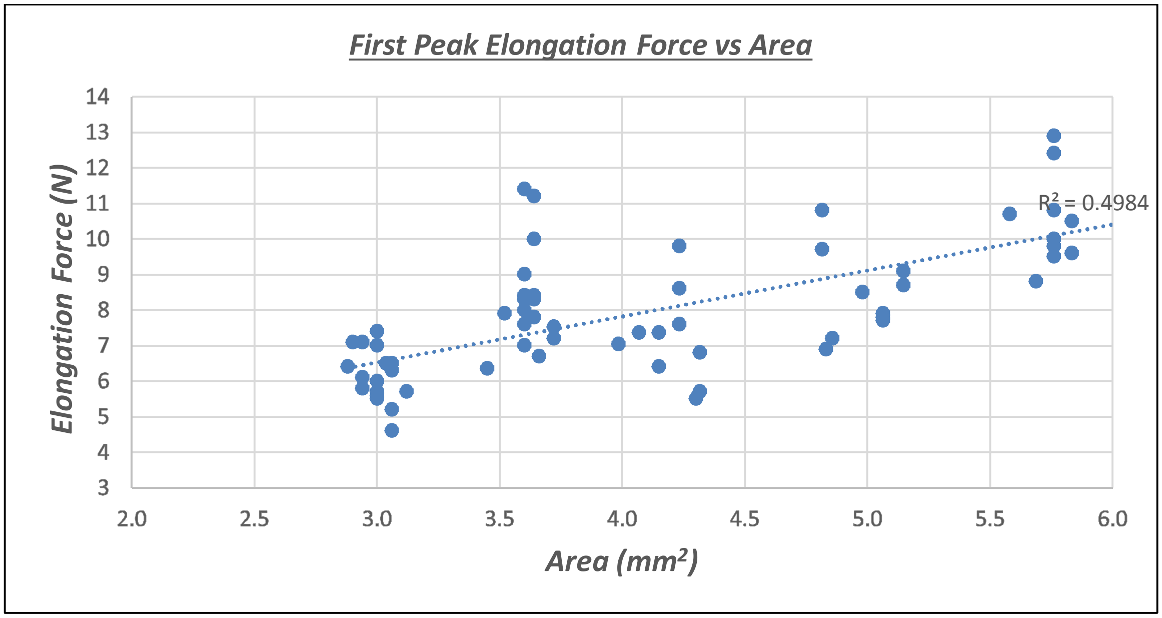

Figure 4-12. First Peak Elongation Force vs. Initial Area

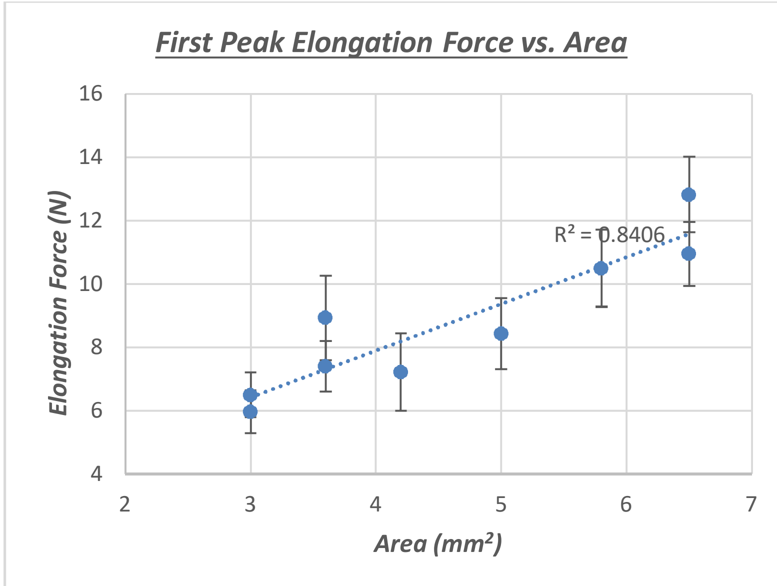

Figure 4-13. Average First Peak Elongation Force vs. Initial Area

4.2.2 Width and thickness effect in the elongation force

4.2.2.1 *Width and thickness effect in the second peak elongation force.* In this study, the effect of the sample's geometry (the width and the thickness) on the average elongation force was investigated. Figure 4-14 shows the average second peak elongation force F_2 vs. width for three different selected initial areas. Every initial area has been tested with two different geometries. It can be observed that for the initial X-sectional area of 3.0 mm^2, samples with dimensions of 5 mm x 0.6 mm have shown an average F_2 of 7.8 N. As for the same initial area with dimensions of 7.5 mm x 0.4 mm where the width increases by 50 %, and the thickness decreases by 33%, average F_2 of 8.7 N was observed, with a force increment of 0.9 N. For the initial area of 3.6 mm^2, the sample's dimensions of 6 mm x 0.6 mm show average F_2 of 9.4 N. The same initial area with dimensions of 9 mm x 0.4 mm, with width increasing by 50%, and thickness decreases by

33%, has shown an average F_2 of 11.6 N with force increment of 2.2 N. For the initial area 6.5 mm^2, the samples with dimensions of 9 mm x 0.72 mm show average F_2 of 15.2 N. Finally, the samples with dimensions of 10.8 mm x 0.6 mm, with width increasing by 20%, and thickness decreasing by 20%, have shown an average F_2 of 17.9 N with an average force increment of 2.7 N.

Figure 4-14 illustrates F_2 for equal initial areas but different width. It can be observed that the second peak elongation force increases due to the increases in width. Also, It can be observed from Figure 4-14 that even though the thickness decreases, the width increases, and the initial cross-section area remains the same, all three tested initial areas have shown increasing in the average second peak elongation force.

To understand the effect of the thickness on the average elongation force, Figure 4-15 illustrates the average second peak elongation force vs. thickness for different initial areas. It can be observed how clearly the elongation force of the samples with the same initial areas decreases due to the increases in the sample's thickness and decreases in width.

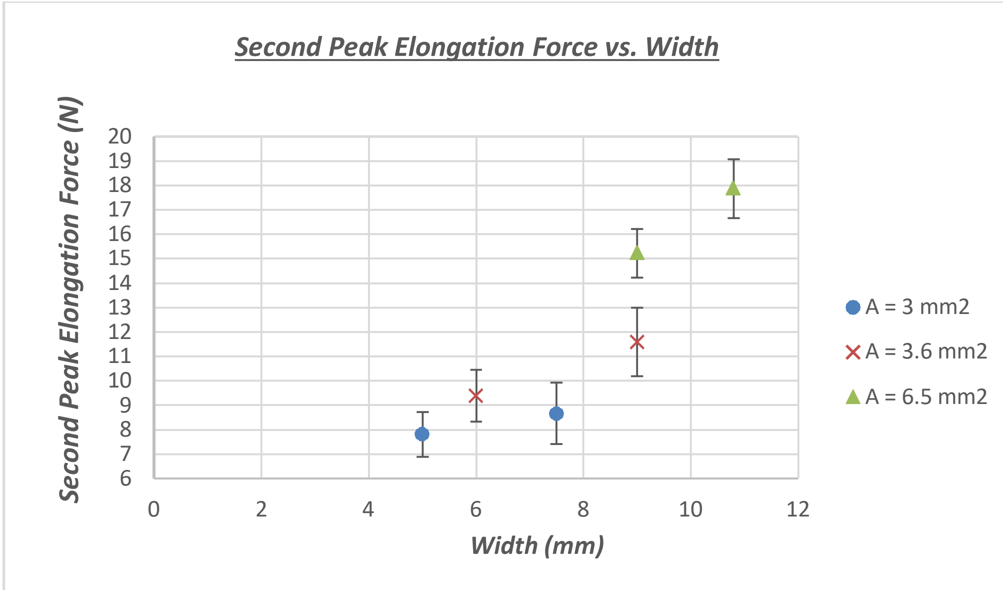

Figure 4-14. Average Second Peak Elongation Force vs. Width

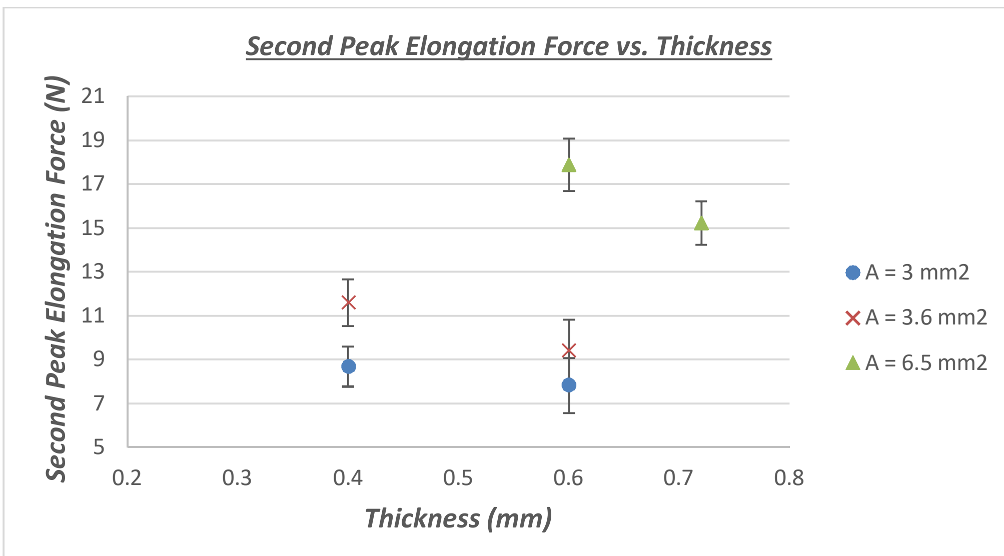

Figure 4-15. Average Second Peak Elongation Force vs. Thickness, for the different initial areas

Furthermore, Figure 4-16 illustrates the relation between the average F_2 and width for the samples with the same thickness but different widths. It can be observed that the force increment between the sample geometry of 5 mm x 0.6 mm and 6 mm x 0.6 mm is equal to 1.59 N, which is almost equal to the force increment between 5 mm x 0.83 mm and 6 mm x 0.83 mm, which is 1.66 N. As for the force increment between 6 mm x 0.6 mm and 10.8 mm x 0.6 mm, the average F_2 increases by 8.5N. In the case of the sample geometries 7.5 mm x 0.4 mm and 9 mm x 0.4 mm, the average F_2 increases by 2.92; this is due to the 1.5 mm increment of the width and, the relatively low thickness value of 0.4 mm. Moreover, it can be observed that at low thicknesses, the effect of the width on the average second peak elongation force behavior is more significant. For geometries 8 mm x 0.72 mm and 9 mm x 0.72 mm, it can be observed that average F_2 increases by just 1.13 N due to the limited percent increment of the width and the relatively high thickness value of 0.72 mm.

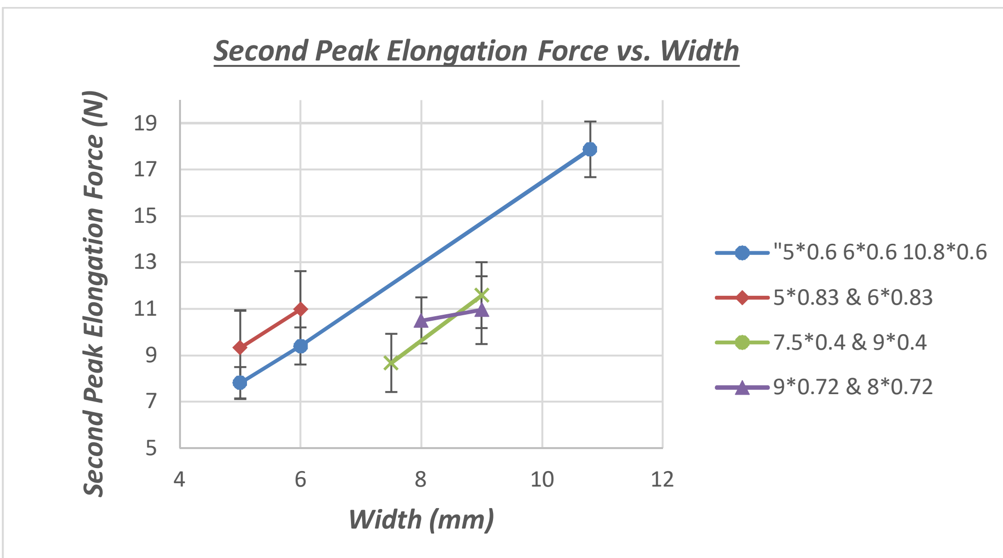

Figure 4-16. Average Second Peak Elongation Force vs. Width, for the different thicknesses

Figure 4-17 shows the correlation between F_2, and thickness for equally width samples. It can be observed that the increasing of F_2 due to the increasing of thickness between the samples with a width of 6 mm is almost equal to the 5 mm width samples.

For the samples with dimensions of 9 mm x 0.4 mm and 9 mm x 0.72 mm, the F_2 increment equal to 3.6 N, which is due to the relatively high width dimension of 9 mm.

The geometry 9 mm x 0.72 mm shows the lowest coefficient of variation among all the geometries by 6.6%. Among the eight geometries, the geometries 9 mm x 0.72 mm, and 10.8 mm x 0.60 mm show the highest two values of the average second peak elongation forces of 15.2 N and 18.2 N, respectively. However, the second mentioned geometry is almost at the SER recommended width threshold, which is equal to 12.7 mm. For the above mentioned details, geometry 9 mm x 0.72 mm was chosen to be the recommended geometry for the developed test method.

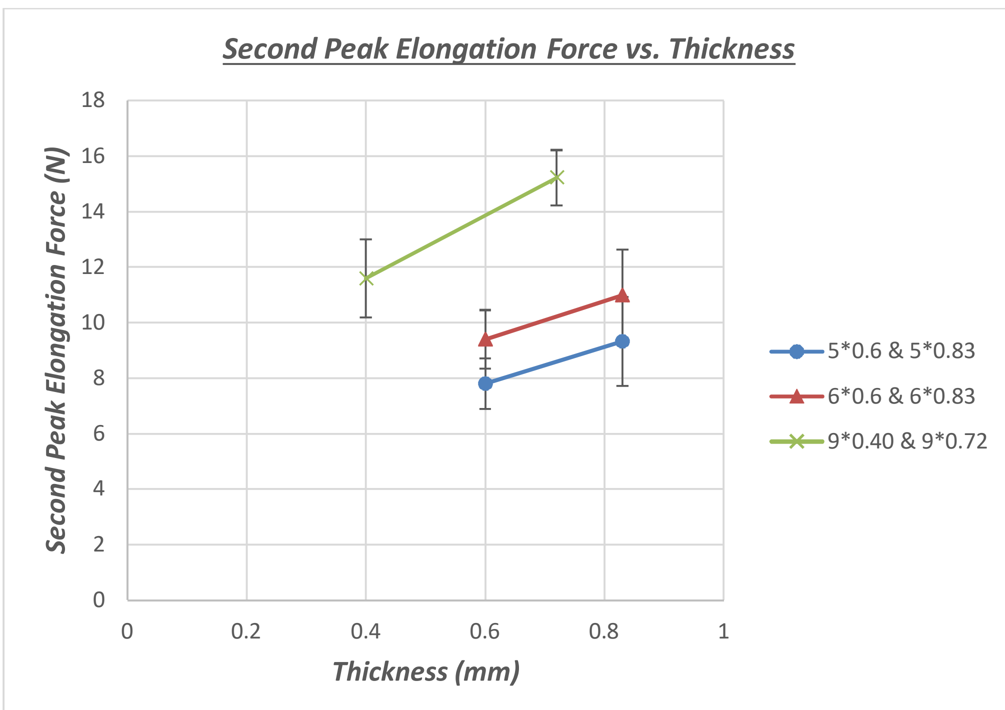

Figure 4-17. Average Second Peak Elongation Force vs. Thickness, for different widths

4.2.2.2 <u>*Width and thickness effect in the first peak elongation force.*</u> Figure 4-18 illustrates the average first peak elongation force F_1 vs width for the same above-mentioned initial areas: 3.0 mm^2, 3.6 mm^2, and 6.5 mm^2. It can be observed that out of the twenty samples that were tested with an initial X-sectional area of 3.0 mm^2, the ten samples with dimensions of 5 mm x 0.6 mm show an average F_1 of 6.0 N. As for the ten samples with dimensions of 7.5 mm x 0.4 mm with width increasing by 50%, and thickness decreasing by 33%, the average F_1 observed was 6.5 N with a force increment of 0.5 N, which is less by 0.4 N than the increment of F_2 of the same geometries mentioned in Section 4.2.2.1.

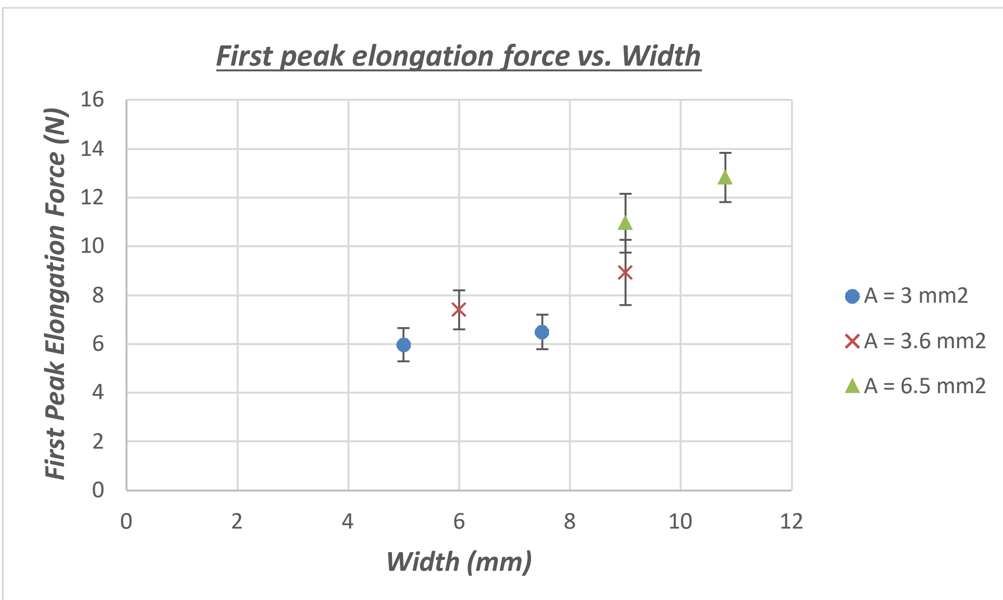

Figure 4-18. Average First Peak Elongation Force vs. Width

As for the initial area 3.6 mm^2, the ten samples with geometry of 6 mm x 0.6 mm show the average F_1 equals to 7.4 N. The samples with the dimension 9 mm x 0.4 mm show an average F_1 of 8.9 N with force increment by 1.5 N, which is 0.7 N less than the F_2 increment mentioned in Section 4.2.2.1. For the initial area 6.5 mm^2, samples dimension of 10.8 mm x 0.6 mm show average F_1 of 12.8 N, as for samples dimension of 9 mm x 0.72 mm show average F_1 equals to 10.9 N with force increases by 1.9 N, which is less than the increment of F_{2f} by 0.4 N. In general, the geometry effect is similar for F_1, and F_2 but it is slightly less for F_1 than F_2.

Figure 4-19 shows that for equal initial areas with different X-sectional dimensions, it can be observed that the average F_1 increases due to the increase in width even though the thickness decreases, and the initial area remains the same. It can also be observed that as the initial area increases the gap in average F_1 for equal initial areas with different dimensions increases.

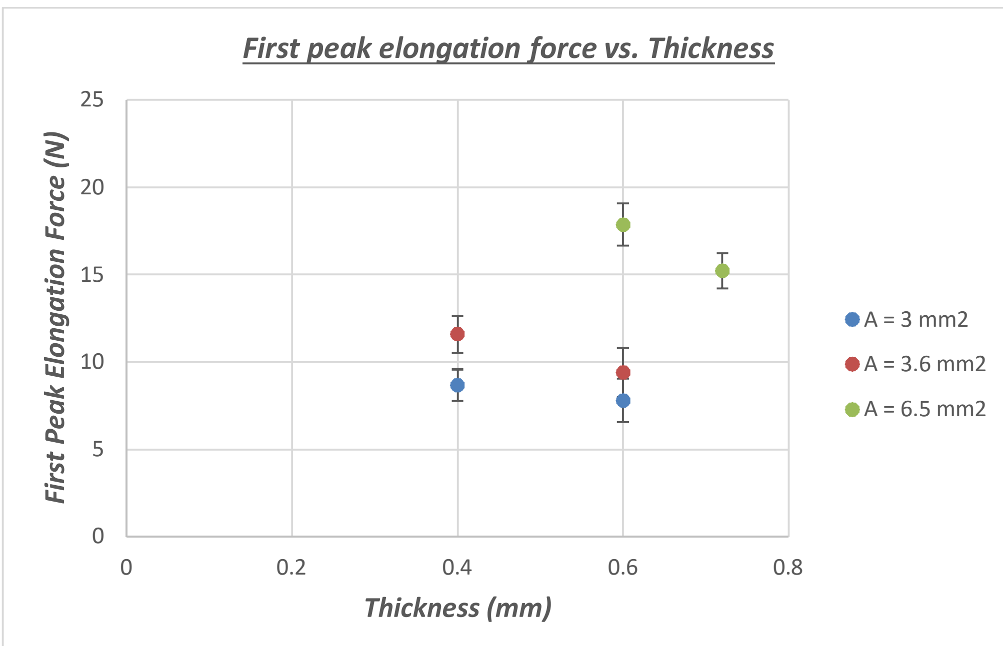

Figure 4-19. Average First Peak Elongation Force vs. Thickness

Figure 4-20 illustrates the average F_1 vs. thickness for the different samples initial areas with the same width. Figure 4-21 shows the average F_1 vs. width for the different samples' initial areas with the same thickness but different width. For samples 5 mm x

0.6 mm and samples 5 mm x 0.83 mm, with thickness increasing by 38%, the elongation force increases from 6 N to 7.2 N by percent increment of 20%. As for samples 5 mm x 0.6 mm and samples 6 mm x 0.6 mm, with the width increasing by 20% but thickness staying the same, the elongation force's increase equals 23%. As for samples 6 mm x 0.6 mm and 6 mm x 0.83 mm, with the same thickness increment percent of 38%, elongation force increases from 7.4 N to 8.4 N by increment percent of 14%, which is less by 6% than the elongation force percent increment of the previous mentioned samples.

Overall, the above detailed analysis indicates that, the average second and first peak elongation forces increase due to the increasing of the sample's initial area, but the same initial areas with different dimensions derived different values of elongation force. In case of all samples with same initial areas but different dimensions, the elongation force increases due to the increase in width and decrease of thickness. The effect of the thickness in the average peak elongation force decreases due to the increasing of the width. We can also derive that second and first peak elongation forces have almost the same characteristics with respect to the sample initial X-sectional area. Therefore, the second peak elongation force is more sensitive towards the sample initial X-sectional area than the first peak elongation force.

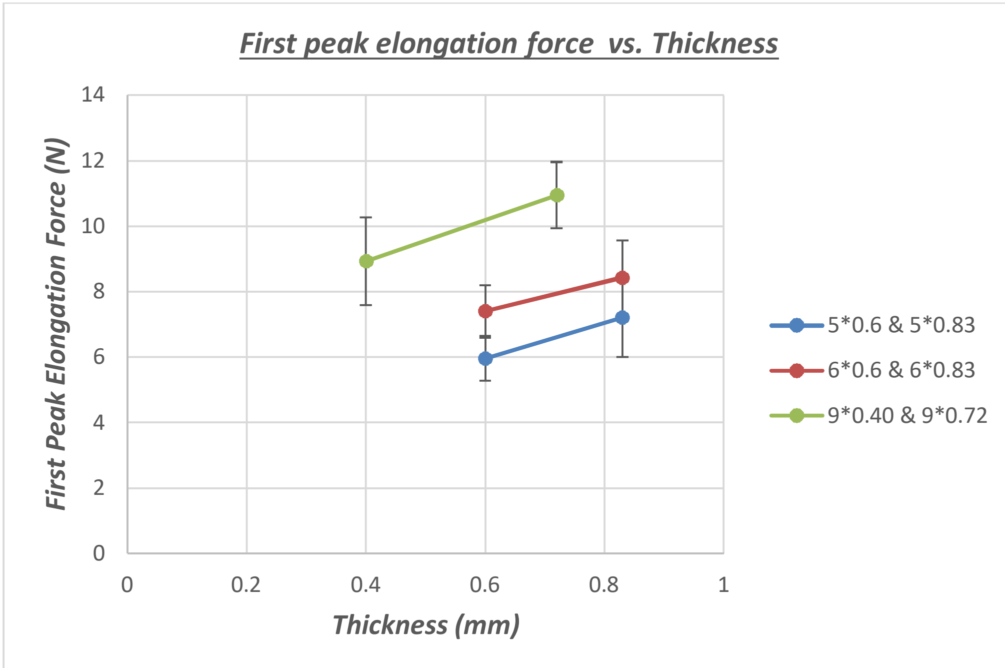

Figure 4-20. Average First Peak Elongation Force vs. Thickness

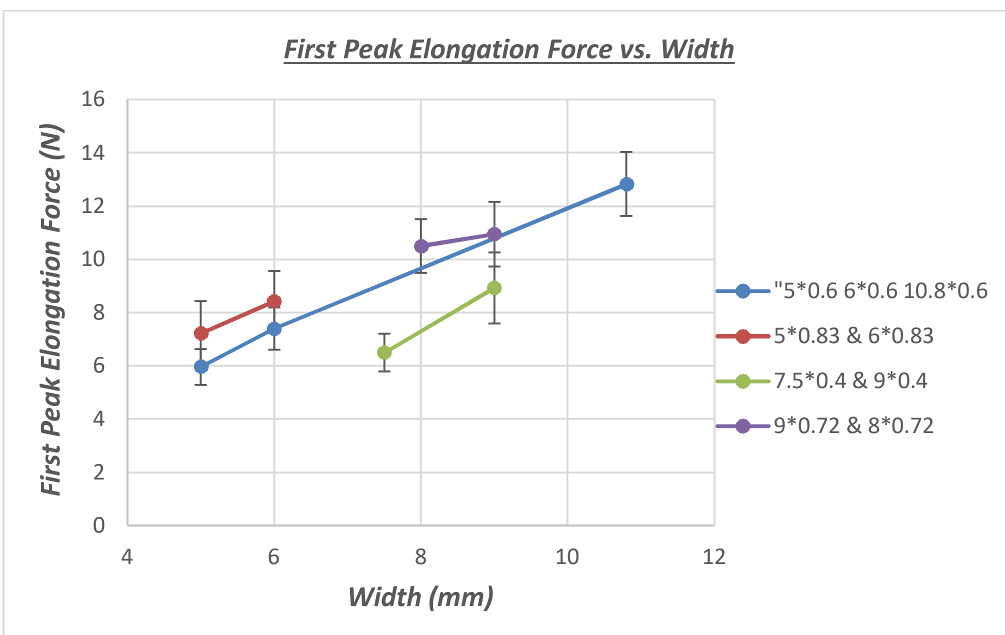

Figure 4-21. Average First Peak Elongation Force vs. Width

4.3 Selection of a Temperature

4.3.1 Temperature effect in the second peak elongation force

State of Louisiana is currently carrying out the force ductility test according to AASHTO T300, which specifies that the test shall be performed at a temperature of 4.0 ± 0.5°C (39.2 ± 1.0 F). In order to evaluate the effect of temperature on the elongation force, two geometries, 8 mm x 0.72 mm and 9 mm x 0.72 mm, were tested at three different temperatures: 4°C, 10°C, and 16°C.

Figure 4-22 shows the correlation between the second peak elongation force and temperature for samples with an initial area of 5.8 mm^2. Figure 4-23 shows the correlation between the average second peak elongation force and temperature for the samples with an initial area of 5.8 mm^2. The second peak elongation force F_2 is almost linearly increased due to the temperature increase with R^2 values of 0.65 and 0.95 for F_2 and average F_2, respectively. It can be observed from Figure 4-23 that the second peak elongation force at 4°C was 14.1 N. At 10°C, elongation force decreases to 12.23 N, and for 16°C, elongation force was 7.7 N, which is the lowest among the three testing temperatures.

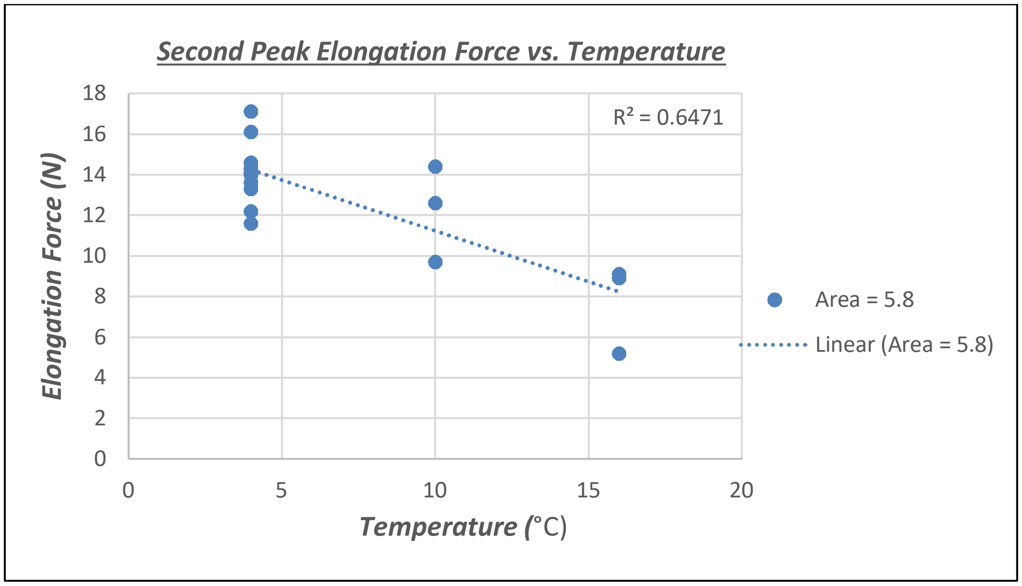

Figure 4-22. Second Peak Elongation Force vs. Temperature

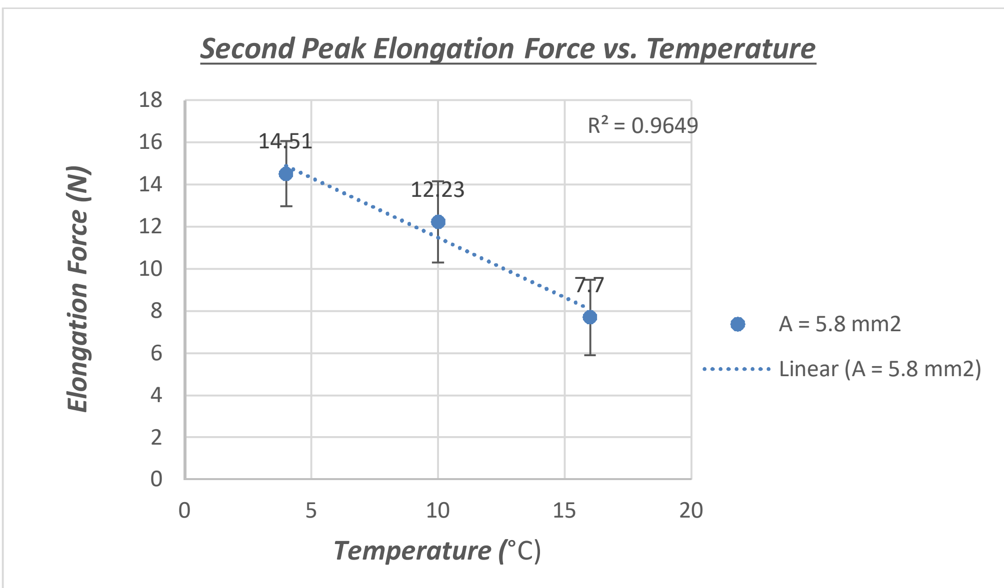

Figure 4-23. Average Second Peak Elongation Force vs. Temperature

For the initial area of 6.5 mm^2, similar behavior was observed from Figure 4-24 and Figure 4-25, which illustrate the correlation between the second peak elongation force and average second peak elongation force with temperature, respectively. From

Figure 4-25, the highest average second peak elongation force was found to be 15.22 N at 4°C. At 10°C, elongation force decreases to 13.6 N, as for 16°C, elongation force observed was 7.7 N. The R^2 value was 0.74 and 0.91 for F_2, and average F_2 respectively. In all the cases in this study, samples tested at 4°C (the lowest temperature among the three testing temperatures) exhibited the highest second peak elongation force.

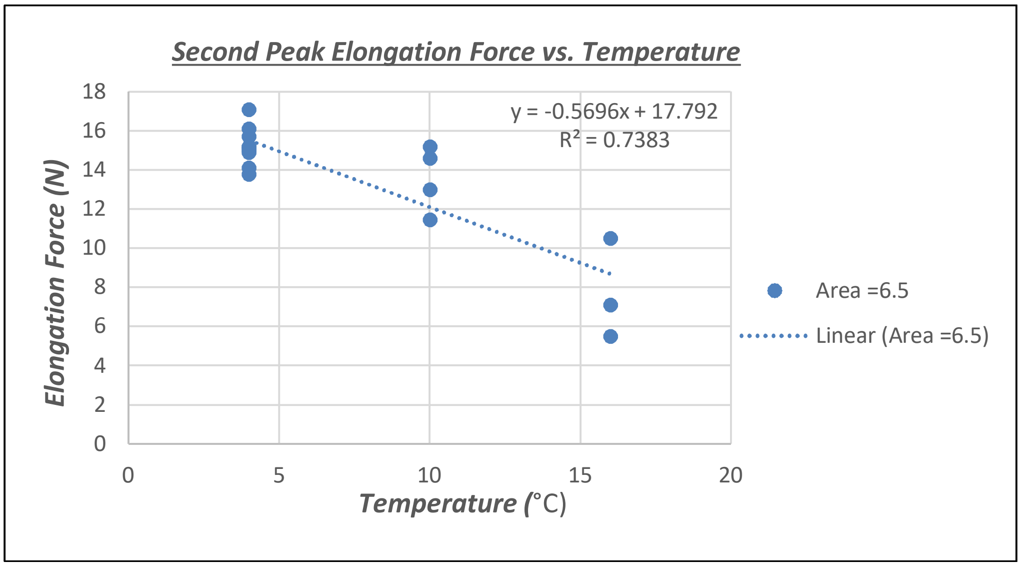

Figure 4-24. Second Peak Elongation Force vs. Temperature

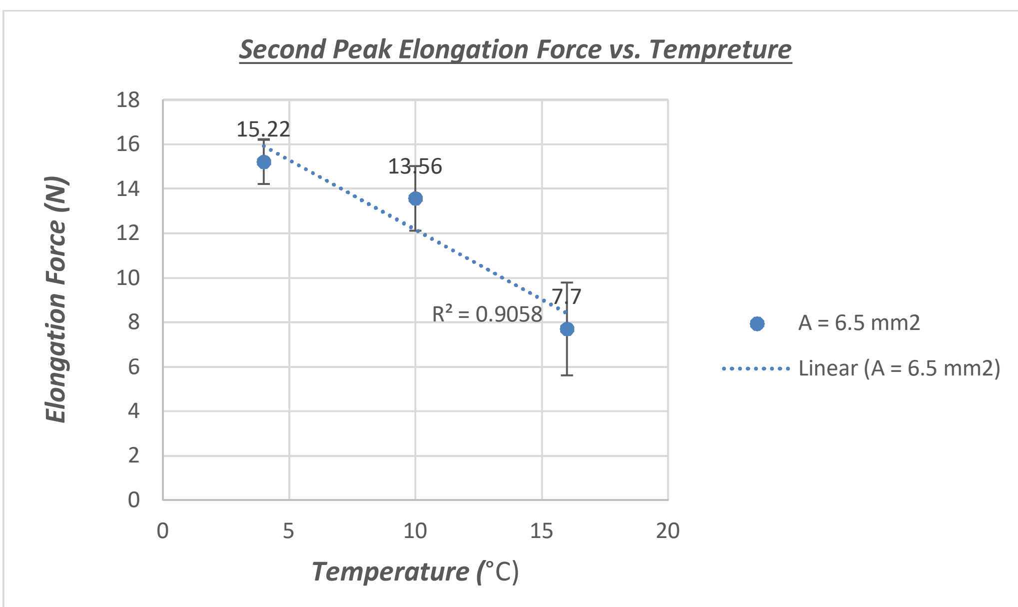

Figure 4-25. Average Second Peak Elongation Force vs. Temperature

4.3.2 Temperature effect in the elongation force vs step time curve characteristics

Figures 4-26, 4-27, and 4-28 show the elongation force vs step time for geometry of 8 mm x 0.72 mm at 4°C, 10°C, and 16°C, respectively. Figures 4-29, 4-30, and 4-31 show the elongation force vs step time for geometry of 9 mm x 0.72 mm at 4°C, 10°C, and 16°C, respectively. It can be observed from Figures 4-26 to 4-31 that, the curve characteristics change due to the temperature changes. At 4°C the inflection point can be clearly determined. However, at 10°C, and 16°C the inflection points almost fully integrated with the first and second peak elongation forces. That is because of the increase of the asphalt resilience due to the temperature increment.

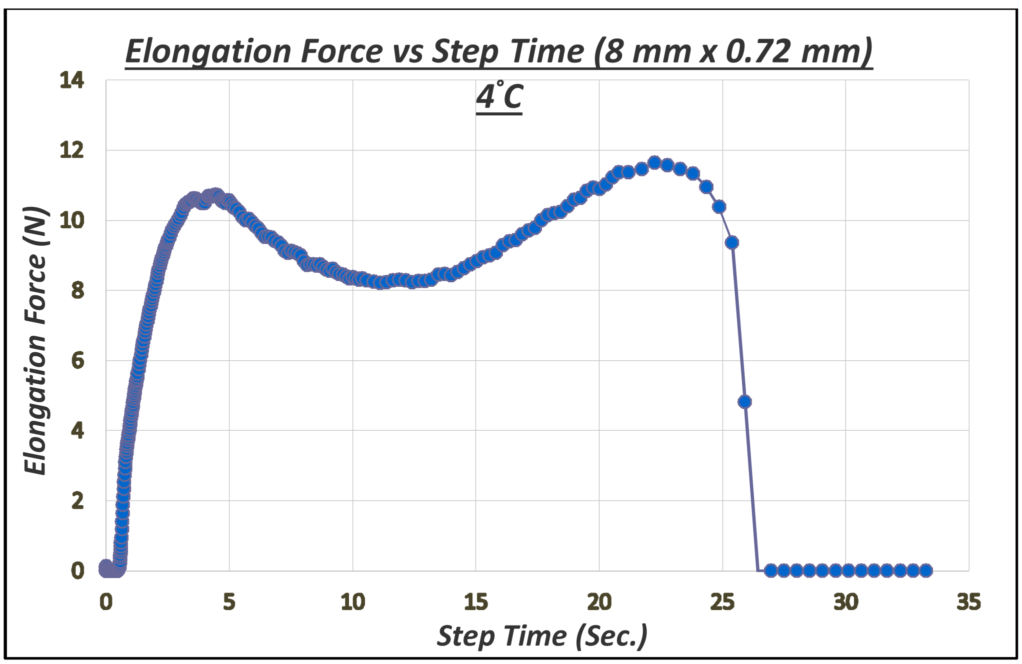

Figure 4-26. Elongation Force vs. Step Time for PG 76-22 geometry of 8 mm x 0.72 mm at 4°C

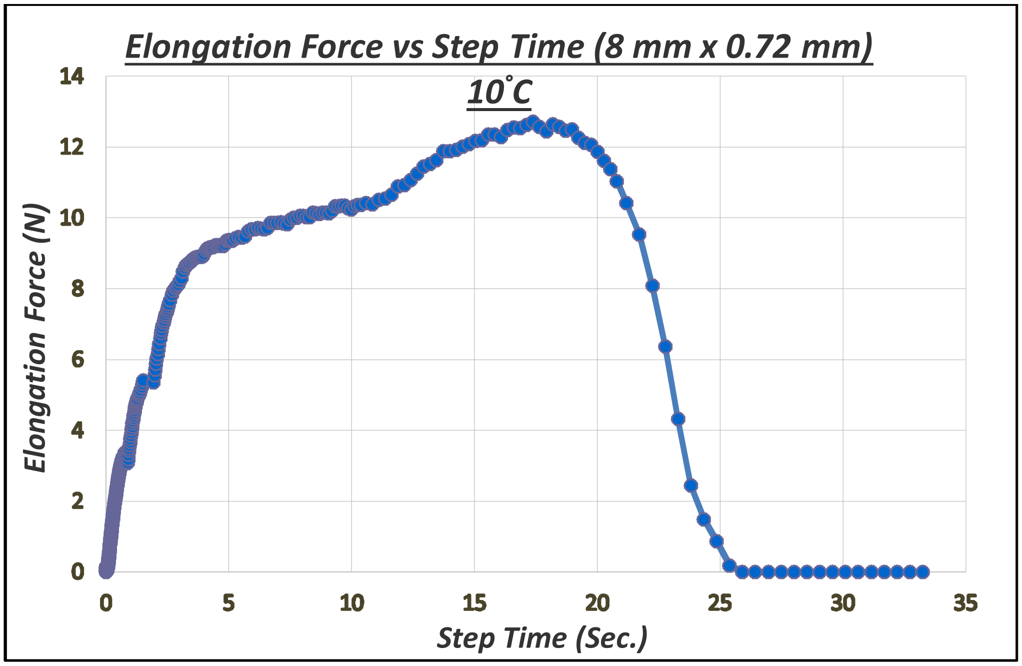

Figure 4-27. Elongation Force vs. Step Time for PG 76-22 geometry of 8 mm x 0.72 mm at 10°C

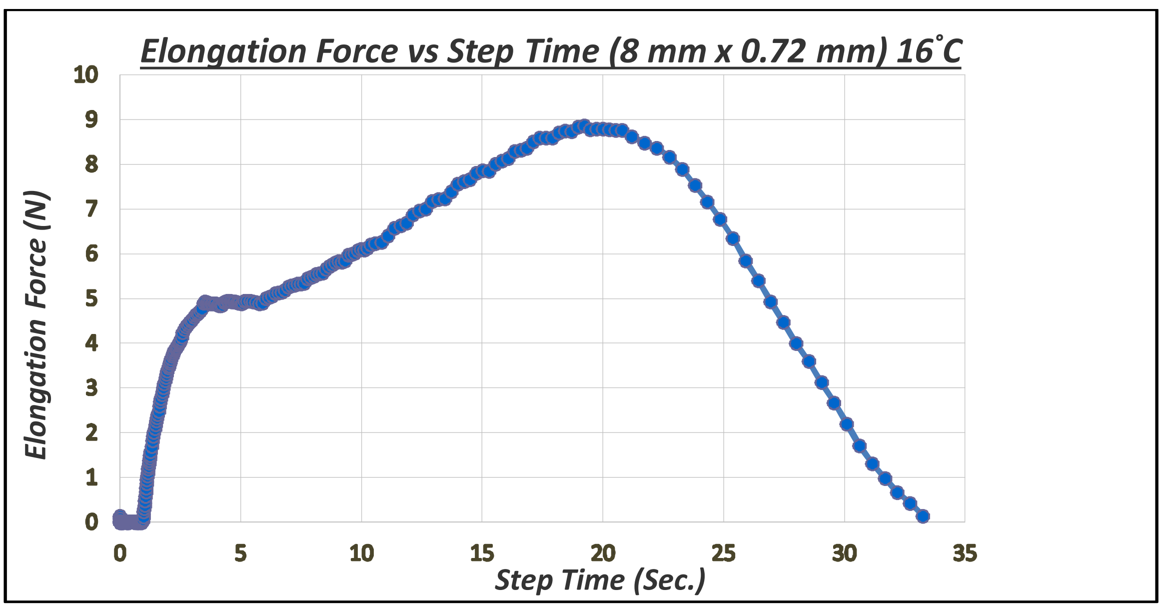

Figure 4-28. Elongation Force vs. Step Time for PG 76-22 geometry of 8 mm x 0.72 mm at 16°C

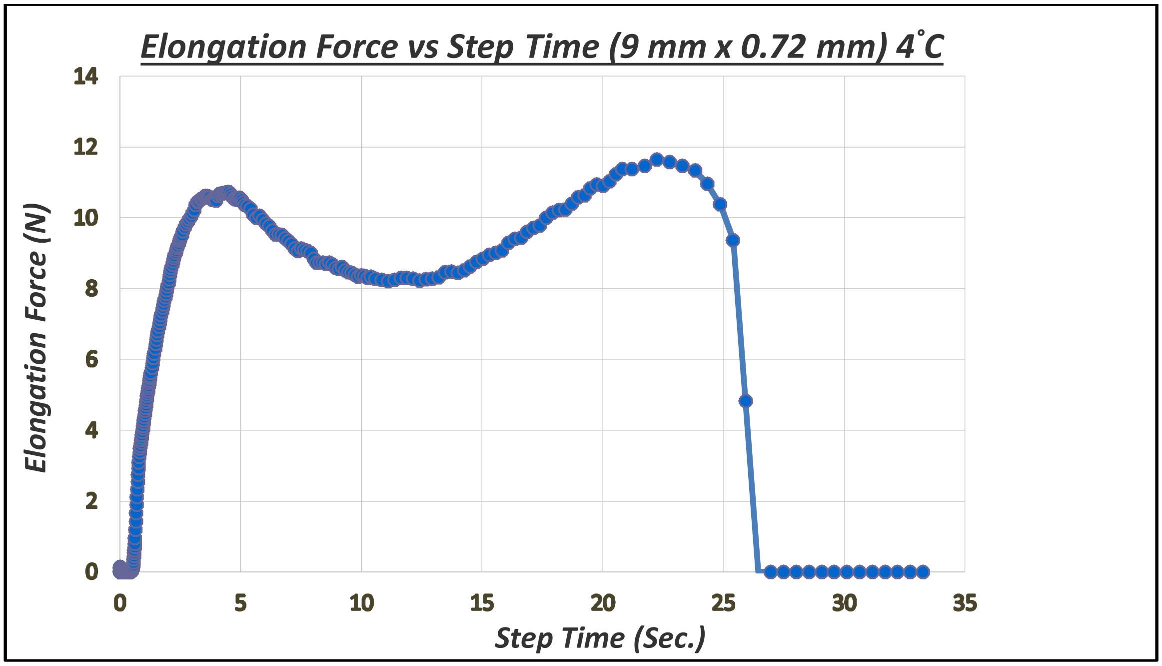

Figure 4-29. Elongation Force vs. Step Time for PG 76-22 geometry of 9 mm x 0.72 mm at 4°C

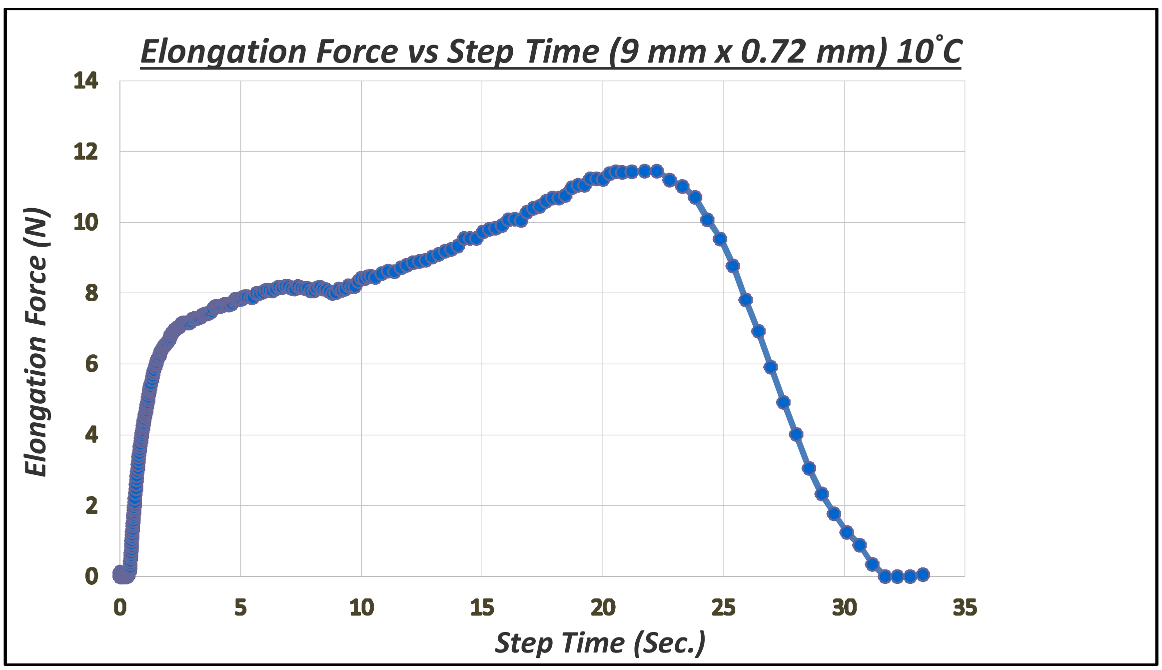

Figure 4-30. Elongation Force vs. Step Time for PG 76-22 geometry of 9 mm x 0.72 mm at 10°C

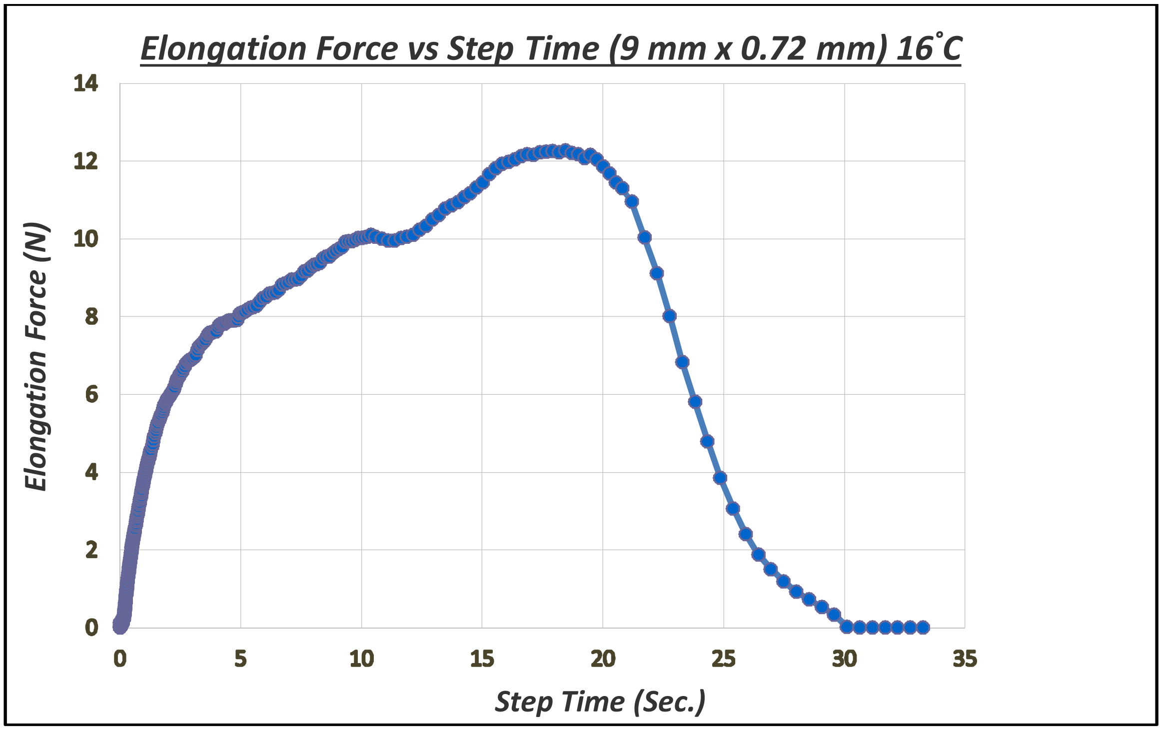

Figure 4-31. Elongation Force vs. Step Time for PG 76-22 geometry of 9 mm x 0.72 mm at 16°C

Furthermore, it can be observed that the failure criteria become more ductile with the temperature increment. For example, for geometry 8 mm x 0.72 mm the final test time was 26 seconds at 4°C. As for the same geometry, the final test time at 16°C was 33 seconds with 8 seconds increment than the 4°C. The same trend was observed for geometry 9 mm x 0.72 mm. From the above-mentioned discussions in Sections 4.3.1 and 4.3.2, 4°C was selected to be the testing temperature for the developed extensional deformation test of asphalt binders.

4.4 Test Parameters and Specifications

As mentioned earlier, different parameters are used by different agencies for different asphalt materials in the current force ductility test (AASHTO 300). The commonly used parameters are F_2/F_1 and value of F_2. Also, F_2 is defined by second peak force or by force at 30 cm elongation. Like the parameters, recommended specifications and testing temperature vary as well by different agencies.

Table 4-1 demonstrates the second peak elongation force results of the selected geometry, 9 mm x 0.72 mm (width x thickness). The lowest F_2 was 13.1 N and the highest F_2 was 17.1 N, with an average F_2 of 15.322 N, standard deviation of 0.998, and coefficient of variation of 6.55%. Table 4-1 also demonstrates that out of the ten samples, the lowest F_2/F_1 obtained was 1.17 and the highest F_2/F_1 obtained was 1.54 with an average of 1.4, and a standard deviation of 0.13. The coefficient of variation for ten F_2 values is 6.19%, whereas coefficient of variation for F_2/F_1 values is 9.21%. The F_2 value has been chosen as a recommended force ductility parameter. The minimum F_2 value recommended is 14 N, which was lower than the lowest limit of 99% confidence interval (14.45N – 15.99 N). Also, minimum F_2/F_1 of 1.25 is recommended for PG76-22. This is also lower than the lowest value of 99% confidence interval (1.29-1.51).

Table 4-1. Statistical Analysis of the Selected Geometry

Sample No.	**F_1 in N**	**F_2 in N**	**F_2/F_1**
Sample1	12.2	15.2	1.25
Sample2	10.6	15	1.42
Sample3	10.1	15.1	1.5
Sample4	11.2	17.1	1.53
Sample5	9.7	14.9	1.54
Sample6	10.8	15.2	1.41
Sample7	9.2	14.1	1.53
Sample8	11.8	13.8	1.17
Sample9	11.5	15.7	1.37
Sample10	12.4	16.1	1.3
Average	10.95	15.22	1.40
Highest	12.4	17.1	1.54
Lowest	9.2	13.8	1.17
Stan. Dev.	1.07	0.94	0.13
Coefficient of Variation (%)	9.74	6.19	9.21
99% Conf. Interval	10.08-11.82	14.45-15.99	1.29-1.51
No. of Sample Outside the Limits of 99% Confidence Int.	4	4	4
Recommended Value (Minimum)		**14 N**	**1.25**

The recommended temperature for the test remains to be 4ºC as the conventional force ductility test. To avoid sample overlapping after a half rotation of each drum, the recommended final strain is 3.4 rad. Based on the findings of this study, the geometry of 9 mm x 0.72 mm was selected.

CHAPTER 5

CONCLUSIONS AND RECOMMENDATIONS

In order to investigate the potential of Sentmanat Extensional Rheometer fixture as a replacement of the force ductility test (AASHTO T300), extensional deformation tests using a DSR-based SER fixture were performed for asphalt binders PG 76-22, PG 64-22, and PG 58-28.

This study focused on PG 76-22 in order to detect the second peak elongation force caused by the polymer modifications. In order to select the sample geometry, nine different geometries were investigated. Three temperatures, 4°C, 10°C, and 16°C, were used to determine the recommended test temperature. Based on the result presented in this study, the following conclusions can be drawn:

- A new test method was developed to fulfill the acknowledged gap in the current PG system and replace the force ductility test by exploring different potential extensional rheology parameters. Second peak elongation force was detected for PG 76-22 polymer modified binder.
- Sample preparation method was developed and simplified so it can be performed with easy access tools. Less than 1 g of the sample is needed, and less than 1 min is needed to perform the test after a temperature equilibrium soaking time of 10

min. The developed test procedure was kept limited to the fixture safety thresholds, and capabilities.

- The newly developed test parameters are F_2 and F_2/F_1. The coefficient of variation for ten F_2 values is 6.19%, and coefficient of variation for F_2/F_1 values is 9.21%.
- A detailed analysis indicates that the average second peak and first peak elongation forces increase due to the increase of the sample's initial area, with R^2 values of 0.85 and 0.84, respectively. However, the same initial areas with different dimensions derived different values of elongation force. The elongation force of all samples with the same initial area but different dimensions increase due to the increase of width even though the thickness decreases.
- The second peak elongation force is almost linearly increasing due to the temperature increment, with R^2 value of 0.96 at 4°C, 10°C, and 16°C.
- Based on the study, the recommended test specifications are as follows: the selected geometry 9 mm x 0.72 mm. The F_2 value has been chosen as a recommended force ductility parameter. The minimum F_2 value recommended is 14 N, which was lower than the lowest limit of 99% confidence interval (14.45N – 15.99 N). Also, minimum F_2/F_1 of 1.25 is recommended for PG76-22. This is also lower than the lowest value of 99% confidence interval (1.29-1.51). The recommended temperature is 4ºC, recommended strain rate 0.1 s^{-1}, and the recommended final strain is 3.4 rad.
- For the future ongoing research, it is recommended that:

- The sample preparation method can be developed in order to minimize its processing time and the sample thickness accuracy.
- Extensional deformation tests can be performed in aged asphalt binders.
- Extensional deformation tests can be performed in polymer asphalt binders with different types of polymers.
- Analyzing the stress and strain curve.
- Analyzing the elastic modulus of the modified asphalt binders.

APPENDIX

This study recommended F_2/F_1 and F_2 as the new developed extensional test parameters, but the true material properties can also be obtained from the stress vs. strain curve and the modulus curve. The following paragraphs discuss on the stress-strain curves and elaborate why the final recommendations are still based on F_2/F_1 and F_2.

Figure A-1, A-2, and A-3 show the elongation force vs. step time, the true stress vs. Hencky strain, and the engineering stress vs. Hencky strain, respectively. It can be observed from Figure A-2 that, for the first part of the curve the true stress was relatively low comparing with the second part. That is because at the start of the test the initial area was 6.5 mm^2, but with the stretching of the sample the area decreases therefore, the stress increases until it reaches the second peak in which the force starts dropping, subsequently, the stress drops.

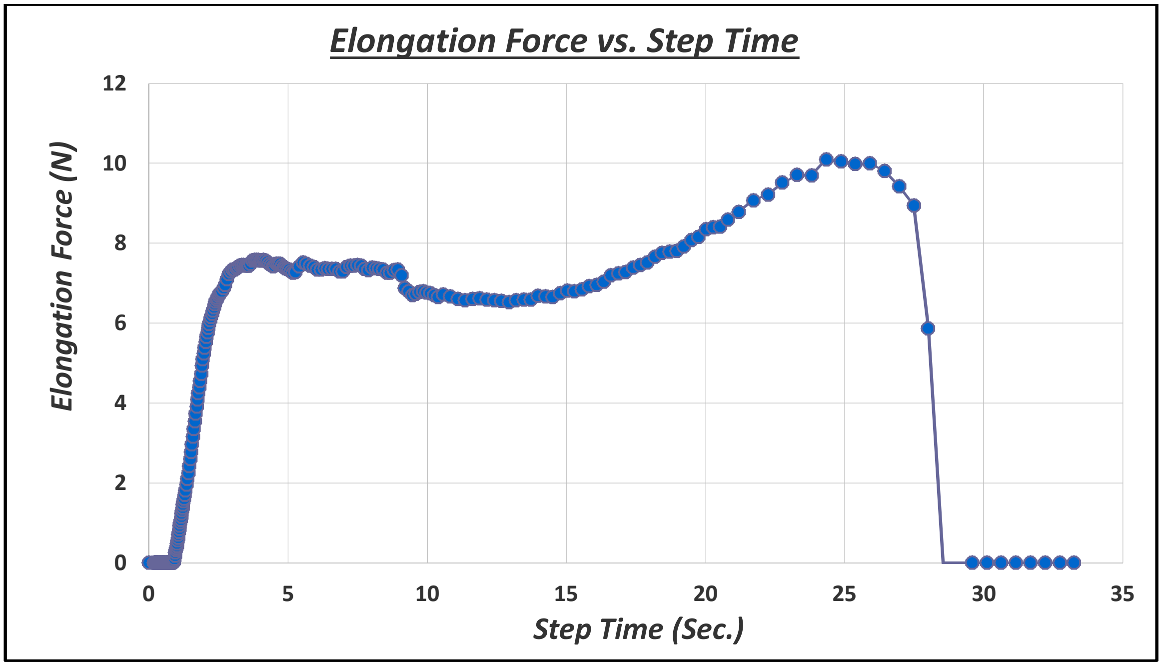

Figure A-1. Elongation Force vs. Step Time for PG 76-22 geometry of 9 mm x 0.72 mm at 4°C

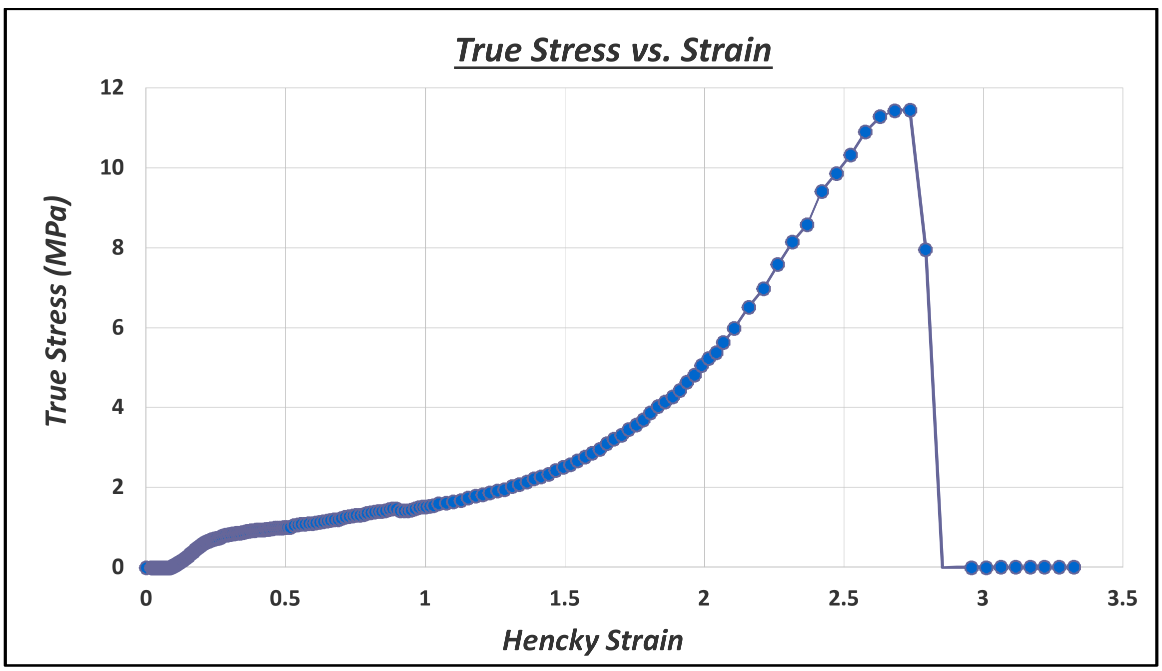

Figure A-2. True Stress vs. Hencky Strain for PG 76-22 geometry of 9 mm x 0.72 mm at 4°C

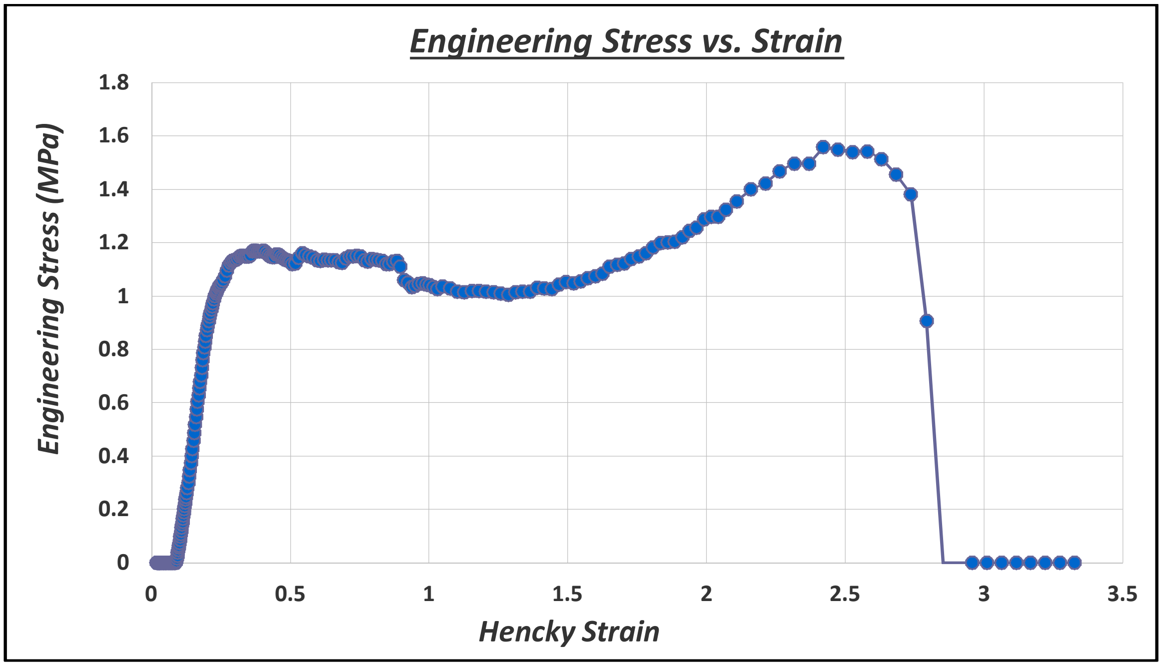

Figure A-3. Engineering Stress vs. Hencky Strain for PG 76-22 geometry of 9 mm x 0.72 mm at 4°C

For Figure A-3, the engineering stress has a similar trend of the elongation force, that is because the area is constant so, the only inconstant in the stress equation is the elongation force.

Figure A-4 and Figure A-5 show the elastic modulus, based on the true stress, vs. step time and the elastic modulus, based on engineering stress, vs. stress time, respectively. From Figure A-4, it can be observed very clearly that the PG 76-22 has two distinct elastic moduli. The first elastic modulus at the first part of the curve is related to the asphalt binder which is equal to 2.9 MPa. As for the elastic modulus obtained at the second part of the curve is related to the polymer, which is equal to 4.3 MPa.

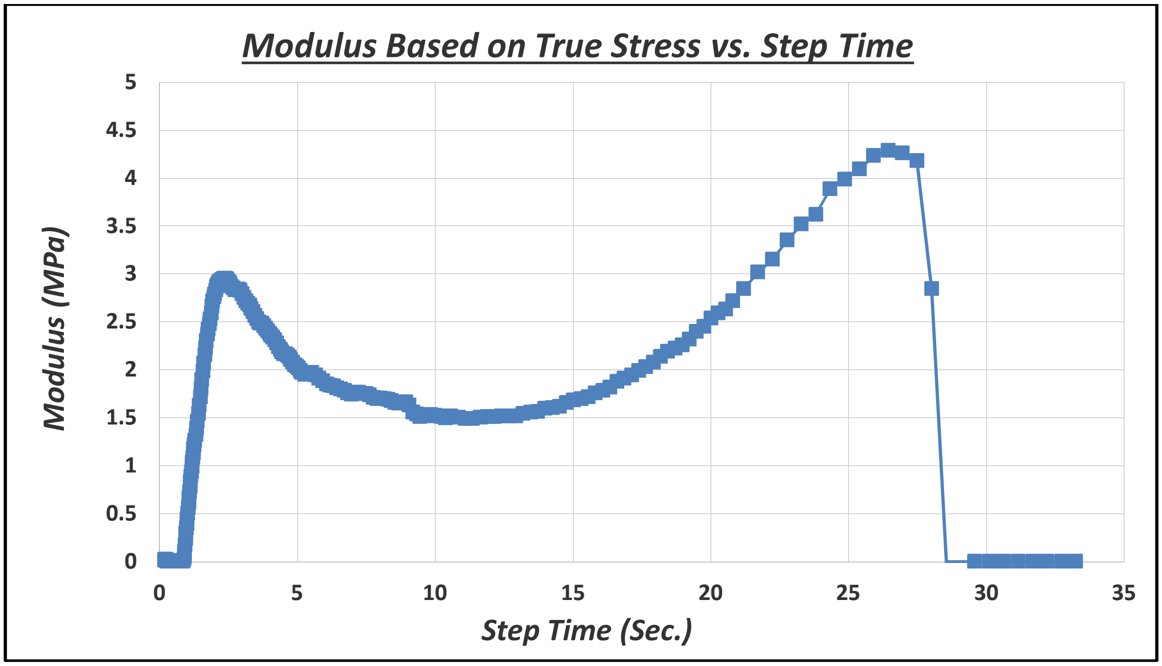

Figure A-4. Elastic Modulus based on true stress vs. Step Time for PG 76-22 geometry of 9 mm x 0.72 mm at 4°C

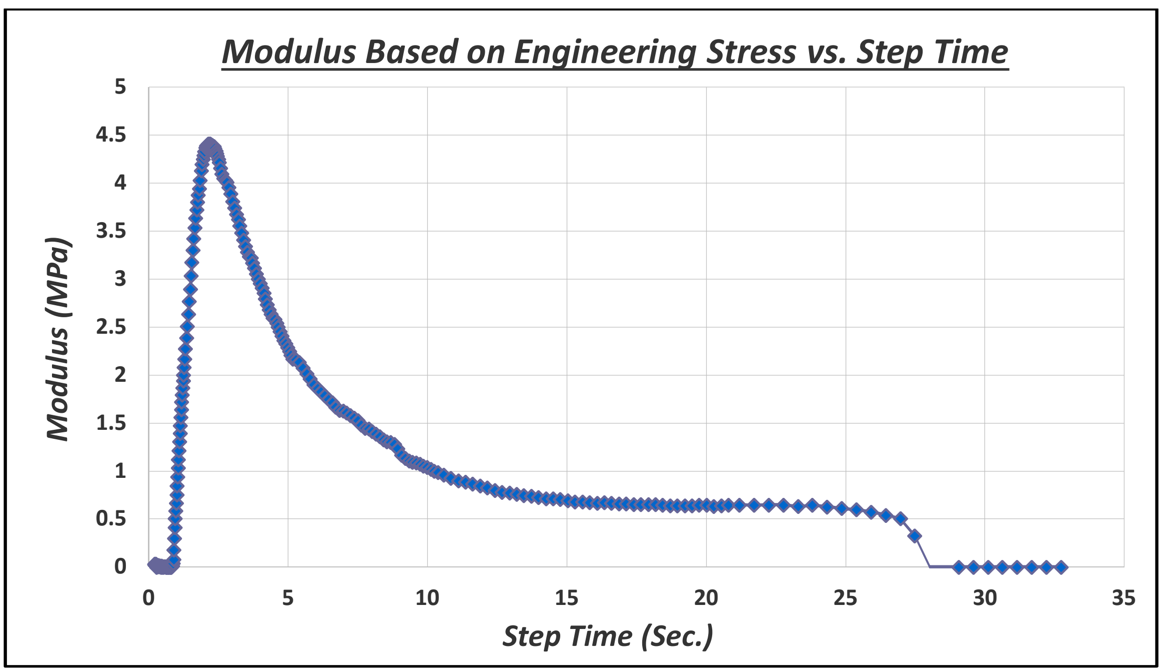

Figure A-5. Elastic Modulus based on Engineering Stress vs. Step Time for PG 76-22 geometry of 9 mm x 0.72 mm at 4°C

It can also be observed from Figures A-1 and A-4 that, the elongation force curve has the same trend of the elastic modulus curve, but there is an insignificant time differences for the peak points as follows: for the elongation force, the step time of the first peak is 4.6 s, as for the modulus, the step time of the first peak is 2.4 s, with time difference of 2.2 s. As for the second part of the curve, the elongation force second peak step time is 25.9 s, but the elastic modulus second peak step time is 26.9 s with time difference of 1 second. That is because the area calculation is theoretical so, insignificant variation expected.

So, the elongation force curve (Figure A-1) and the modulus curve (based on true stress and Hencky strain in Figure A-5) exhibit very similar material trends with a first peak and an increased second peak. This study recommends F_2/F_1 and F_2 parameters for the newly developed test because forces are actual in this case whereas, for modulus curve, stresses are derived from theoretically calculated area. Figures A-1 to A-5 and Table A-1 were prepared from one sample of the selected geometry.

Table A-1. Typical test results extracted from a SER

Number of result	Step time	Temperature	Hencky strain	Hencky rate	Stress	Elongation viscosity	Velocity	Displacement	Elongation Force
	s	°C		1/s	Pa	Pa.s	rad/s	rad	N
1.	0.000	3.967	0.0000	0.0003	0.00E+00	0.0E+00	0.0003	-18.276	0.000
2.	0.001	3.967	0.0000	0.0003	1.22E+03	4.0E+06	0.0004	-18.276	0.016
3.	0.002	3.967	0.0000	0.0080	8.66E+03	1.1E+06	0.0099	-18.276	0.116
4.	0.003	3.967	0.0001	0.0366	1.04E+04	2.9E+05	0.0452	-18.276	0.140
5.	0.004	3.967	0.0001	0.0687	6.15E+03	8.9E+04	0.0847	-18.276	0.082
6.	0.005	3.967	0.0002	0.0875	2.06E+03	2.4E+04	0.1079	-18.276	0.028
7.	0.006	3.967	0.0003	0.0937	2.81E+02	3.0E+03	0.1155	-18.275	0.004
8.	0.007	3.967	0.0004	0.0943	7.47E+01	7.9E+02	0.1163	-18.275	0.001
9.	0.008	3.967	0.0005	0.0938	4.22E+02	4.5E+03	0.1157	-18.275	0.006
10.	0.009	3.967	0.0006	0.0943	6.92E+02	7.3E+03	0.1163	-18.275	0.009
11.	0.010	3.967	0.0007	0.0959	6.70E+02	7.0E+03	0.1182	-18.275	0.009
12.	0.011	3.967	0.0008	0.0972	4.98E+02	5.1E+03	0.1199	-18.275	0.007
13.	0.012	3.967	0.0009	0.0978	4.52E+02	4.6E+03	0.1206	-18.275	0.006
14.	0.013	3.967	0.0010	0.0985	4.23E+02	4.3E+03	0.1215	-18.275	0.006
15.	0.014	3.967	0.0011	0.0992	3.08E+02	3.1E+03	0.1224	-18.274	0.004
16.	0.015	3.967	0.0012	0.0994	2.75E+02	2.8E+03	0.1225	-18.274	0.004
17.	0.016	3.967	0.0013	0.0993	3.09E+02	3.1E+03	0.1225	-18.274	0.004
18.	0.017	3.967	0.0014	0.0991	3.85E+02	3.9E+03	0.1222	-18.274	0.005
19.	0.018	3.967	0.0015	0.0991	4.71E+02	4.8E+03	0.1221	-18.274	0.006
20.	0.019	3.967	0.0016	0.0994	4.68E+02	4.7E+03	0.1226	-18.274	0.006
21.	0.020	3.967	0.0017	0.0999	3.90E+02	3.9E+03	0.1231	-18.274	0.005
22.	0.021	3.967	0.0018	0.1002	3.03E+02	3.0E+03	0.1236	-18.274	0.004
23.	0.022	3.967	0.0019	0.1003	2.34E+02	2.3E+03	0.1237	-18.273	0.003
24.	0.023	3.967	0.0021	0.1003	2.24E+02	2.2E+03	0.1236	-18.273	0.003
25.	0.024	3.967	0.0022	0.1000	2.47E+02	2.5E+03	0.1234	-18.273	0.003
26.	0.025	3.967	0.0023	0.0999	3.11E+02	3.1E+03	0.1232	-18.273	0.004
27.	0.026	3.967	0.0024	0.1005	2.20E+02	2.2E+03	0.1239	-18.273	0.003
28.	0.027	3.967	0.0025	0.1012	-1.13E+00	-1.1E+01	0.1248	-18.273	0.000
29.	0.028	3.967	0.0026	0.1012	-1.24E+02	-1.2E+03	0.1247	-18.273	-0.002
30.	0.029	3.967	0.0027	0.1005	-6.75E+01	-6.7E+02	0.1239	-18.273	-0.001
31.	0.030	3.967	0.0028	0.0997	1.12E+02	1.1E+03	0.1229	-18.272	0.001
32.	0.031	3.967	0.0029	0.0994	2.29E+02	2.3E+03	0.1226	-18.272	0.003

Table A-1 Continued.

33.	0.032	3.967	0.0030	0.0991	3.42E+02	3.4E+03	0.1222	-18.272	0.005
34.	0.033	3.967	0.0031	0.0994	3.68E+02	3.7E+03	0.1226	-18.272	0.005
35.	0.034	3.967	0.0032	0.0996	3.33E+02	3.3E+03	0.1228	-18.272	0.004
36.	0.035	3.967	0.0033	0.0996	3.48E+02	3.5E+03	0.1228	-18.272	0.005
37.	0.036	3.967	0.0034	0.0995	3.87E+02	3.9E+03	0.1227	-18.272	0.005
38.	0.037	3.967	0.0035	0.0998	3.66E+02	3.7E+03	0.1231	-18.272	0.005
39.	0.038	3.967	0.0036	0.0998	3.61E+02	3.6E+03	0.1231	-18.271	0.005
40.	0.039	3.967	0.0037	0.0999	3.59E+02	3.6E+03	0.1232	-18.271	0.005
41.	0.040	3.967	0.0038	0.1003	2.92E+02	2.9E+03	0.1237	-18.271	0.004
42.	0.042	3.967	0.0039	0.1005	1.46E+02	1.5E+03	0.1239	-18.271	0.002
43.	0.044	3.967	0.0042	0.0998	2.87E+02	2.9E+03	0.1231	-18.271	0.004
44.	0.046	3.967	0.0044	0.1001	2.61E+02	2.6E+03	0.1234	-18.270	0.003
45.	0.048	3.967	0.0046	0.1009	1.99E+01	2.0E+02	0.1245	-18.270	0.000
46.	0.050	3.967	0.0048	0.1000	6.84E+01	6.8E+02	0.1233	-18.270	0.001
47.	0.052	3.967	0.0050	0.0995	2.83E+02	2.8E+03	0.1227	-18.270	0.004
48.	0.054	3.967	0.0052	0.0998	2.73E+02	2.7E+03	0.1231	-18.269	0.004
49.	0.056	3.967	0.0054	0.0997	2.72E+02	2.7E+03	0.1230	-18.269	0.004
50.	0.058	3.967	0.0056	0.0994	4.21E+02	4.2E+03	0.1226	-18.269	0.006
51.	0.060	3.967	0.0058	0.0998	4.01E+02	4.0E+03	0.1231	-18.269	0.005
52.	0.062	3.967	0.0060	0.1007	1.91E+02	1.9E+03	0.1242	-18.268	0.003
53.	0.065	3.967	0.0062	0.1003	1.14E+02	1.1E+03	0.1237	-18.268	0.002
54.	0.067	3.967	0.0064	0.0998	2.91E+02	2.9E+03	0.1231	-18.268	0.004
55.	0.069	3.967	0.0066	0.1003	1.67E+02	1.7E+03	0.1237	-18.268	0.002
56.	0.071	3.967	0.0068	0.1001	1.48E+02	1.5E+03	0.1234	-18.267	0.002
57.	0.073	3.967	0.0070	0.0992	3.89E+02	3.9E+03	0.1223	-18.267	0.005
58.	0.075	3.967	0.0072	0.0995	4.77E+02	4.8E+03	0.1227	-18.267	0.006
59.	0.077	3.967	0.0074	0.1004	2.51E+02	2.5E+03	0.1238	-18.267	0.003
60.	0.079	3.967	0.0076	0.0995	4.16E+02	4.2E+03	0.1227	-18.266	0.006
61.	0.081	3.967	0.0078	0.1002	3.68E+02	3.7E+03	0.1235	-18.266	0.005
62.	0.083	3.967	0.0080	0.1007	1.33E+02	1.3E+03	0.1242	-18.266	0.002
63.	0.085	3.967	0.0082	0.0999	2.48E+02	2.5E+03	0.1232	-18.266	0.003
64.	0.087	3.967	0.0085	0.1003	2.50E+02	2.5E+03	0.1236	-18.265	0.003
65.	0.089	3.967	0.0087	0.1012	-8.79E+01	-8.7E+02	0.1248	-18.265	-0.001
66.	0.091	3.967	0.0089	0.0999	3.78E+01	3.8E+02	0.1232	-18.265	0.001
67.	0.093	3.967	0.0091	0.0990	3.84E+02	3.9E+03	0.1220	-18.265	0.005
68.	0.095	3.967	0.0093	0.0993	4.38E+02	4.4E+03	0.1225	-18.264	0.006
69.	0.097	3.967	0.0095	0.0998	3.62E+02	3.6E+03	0.1231	-18.264	0.005
70.	0.099	3.967	0.0097	0.0997	4.07E+02	4.1E+03	0.1229	-18.264	0.005

Table A-1 Continued.

71.	0.101	3.967	0.0099	0.1003	3.27E+02	3.3E+03	0.1237	-18.264	0.004
72.	0.103	3.967	0.0101	0.1013	-2.22E+01	-2.2E+02	0.1248	-18.263	0.000
73.	0.106	3.967	0.0103	0.1001	8.37E+01	8.4E+02	0.1234	-18.263	0.001
74.	0.108	3.967	0.0105	0.1000	2.09E+02	2.1E+03	0.1233	-18.263	0.003
75.	0.110	3.967	0.0107	0.1003	6.00E+01	6.0E+02	0.1237	-18.263	0.001
76.	0.112	3.967	0.0109	0.0995	2.25E+02	2.3E+03	0.1227	-18.262	0.003
77.	0.114	3.967	0.0111	0.0992	4.26E+02	4.3E+03	0.1223	-18.262	0.006
78.	0.116	3.967	0.0113	0.0997	4.00E+02	4.0E+03	0.1229	-18.262	0.005
79.	0.118	3.967	0.0115	0.1000	3.32E+02	3.3E+03	0.1233	-18.262	0.004
80.	0.120	3.967	0.0117	0.1003	2.43E+02	2.4E+03	0.1237	-18.261	0.003
81.	0.122	3.967	0.0119	0.1008	8.31E+01	8.2E+02	0.1242	-18.261	0.001
82.	0.125	3.967	0.0122	0.1002	7.89E+01	7.9E+02	0.1235	-18.261	0.001
83.	0.129	3.967	0.0127	0.1001	1.75E+02	1.8E+03	0.1234	-18.260	0.002
84.	0.133	3.967	0.0131	0.0996	2.50E+02	2.5E+03	0.1228	-18.260	0.003
85.	0.137	3.967	0.0135	0.1002	1.66E+02	1.7E+03	0.1235	-18.259	0.002
86.	0.141	3.967	0.0139	0.0998	2.73E+02	2.7E+03	0.1230	-18.259	0.004
87.	0.145	3.967	0.0143	0.0998	2.62E+02	2.6E+03	0.1231	-18.258	0.003
88.	0.150	3.967	0.0147	0.1004	1.92E+02	1.9E+03	0.1238	-18.258	0.003
89.	0.154	3.967	0.0151	0.1000	1.47E+02	1.5E+03	0.1233	-18.257	0.002
90.	0.158	3.967	0.0155	0.0999	1.93E+02	1.9E+03	0.1231	-18.257	0.003
91.	0.162	3.967	0.0159	0.0997	3.48E+02	3.5E+03	0.1230	-18.256	0.005
92.	0.166	3.967	0.0163	0.0999	2.90E+02	2.9E+03	0.1232	-18.256	0.004
93.	0.170	3.967	0.0167	0.1005	1.73E+02	1.7E+03	0.1240	-18.255	0.002
94.	0.174	3.967	0.0172	0.1000	1.53E+02	1.5E+03	0.1233	-18.255	0.002
95.	0.178	3.967	0.0176	0.1001	1.82E+02	1.8E+03	0.1234	-18.254	0.002
96.	0.182	3.967	0.0180	0.0997	2.65E+02	2.7E+03	0.1229	-18.254	0.003
97.	0.186	3.967	0.0184	0.0998	3.00E+02	3.0E+03	0.1230	-18.253	0.004
98.	0.190	3.967	0.0188	0.1006	1.30E+02	1.3E+03	0.1240	-18.253	0.002
99.	0.195	3.967	0.0192	0.0999	1.78E+02	1.8E+03	0.1232	-18.252	0.002
100.	0.199	3.967	0.0196	0.1000	1.43E+02	1.4E+03	0.1233	-18.252	0.002
101.	0.203	3.967	0.0200	0.0998	2.75E+02	2.8E+03	0.1230	-18.251	0.004
102.	0.207	3.967	0.0204	0.0996	3.39E+02	3.4E+03	0.1227	-18.251	0.004
103.	0.211	3.967	0.0208	0.1005	1.99E+02	2.0E+03	0.1240	-18.250	0.003
104.	0.215	3.967	0.0213	0.1002	1.41E+02	1.4E+03	0.1235	-18.250	0.002
105.	0.219	3.967	0.0217	0.1002	6.96E+01	6.9E+02	0.1235	-18.249	0.001
106.	0.223	3.967	0.0221	0.0990	4.86E+02	4.9E+03	0.1221	-18.249	0.006
107.	0.227	3.967	0.0225	0.1000	3.96E+02	4.0E+03	0.1233	-18.248	0.005
108.	0.231	3.967	0.0229	0.1013	-8.10E+01	-8.0E+02	0.1250	-18.248	-0.001

Table A-1 Continued.

109.	0.236	3.967	0.0233	0.0994	2.00E+02	2.0E+03	0.1226	-18.247	0.003
110.	0.240	3.967	0.0237	0.0995	3.28E+02	3.3E+03	0.1227	-18.247	0.004
111.	0.244	3.967	0.0241	0.1000	4.17E+02	4.2E+03	0.1233	-18.246	0.005
112.	0.248	3.967	0.0245	0.1007	2.25E+01	2.2E+02	0.1241	-18.246	0.000
113.	0.252	3.967	0.0249	0.1004	-1.77E+01	-1.8E+02	0.1238	-18.245	0.000
114.	0.256	3.967	0.0253	0.0993	3.20E+02	3.2E+03	0.1224	-18.245	0.004
115.	0.260	3.967	0.0258	0.0997	3.49E+02	3.5E+03	0.1229	-18.244	0.005
116.	0.264	3.967	0.0262	0.1003	2.25E+02	2.2E+03	0.1237	-18.244	0.003
117.	0.268	3.967	0.0266	0.1001	1.69E+02	1.7E+03	0.1235	-18.243	0.002
118.	0.272	3.967	0.0270	0.1002	1.15E+02	1.1E+03	0.1236	-18.243	0.001
119.	0.277	3.967	0.0274	0.0993	4.22E+02	4.3E+03	0.1224	-18.242	0.006
120.	0.281	3.967	0.0278	0.1005	1.40E+02	1.4E+03	0.1239	-18.242	0.002
121.	0.285	3.967	0.0282	0.0997	3.28E+02	3.3E+03	0.1230	-18.241	0.004
122.	0.291	3.967	0.0288	0.1000	2.29E+02	2.3E+03	0.1234	-18.240	0.003
123.	0.299	3.967	0.0297	0.1002	2.04E+02	2.0E+03	0.1235	-18.239	0.003
124.	0.307	3.967	0.0305	0.0996	3.36E+02	3.4E+03	0.1228	-18.238	0.004
125.	0.315	3.967	0.0313	0.1005	9.55E+01	9.5E+02	0.1239	-18.237	0.001
126.	0.324	3.971	0.0321	0.0995	3.15E+02	3.2E+03	0.1227	-18.236	0.004
127.	0.332	3.971	0.0329	0.1006	1.10E+02	1.1E+03	0.1241	-18.235	0.001
128.	0.340	3.971	0.0337	0.0994	3.14E+02	3.2E+03	0.1226	-18.234	0.004
129.	0.348	3.971	0.0346	0.1003	2.58E+02	2.6E+03	0.1237	-18.233	0.003
130.	0.356	3.971	0.0354	0.0997	2.03E+02	2.0E+03	0.1230	-18.232	0.003
131.	0.365	3.971	0.0362	0.1002	2.59E+02	2.6E+03	0.1235	-18.231	0.003
132.	0.373	3.971	0.0370	0.1002	9.72E+01	9.7E+02	0.1235	-18.230	0.001
133.	0.381	3.971	0.0378	0.0998	3.28E+02	3.3E+03	0.1230	-18.229	0.004
134.	0.389	3.971	0.0387	0.1000	1.97E+02	2.0E+03	0.1233	-18.228	0.003
135.	0.397	3.971	0.0395	0.1000	2.79E+02	2.8E+03	0.1233	-18.227	0.004
136.	0.406	3.971	0.0403	0.1000	1.78E+02	1.8E+03	0.1233	-18.226	0.002
137.	0.414	3.971	0.0411	0.1000	2.91E+02	2.9E+03	0.1233	-18.225	0.004
138.	0.422	3.971	0.0419	0.1003	3.18E+00	3.2E+01	0.1237	-18.224	0.000
139.	0.430	3.971	0.0428	0.0995	4.30E+02	4.3E+03	0.1227	-18.223	0.006
140.	0.438	3.971	0.0436	0.1004	3.49E+01	3.5E+02	0.1238	-18.222	0.000
141.	0.446	3.971	0.0444	0.0996	4.13E+02	4.1E+03	0.1228	-18.221	0.005
142.	0.455	3.971	0.0452	0.1005	1.04E+02	1.0E+03	0.1239	-18.220	0.001
143.	0.463	3.971	0.0460	0.0996	2.69E+02	2.7E+03	0.1228	-18.219	0.003
144.	0.471	3.971	0.0469	0.1002	2.76E+02	2.8E+03	0.1236	-18.218	0.004
145.	0.479	3.971	0.0477	0.1000	1.88E+02	1.9E+03	0.1232	-18.217	0.002
146.	0.487	3.971	0.0485	0.1000	2.30E+02	2.3E+03	0.1233	-18.216	0.003

Table A-1 Continued.

147.	0.496	3.971	0.0493	0.0998	2.82E+02	2.8E+03	0.1231	-18.215	0.004
148.	0.504	3.971	0.0501	0.1003	1.74E+02	1.7E+03	0.1236	-18.214	0.002
149.	0.512	3.971	0.0509	0.0997	3.71E+02	3.7E+03	0.1229	-18.213	0.005
150.	0.520	3.971	0.0518	0.1005	1.52E+02	1.5E+03	0.1239	-18.212	0.002
151.	0.528	3.971	0.0526	0.0995	2.92E+02	2.9E+03	0.1226	-18.211	0.004
152.	0.537	3.971	0.0534	0.1004	2.54E+02	2.5E+03	0.1237	-18.210	0.003
153.	0.545	3.971	0.0542	0.1000	5.93E+01	5.9E+02	0.1233	-18.209	0.001
154.	0.553	3.971	0.0550	0.0998	4.66E+02	4.7E+03	0.1230	-18.208	0.006
155.	0.561	3.971	0.0559	0.1003	8.94E+01	8.9E+02	0.1236	-18.207	0.001
156.	0.569	3.971	0.0567	0.0996	4.61E+02	4.6E+03	0.1228	-18.206	0.006
157.	0.578	3.971	0.0575	0.1006	2.94E+01	2.9E+02	0.1241	-18.205	0.000
158.	0.586	3.971	0.0583	0.0995	3.30E+02	3.3E+03	0.1227	-18.204	0.004
159.	0.594	3.971	0.0591	0.1004	1.63E+02	1.6E+03	0.1238	-18.203	0.002
160.	0.602	3.971	0.0600	0.0998	2.61E+02	2.6E+03	0.1231	-18.202	0.003
161.	0.610	3.971	0.0608	0.0999	2.64E+02	2.6E+03	0.1232	-18.201	0.003
162.	0.623	3.971	0.0620	0.1001	2.23E+02	2.2E+03	0.1234	-18.199	0.003
163.	0.639	3.971	0.0636	0.1001	2.79E+02	2.8E+03	0.1234	-18.197	0.004
164.	0.655	3.971	0.0653	0.1000	3.14E+02	3.1E+03	0.1233	-18.195	0.004
165.	0.672	3.971	0.0669	0.1000	3.08E+02	3.1E+03	0.1232	-18.193	0.004
166.	0.688	3.971	0.0686	0.0999	2.32E+02	2.3E+03	0.1232	-18.191	0.003
167.	0.705	3.971	0.0702	0.1000	2.16E+02	2.2E+03	0.1233	-18.189	0.003
168.	0.721	3.971	0.0718	0.1002	2.48E+02	2.5E+03	0.1235	-18.187	0.003
169.	0.737	3.977	0.0735	0.0998	2.93E+02	2.9E+03	0.1230	-18.185	0.004
170.	0.754	3.977	0.0751	0.1000	2.58E+02	2.6E+03	0.1234	-18.183	0.003
171.	0.770	3.977	0.0768	0.0999	2.52E+02	2.5E+03	0.1232	-18.181	0.003
172.	0.786	3.977	0.0784	0.1001	1.94E+02	1.9E+03	0.1234	-18.179	0.002
173.	0.803	3.977	0.0800	0.1002	2.15E+02	2.1E+03	0.1235	-18.177	0.003
174.	0.819	3.977	0.0817	0.0999	3.08E+02	3.1E+03	0.1232	-18.175	0.004
175.	0.836	3.977	0.0833	0.0997	4.18E+02	4.2E+03	0.1230	-18.173	0.005
176.	0.852	3.977	0.0849	0.0999	6.56E+02	6.6E+03	0.1231	-18.171	0.008
177.	0.868	3.977	0.0866	0.1000	5.03E+02	5.0E+03	0.1233	-18.169	0.006
178.	0.885	3.977	0.0882	0.0984	1.41E+03	1.4E+04	0.1214	-18.167	0.017
179.	0.901	3.977	0.0898	0.0943	6.44E+03	6.8E+04	0.1163	-18.165	0.079
180.	0.918	3.977	0.0913	0.0939	1.18E+04	1.3E+05	0.1158	-18.163	0.144
181.	0.934	3.977	0.0928	0.0897	2.27E+04	2.5E+05	0.1106	-18.161	0.277
182.	0.950	3.977	0.0943	0.0922	3.11E+04	3.4E+05	0.1136	-18.160	0.379
183.	0.967	3.977	0.0958	0.0908	4.04E+04	4.5E+05	0.1119	-18.158	0.493
184.	0.983	3.977	0.0973	0.0884	5.18E+04	5.9E+05	0.1089	-18.156	0.630

Table A-1 Continued.

185.	0.999	3.977	0.0987	0.0851	6.66E+04	7.8E+05	0.1049	-18.154	0.809
186.	1.016	3.977	0.1001	0.0836	8.35E+04	1.0E+06	0.1031	-18.152	1.013
187.	1.032	3.977	0.1014	0.0815	1.02E+05	1.3E+06	0.1005	-18.151	1.241
188.	1.049	3.977	0.1028	0.0808	1.23E+05	1.5E+06	0.0996	-18.149	1.485
189.	1.065	3.977	0.1041	0.0808	1.43E+05	1.8E+06	0.0996	-18.148	1.730
190.	1.081	3.977	0.1054	0.0810	1.63E+05	2.0E+06	0.0999	-18.146	1.973
191.	1.098	3.977	0.1067	0.0814	1.83E+05	2.3E+06	0.1004	-18.144	2.211
192.	1.114	3.977	0.1081	0.0819	2.03E+05	2.5E+06	0.1010	-18.143	2.442
193.	1.131	3.977	0.1094	0.0823	2.22E+05	2.7E+06	0.1015	-18.141	2.669
194.	1.147	3.977	0.1108	0.0827	2.41E+05	2.9E+06	0.1020	-18.139	2.891
195.	1.163	3.983	0.1121	0.0831	2.59E+05	3.1E+06	0.1025	-18.138	3.107
196.	1.180	3.983	0.1135	0.0837	2.77E+05	3.3E+06	0.1032	-18.136	3.317
197.	1.196	3.983	0.1149	0.0840	2.95E+05	3.5E+06	0.1036	-18.134	3.522
198.	1.212	3.983	0.1163	0.0844	3.12E+05	3.7E+06	0.1040	-18.132	3.721
199.	1.229	3.983	0.1176	0.0844	3.29E+05	3.9E+06	0.1041	-18.131	3.920
200.	1.245	3.983	0.1190	0.0847	3.46E+05	4.1E+06	0.1044	-18.129	4.116
201.	1.262	3.983	0.1204	0.0846	3.63E+05	4.3E+06	0.1043	-18.127	4.312
202.	1.286	3.983	0.1225	0.0852	3.88E+05	4.5E+06	0.1051	-18.125	4.598
203.	1.319	3.983	0.1253	0.0860	4.19E+05	4.9E+06	0.1061	-18.121	4.963
204.	1.352	3.983	0.1281	0.0866	4.50E+05	5.2E+06	0.1068	-18.118	5.307
205.	1.384	3.983	0.1310	0.0876	4.79E+05	5.5E+06	0.1081	-18.114	5.635
206.	1.417	3.983	0.1339	0.0897	5.04E+05	5.6E+06	0.1106	-18.111	5.916
207.	1.450	3.983	0.1368	0.0886	5.30E+05	6.0E+06	0.1093	-18.107	6.195
208.	1.483	3.983	0.1397	0.0895	5.55E+05	6.2E+06	0.1103	-18.104	6.471
209.	1.516	3.983	0.1427	0.0902	5.79E+05	6.4E+06	0.1112	-18.100	6.727
210.	1.548	3.991	0.1456	0.0909	6.01E+05	6.6E+06	0.1121	-18.096	6.966
211.	1.581	3.991	0.1486	0.0913	6.22E+05	6.8E+06	0.1126	-18.093	7.191
212.	1.614	3.991	0.1516	0.0921	6.42E+05	7.0E+06	0.1136	-18.089	7.399
213.	1.647	3.991	0.1547	0.0927	6.61E+05	7.1E+06	0.1143	-18.085	7.592
214.	1.679	3.991	0.1577	0.0933	6.78E+05	7.3E+06	0.1151	-18.081	7.767
215.	1.712	3.991	0.1608	0.0937	6.95E+05	7.4E+06	0.1155	-18.078	7.933
216.	1.745	3.991	0.1638	0.0927	7.12E+05	7.7E+06	0.1142	-18.074	8.106
217.	1.778	3.991	0.1669	0.0921	7.32E+05	7.9E+06	0.1136	-18.070	8.305
218.	1.810	3.991	0.1699	0.0925	7.51E+05	8.1E+06	0.1141	-18.066	8.499
219.	1.843	3.991	0.1729	0.0925	7.70E+05	8.3E+06	0.1141	-18.063	8.690
220.	1.876	3.991	0.1760	0.0934	7.88E+05	8.4E+06	0.1152	-18.059	8.868
221.	1.909	3.991	0.1790	0.0939	8.05E+05	8.6E+06	0.1158	-18.055	9.026
222.	1.942	3.996	0.1821	0.0946	8.21E+05	8.7E+06	0.1166	-18.051	9.172

Table A-1 Continued.

223.	1.974	3.996	0.1852	0.0947	8.35E+05	8.8E+06	0.1168	-18.047	9.308
224.	2.007	3.996	0.1883	0.0948	8.50E+05	9.0E+06	0.1169	-18.044	9.441
225.	2.040	3.996	0.1914	0.0950	8.64E+05	9.1E+06	0.1171	-18.040	9.570
226.	2.073	3.996	0.1945	0.0948	8.79E+05	9.3E+06	0.1169	-18.036	9.702
227.	2.105	3.996	0.1977	0.0949	8.93E+05	9.4E+06	0.1171	-18.032	9.831
228.	2.138	3.996	0.2008	0.0952	9.08E+05	9.5E+06	0.1173	-18.028	9.958
229.	2.171	3.996	0.2039	0.0952	9.22E+05	9.7E+06	0.1174	-18.024	10.080
230.	2.204	3.996	0.2070	0.0952	9.36E+05	9.8E+06	0.1174	-18.021	10.200
231.	2.236	3.996	0.2101	0.0951	9.50E+05	1.0E+07	0.1172	-18.017	10.325
232.	2.269	3.996	0.2132	0.0951	9.64E+05	1.0E+07	0.1173	-18.013	10.449
233.	2.302	3.996	0.2164	0.0956	9.78E+05	1.0E+07	0.1179	-18.009	10.567
234.	2.335	3.996	0.2195	0.0962	9.91E+05	1.0E+07	0.1186	-18.005	10.668
235.	2.368	4.004	0.2227	0.0966	1.00E+06	1.0E+07	0.1191	-18.001	10.760
236.	2.400	4.004	0.2258	0.0965	1.01E+06	1.0E+07	0.1190	-17.997	10.847
237.	2.433	4.004	0.2290	0.0970	1.02E+06	1.1E+07	0.1196	-17.993	10.926
238.	2.466	4.004	0.2322	0.0971	1.03E+06	1.1E+07	0.1197	-17.990	11.002
239.	2.499	4.004	0.2354	0.0974	1.04E+06	1.1E+07	0.1201	-17.986	11.073
240.	2.531	4.004	0.2386	0.0976	1.05E+06	1.1E+07	0.1204	-17.982	11.136
241.	2.564	4.004	0.2418	0.0979	1.06E+06	1.1E+07	0.1207	-17.978	11.191
242.	2.613	4.004	0.2466	0.0975	1.08E+06	1.1E+07	0.1202	-17.972	11.278
243.	2.679	4.004	0.2530	0.0974	1.10E+06	1.1E+07	0.1202	-17.964	11.408
244.	2.744	4.013	0.2593	0.0961	1.12E+06	1.2E+07	0.1185	-17.956	11.574
245.	2.810	4.013	0.2656	0.0967	1.15E+06	1.2E+07	0.1192	-17.948	11.777
246.	2.875	4.013	0.2720	0.0982	1.16E+06	1.2E+07	0.1211	-17.940	11.889
247.	2.941	4.013	0.2784	0.0986	1.18E+06	1.2E+07	0.1216	-17.933	11.970
248.	3.007	4.013	0.2849	0.0992	1.19E+06	1.2E+07	0.1224	-17.925	12.020
249.	3.072	4.013	0.2914	0.0992	1.20E+06	1.2E+07	0.1223	-17.916	12.059
250.	3.138	4.013	0.2979	0.0986	1.22E+06	1.2E+07	0.1216	-17.908	12.117
251.	3.203	4.012	0.3044	0.0992	1.23E+06	1.2E+07	0.1223	-17.901	12.174
252.	3.269	4.012	0.3109	0.0999	1.24E+06	1.2E+07	0.1232	-17.892	12.192
253.	3.334	4.012	0.3175	0.1003	1.25E+06	1.2E+07	0.1236	-17.884	12.186
254.	3.400	4.012	0.3241	0.1008	1.25E+06	1.2E+07	0.1243	-17.876	12.156
255.	3.465	4.012	0.3307	0.1006	1.26E+06	1.2E+07	0.1241	-17.868	12.112
256.	3.531	4.012	0.3373	0.1004	1.26E+06	1.3E+07	0.1238	-17.860	12.096
257.	3.596	4.012	0.3438	0.0999	1.27E+06	1.3E+07	0.1232	-17.852	12.078
258.	3.662	4.012	0.3503	0.0979	1.29E+06	1.3E+07	0.1207	-17.844	12.141
259.	3.727	4.012	0.3568	0.0995	1.30E+06	1.3E+07	0.1226	-17.836	12.224
260.	3.793	4.012	0.3633	0.1009	1.31E+06	1.3E+07	0.1244	-17.828	12.200

Table A-1 Continued.

261.	3.858	4.012	0.3700	0.1016	1.31E+06	1.3E+07	0.1253	-17.820	12.132
262.	3.924	4.012	0.3766	0.1015	1.31E+06	1.3E+07	0.1252	-17.811	12.044
263.	3.990	4.015	0.3833	0.1003	1.31E+06	1.3E+07	0.1236	-17.803	12.002
264.	4.055	4.015	0.3898	0.0994	1.32E+06	1.3E+07	0.1226	-17.795	12.019
265.	4.121	4.015	0.3963	0.1000	1.33E+06	1.3E+07	0.1233	-17.787	12.030
266.	4.186	4.015	0.4029	0.1001	1.34E+06	1.3E+07	0.1234	-17.779	12.028
267.	4.252	4.015	0.4095	0.1006	1.35E+06	1.3E+07	0.1241	-17.771	12.010
268.	4.317	4.015	0.4161	0.1004	1.35E+06	1.3E+07	0.1238	-17.763	11.974
269.	4.383	4.011	0.4226	0.1005	1.36E+06	1.4E+07	0.1239	-17.755	11.962
270.	4.448	4.011	0.4292	0.1001	1.37E+06	1.4E+07	0.1234	-17.747	11.935
271.	4.514	4.011	0.4357	0.0981	1.38E+06	1.4E+07	0.1210	-17.739	11.986
272.	4.579	4.011	0.4422	0.0992	1.40E+06	1.4E+07	0.1223	-17.731	12.073
273.	4.645	4.011	0.4487	0.1004	1.41E+06	1.4E+07	0.1238	-17.723	12.071
274.	4.710	4.011	0.4553	0.1006	1.42E+06	1.4E+07	0.1240	-17.714	12.047
275.	4.776	4.006	0.4619	0.1002	1.42E+06	1.4E+07	0.1235	-17.706	12.024
276.	4.842	4.006	0.4684	0.0993	1.43E+06	1.4E+07	0.1224	-17.698	12.037
277.	4.907	4.006	0.4749	0.0991	1.45E+06	1.5E+07	0.1221	-17.690	12.089
278.	4.973	4.006	0.4814	0.0997	1.46E+06	1.5E+07	0.1229	-17.682	12.119
279.	5.038	4.006	0.4880	0.1004	1.47E+06	1.5E+07	0.1238	-17.674	12.117
280.	5.104	4.006	0.4946	0.1010	1.48E+06	1.5E+07	0.1246	-17.666	12.081
281.	5.169	4.006	0.5012	0.1010	1.48E+06	1.5E+07	0.1245	-17.658	12.019
282.	5.267	4.003	0.5111	0.0998	1.49E+06	1.5E+07	0.1230	-17.646	11.995
283.	5.399	4.003	0.5241	0.0992	1.52E+06	1.5E+07	0.1224	-17.630	12.082
284.	5.530	4.003	0.5372	0.1007	1.54E+06	1.5E+07	0.1242	-17.613	12.066
285.	5.661	4.006	0.5504	0.1002	1.55E+06	1.5E+07	0.1236	-17.597	11.999
286.	5.792	4.006	0.5634	0.0996	1.58E+06	1.6E+07	0.1229	-17.581	12.035
287.	5.923	4.006	0.5766	0.1010	1.59E+06	1.6E+07	0.1245	-17.565	12.000
288.	6.054	4.006	0.5899	0.1010	1.60E+06	1.6E+07	0.1246	-17.549	11.874
289.	6.185	4.006	0.6030	0.0989	1.62E+06	1.6E+07	0.1220	-17.532	11.860
290.	6.316	4.006	0.6160	0.1000	1.65E+06	1.7E+07	0.1233	-17.516	11.960
291.	6.447	4.001	0.6291	0.1008	1.67E+06	1.7E+07	0.1243	-17.500	11.911
292.	6.578	4.001	0.6423	0.1002	1.68E+06	1.7E+07	0.1236	-17.484	11.865
293.	6.709	4.001	0.6555	0.1013	1.69E+06	1.7E+07	0.1249	-17.468	11.779
294.	6.840	3.999	0.6688	0.1014	1.69E+06	1.7E+07	0.1250	-17.451	11.633
295.	6.971	3.999	0.6821	0.1005	1.70E+06	1.7E+07	0.1239	-17.435	11.533
296.	7.103	3.999	0.6951	0.0989	1.73E+06	1.8E+07	0.1219	-17.419	11.610
297.	7.234	3.998	0.7082	0.1008	1.76E+06	1.7E+07	0.1243	-17.403	11.600
298.	7.365	3.998	0.7214	0.1002	1.77E+06	1.8E+07	0.1236	-17.386	11.540

Table A-1 Continued.

299.	7.496	3.998	0.7345	0.1005	1.79E+06	1.8E+07	0.1240	-17.370	11.519
300.	7.627	3.994	0.7477	0.1014	1.80E+06	1.8E+07	0.1251	-17.354	11.412
301.	7.758	3.994	0.7610	0.1011	1.80E+06	1.8E+07	0.1246	-17.337	11.273
302.	7.889	3.994	0.7742	0.0992	1.82E+06	1.8E+07	0.1223	-17.321	11.246
303.	8.020	3.983	0.7872	0.1007	1.85E+06	1.8E+07	0.1242	-17.305	11.283
304.	8.151	3.983	0.8005	0.1013	1.85E+06	1.8E+07	0.1248	-17.289	11.162
305.	8.282	3.983	0.8137	0.0999	1.87E+06	1.9E+07	0.1232	-17.273	11.103
306.	8.413	3.981	0.8268	0.1011	1.89E+06	1.9E+07	0.1246	-17.256	11.069
307.	8.544	3.981	0.8401	0.1015	1.89E+06	1.9E+07	0.1251	-17.240	10.915
308.	8.675	3.981	0.8534	0.1000	1.90E+06	1.9E+07	0.1234	-17.224	10.828
309.	8.806	3.981	0.8664	0.0996	1.93E+06	1.9E+07	0.1228	-17.208	10.903
310.	8.938	3.981	0.8795	0.1007	1.95E+06	1.9E+07	0.1242	-17.191	10.857
311.	9.069	3.981	0.8927	0.0997	1.97E+06	2.0E+07	0.1230	-17.175	10.818
312.	9.200	3.981	0.9058	0.1004	2.00E+06	2.0E+07	0.1238	-17.159	10.838
313.	9.331	3.978	0.9190	0.1011	2.01E+06	2.0E+07	0.1247	-17.143	10.754
314.	9.462	3.978	0.9322	0.1008	2.02E+06	2.0E+07	0.1243	-17.126	10.651
315.	9.593	3.978	0.9453	0.0989	2.04E+06	2.1E+07	0.1219	-17.110	10.653
316.	9.724	3.969	0.9584	0.1008	2.08E+06	2.1E+07	0.1243	-17.094	10.690
317.	9.855	3.969	0.9716	0.1011	2.08E+06	2.1E+07	0.1246	-17.078	10.582
318.	9.986	3.969	0.9848	0.1004	2.10E+06	2.1E+07	0.1237	-17.062	10.513
319.	10.117	3.969	0.9980	0.1010	2.11E+06	2.1E+07	0.1245	-17.045	10.447
320.	10.248	3.969	1.0113	0.1009	2.12E+06	2.1E+07	0.1244	-17.029	10.342
321.	10.379	3.969	1.0244	0.0999	2.14E+06	2.1E+07	0.1232	-17.013	10.298
322.	10.576	3.969	1.0440	0.0997	2.20E+06	2.2E+07	0.1230	-16.989	10.400
323.	10.838	3.967	1.0702	0.1001	2.26E+06	2.3E+07	0.1235	-16.956	10.384
324.	11.100	3.967	1.0966	0.1008	2.29E+06	2.3E+07	0.1243	-16.924	10.244
325.	11.362	3.962	1.1228	0.0998	2.35E+06	2.4E+07	0.1231	-16.891	10.262
326.	11.625	3.963	1.1491	0.1001	2.40E+06	2.4E+07	0.1234	-16.859	10.196
327.	11.887	3.963	1.1754	0.1006	2.45E+06	2.4E+07	0.1240	-16.827	10.138
328.	12.149	3.969	1.2015	0.0991	2.52E+06	2.5E+07	0.1222	-16.794	10.173
329.	12.411	3.969	1.2277	0.1003	2.60E+06	2.6E+07	0.1237	-16.762	10.206
330.	12.673	3.968	1.2540	0.1008	2.65E+06	2.6E+07	0.1242	-16.730	10.134
331.	12.935	3.964	1.2803	0.0993	2.71E+06	2.7E+07	0.1224	-16.697	10.091
332.	13.197	3.964	1.3064	0.0998	2.81E+06	2.8E+07	0.1231	-16.665	10.210
333.	13.460	3.965	1.3325	0.1003	2.89E+06	2.9E+07	0.1236	-16.633	10.229
334.	13.722	3.969	1.3588	0.0992	2.95E+06	3.0E+07	0.1224	-16.600	10.178
335.	13.984	3.969	1.3848	0.0999	3.09E+06	3.1E+07	0.1231	-16.568	10.376
336.	14.246	3.97	1.4110	0.0999	3.18E+06	3.2E+07	0.1232	-16.536	10.394

Table A-1 Continued.

337.	14.508	3.97	1.4372	0.1001	3.25E+06	3.2E+07	0.1235	-16.504	10.349
338.	14.770	3.97	1.4632	0.0988	3.40E+06	3.4E+07	0.1218	-16.472	10.554
339.	15.032	3.98	1.4893	0.0995	3.52E+06	3.5E+07	0.1227	-16.440	10.648
340.	15.295	3.986	1.5154	0.1000	3.63E+06	3.6E+07	0.1233	-16.407	10.703
341.	15.557	3.986	1.5415	0.0991	3.76E+06	3.8E+07	0.1222	-16.375	10.805
342.	15.819	3.994	1.5676	0.0993	3.91E+06	3.9E+07	0.1224	-16.343	10.931
343.	16.081	3.994	1.5936	0.0996	4.07E+06	4.1E+07	0.1228	-16.311	11.104
344.	16.343	3.997	1.6197	0.0990	4.21E+06	4.3E+07	0.1221	-16.279	11.182
345.	16.605	4.007	1.6457	0.0999	4.38E+06	4.4E+07	0.1232	-16.247	11.338
346.	16.867	4.007	1.6717	0.0989	4.55E+06	4.6E+07	0.1220	-16.215	11.471
347.	17.130	4.01	1.6977	0.0990	4.74E+06	4.8E+07	0.1221	-16.183	11.634
348.	17.392	4.009	1.7236	0.0992	4.97E+06	5.0E+07	0.1223	-16.151	11.897
349.	17.654	4.009	1.7497	0.0995	5.15E+06	5.2E+07	0.1226	-16.118	12.005
350.	17.916	4.008	1.7759	0.0999	5.30E+06	5.3E+07	0.1232	-16.086	12.025
351.	18.178	4.01	1.8018	0.0980	5.55E+06	5.7E+07	0.1208	-16.054	12.289
352.	18.440	4.01	1.8276	0.0989	5.83E+06	5.9E+07	0.1219	-16.022	12.565
353.	18.702	4.012	1.8536	0.0998	6.05E+06	6.1E+07	0.1231	-15.990	12.712
354.	18.965	4.008	1.8796	0.0983	6.30E+06	6.4E+07	0.1212	-15.958	12.895
355.	19.227	4.008	1.9055	0.0995	6.57E+06	6.6E+07	0.1227	-15.926	13.113
356.	19.489	4.006	1.9316	0.0998	6.80E+06	6.8E+07	0.1231	-15.894	13.218
357.	19.751	4.006	1.9577	0.0984	7.03E+06	7.1E+07	0.1213	-15.862	13.304
358.	20.013	4.004	1.9835	0.0991	7.41E+06	7.5E+07	0.1222	-15.830	13.673
359.	20.275	4.002	2.0095	0.0992	7.69E+06	7.8E+07	0.1223	-15.798	13.828
360.	20.537	4.002	2.0356	0.0998	7.93E+06	7.9E+07	0.1231	-15.766	13.885
361.	20.800	3.992	2.0615	0.0985	8.29E+06	8.4E+07	0.1214	-15.734	14.153
362.	21.193	3.989	2.1007	0.0997	8.70E+06	8.7E+07	0.1230	-15.686	14.276
363.	21.717	3.987	2.1526	0.0990	9.39E+06	9.5E+07	0.1220	-15.622	14.625
364.	22.241	3.98	2.2048	0.0995	1.00E+07	1.0E+08	0.1227	-15.557	14.802
365.	22.766	3.978	2.2570	0.0999	1.07E+07	1.1E+08	0.1232	-15.493	15.006
366.	23.290	3.982	2.3093	0.0993	1.14E+07	1.1E+08	0.1224	-15.428	15.137
367.	23.814	3.977	2.3616	0.1007	1.20E+07	1.2E+08	0.1241	-15.364	15.199
368.	24.339	3.978	2.4144	0.1007	1.24E+07	1.2E+08	0.1242	-15.299	14.896
369.	24.863	3.989	2.4673	0.1005	1.28E+07	1.3E+08	0.1239	-15.234	14.548
370.	25.387	3.993	2.5204	0.1028	1.30E+07	1.3E+08	0.1267	-15.168	14.011
371.	25.911	3.993	2.5746	0.1036	1.24E+07	1.2E+08	0.1277	-15.101	12.683
372.	26.436	3.998	2.6293	0.1052	1.13E+07	1.1E+08	0.1297	-15.034	10.905
373.	26.960	3.999	2.6865	0.1225	7.83E+06	6.4E+07	0.1511	-14.963	7.155
374.	27.484	3.987	2.7482	0.1016	-5.09E+03	-5.0E+04	0.1252	-14.887	-0.004

Table A-1 Continued.

375.	28.009	3.982	2.8006	0.1000	-7.59E+02	-7.6E+03	0.1233	-14.823	-0.001
376.	28.533	3.978	2.8530	0.1000	9.23E+02	9.2E+03	0.1233	-14.758	0.001
377.	29.057	3.967	2.9055	0.1000	5.74E+01	5.7E+02	0.1233	-14.693	0.000
378.	29.581	3.973	2.9579	0.1000	2.85E+02	2.8E+03	0.1233	-14.629	0.000
379.	30.106	3.975	3.0103	0.1000	6.68E+02	6.7E+03	0.1233	-14.564	0.000
380.	30.630	3.971	3.0627	0.1000	-5.84E+01	-5.8E+02	0.1233	-14.499	0.000
381.	31.154	3.968	3.1152	0.1000	1.53E+03	1.5E+04	0.1233	-14.435	0.001
382.	31.679	3.964	3.1676	0.1000	1.49E+03	1.5E+04	0.1233	-14.370	0.001
383.	32.203	3.953	3.2200	0.1000	3.10E+03	3.1E+04	0.1233	-14.306	0.002
384.	32.727	3.954	3.2725	0.1000	1.74E+03	1.7E+04	0.1233	-14.241	0.001
385.	33.251	3.953	3.3249	0.1000	2.01E+03	2.0E+04	0.1233	-14.176	0.001

REFERENCES

1. Roberts, F. L., Kandhal, P. S., Brown, R. E., Lee, D.-Y., Kennedy, T. W. Hot Mix Asphalt Materials, Mixture Design, and Construction, 2nd ed., *National Asphalt Pavement Association Research and Education Foundation*: Lanham, MD, 1996, pp 47-48.

2. Sentmant, M. L. Miniature universal platform: from extensional melt rheology to solid state deformation behavior. *Journal of Rheologica Acta*. Vol. 43, No. 6, 2004, pp. 657-669.

3. Gogoi, R., K. P. Biligiri, and N. C. Das. Performance prediction analyses of styrene-butadiene rubber and crumb rubber materials in asphalt road applications. *Materials and Structures*. Vol. 49, No. 9, 2015, pp. 3479–3493.

4. Anderson, M. Force Ductility Testing of Asphalt Binders. *Asphalt Magazine of the Asphalt Institute*. Vol. 18, No. 2, 2003.

5. Shuler, T. S., C. K. Adams, and M. Lamborn. *Asphalt-Rubber Binder Laboratory Performance*. Texas State Department of Highways and Public Transportation (SDHPT) Research Report 347-1F, Texas Transportation Institute, College Station, Texas, 1985.

6. Shuler, T. S., J. H. Collins, and J. P. Kirkpatrick. Polymer-Modified Asphalt Properties Related to Asphalt Concrete Performance. *Asphalt Rheology: Relationship to Mixture ASTM STP 941*, 1987, pp. 179-193.

7. King, G., H. King, R. D. Pavlovich, A. L. Epps, and K. Prithvi. Additives in Asphalt. Presented at the 75th Anniversary Historical Review of the Association of Asphalt Paving Technologists. 1998.

8. Glover, C. J., R. R. Davison, C. H. Domke, Y. Ruan, Y., P. Juristyarini, D. B. Knorr, and S. H. Jung. *Development of a New Method for Assessing Asphalt Binder Durability with Field Validation*. Texas Transportation Report No. 0-1872-2, 2005.

9. D'Angelo, J. Development of Standard Practice for Superpave Plus Specifications. Presented at the North-East Asphalt User/Producer Group (NEAUPG) Conference, Burlington, VT, 2005.

10. Airey, G. D. Fundamental Binder and Practical Mixture Evaluation of Polymer Modified Bituminous Materials, *International Journal of Pavement Engineering*. Vol. 5(3), 2004, pp. 137-151.

11. Takamura, K. Pavement Preservation Using the SBR Latex Modified Asphalt Emulsion. BASF Corporation, Presented at the International Latex Conference, Charlotte, NC, 2005.

12. Tabatabaee, H., C. Clopotel, A. Arshadi, and H. Bahia. Critical Problems with Using the Asphalt Ductility Test as a Performance Index for Modified Binders. *Transportation Research Record: Journal of the Transportation Research Board*. Vol. 2370, 2013, pp. 84–91.

13. Wasiuddin Nazimuddin, S. S. Ashani, and R. M. Islam. Evaluation of Dynamic Shear Rheometer Test for Emulsions. Publication LTRC Project No. 11-2B. Louisiana Department of Transportation, 2014.

14. Bahia, H., D. I. Hanson, M. Zeng, H. Zahi, M. A. Khatri, and R. M. Anderson. NCHRP Report 459: *Characterization of Modified Asphalt Binders in Superpave Mix Design*. Transportation Research Board, Washington D. C., 2001. http://onlinepubs.trb.org/onlinepubs/nchrp/nchrp_rpt_459-a.pdf.

15. Wasage, T. L., J. Stastna, and L. Zanzotto. Rheological analysis of multi-stress creep recovery (MSCR) test. *International Journal of Pavement Engineering*. Vol. 12, No. 6, 2011, pp. 561–568.

16. Newscripts. *Chemical & Engineering News*. Vol. 63, No. 23, 1985, p. 80.

17. Laun, H. M., and H. Schuch. Transient Elongational Viscosities and Drawability of Polymer Melts. *Journal of Rheology*. Vol. 33, No. 1, 1989, pp. 119–175.

18. Sentmanat, M., B. N. Wang, and G. H. Mckinley. Measuring the transient extensional rheology of polyethylene melts using the SER universal testing platform. *Journal of Rheology*. Vol. 49, No. 3, 2005, pp. 585–606.

19. Navarro F. J., Partal P., M-Boza F., and Gallegos C. Influence of crumb rubber concentration on the rheological behavior of a crumb rubber modified bitumen. *Energy Fuels*. Vol. 19, 2005, pp. 1984–1990.

20. Al-Abdul-Wahhab H., and Al-Amri G. Laboratory evaluation of reclaimed rubber asphaltic concrete mixes. *Journal of Materials in Civil Engineering*. Vol. 3(3), 1991, pp. 189–203.

21. Albayati A. H., and Mohammed H. K. Influence of styrene butadiene rubber on the mechanical properties of asphalt concrete mixtures. *Al-Qadisiya J Eng Sci.* Vol. 4(3), 2011, pp. 258–274.

22. Khadivar A, and Kavussi A. Rheological characteristics of SBR and NR polymer modified bitumen emulsions at average pavement temperatures. *Construction and Build Materials*. Vol. 47, 2013, pp. 1099–1105.

23. Tamimi A. A., Zubaidy I. A. H. A., Upadhye A, and Ali L. Evaluation of sustainable asphalt mixture. *Study Civil Eng Archit.* Vol. 3, 2014, pp. 41–47.

24. Chen, J. C., M. C. Lio, and M. S. Shian. Asphalt Modified by Styrene-Butadiene-Styrene Triblock Copolymer: Morphology and Model. *Journal of Materials in Civil Engineering*. Vol. 14, No. 2, 2002, pp. 224-229.

25. Read, J., and D. Whiteoak. The Shell Bitumen handbook. Thomas Telford, 2003.